# On Nonlinear Cointegration Methods for Structural Health Monitoring

*A thesis submitted to the University of Sheffield for the degree of Doctor of Philosophy in the faculty of Engineering*

*by*

**Haichen Shi**


The University Of Sheffield.

Department of Mechanical Engineering
University of Sheffield

March 2018

# Abstract

*Structural health monitoring* (SHM) is emerging as a crucial technology for the assessment and management of important assets in various industries. Thanks to the rapid developments of sensing technology and computing machines, large amounts of sensor data are now becoming much easier and cheaper to obtain from monitored structures, which consequently has enabled data-driven methods to become the main work forces for real world SHM systems. However, SHM practitioners soon discover a major problem for in-service SHM systems; that is the effect of *environmental and operational variations* (EOVs). Most assets (bridges, aircraft engines, wind turbines) are so important that they are too costly to be isolated for testing and examination purposes. Often, their structural properties are heavily influenced by ambient environmental and operational conditions, or EOVs. So, the most important question raised for an effective SHM system is, how one could tell whether an alarm signal comes from structural damage or from EOVs?

*Cointegration*, a method originating from econometric time series analysis, has proven to be one of the most promising approaches to address the above question. Cointegration is a property of nonstationary time series, it models the long-run relationship among multiple nonstationary time series. The idea of employing the cointegration method in the SHM context relies on the fact that this long-run relationship is immune to the changes caused by EOVs, but when damage occurs, this relationship no longer stands. The work in this thesis aims to further strengthen and extend conventional linear cointegration methods to a nonlinear context, by hybridising cointegration with machine learning and time series models. There are three contributions presented in this thesis:

The first part is about a nonlinear cointegration method based on *Gaussian process*

(GP) regression. Instead of using a linear regression, this part attempts to establish a nonlinear cointegrating regression with a GP. GP regression is a powerful Bayesian machine learning approach that can produce probabilistic predictions and avoid overfitting. The proposed method is tested with one simulated case study and with the Z24 Bridge SHM data.

The second part concerns developing a regime-switching cointegration approach. Instead of modelling nonlinear cointegration as a smooth function, this part sees cointegration as a piecewise-linear function, which is triggered by some external variable. The model is trained with the aid of the augmented Dickey-Fuller (ADF) test statistics. Two case studies are presented in this part, one simulated muliti-degree-of-freedom system, and also the Z24 Bridge data.

The third part of this work introduces a cointegration method for heteroscedastic data. *Heteroscedasticity*, or time-dependent noise is often observed in SHM data, normally caused by seasonal variations. In order to address this issue, the TBATS ( an acronym for key features of the model: Trigonometric, Box-Cox transformation, ARMA error, Trend, Seasonal components) model is employed to decompose the seasonal-corrupted time series, followed by conventional cointegration analysis. A simulated cantilever beam and real measurement data from the NPL Bridge are used to validate the proposed method.

# Table of Contents

**Abstract** **i**

**1 Introduction to Structural Health Monitoring** **1**
1.1 Motivations for SHM . . . 3
1.2 Overview of Some Related Research Topics . . . 4
1.3 Data Acquisition and Sensing Technology . . . 6
1.4 Damage-Sensitive Feature Extraction . . . 9
1.5 Damage Detection Algorithms . . . 10
1.6 Scope of the Thesis . . . 12

**2 Literature Review on Environmental and Operational Variations** **14**
2.1 Sources of EOVs . . . 15
2.2 Machine Learning Methods . . . 20
2.3 Time Series Methods . . . 25
2.4 Summary . . . 31

**3 The Z24 Bridge Benchmark** **33**
3.1 Overview of SHM of the Z24 Bridge . . . 33
3.2 Damage Detection Algorithms . . . 37
3.3 Summary . . . 43

**4 Cointegration Overview** **44**
4.1 Why Cointegration . . . 44
4.2 Nonstationary Time Series and Unit Roots . . . 46
4.2.1 Nonstationarity . . . 46
4.2.2 Trend-Stationary VS Difference-Stationary Time Series . . . 47

4.3 Statistical Tests for Unit Roots . . . 50
4.4 Cointegration . . . 52
4.4.1 Cointegration I: the Engle-Granger Approach . . . 52
4.4.2 Cointegration II: the Johansen Procedures . . . 55
4.5 A Review of Cointegration Method on SHM . . . 57
4.6 Conclusions . . . 65

**5 Gaussian Processes for Nonlinear Cointegration 66**
5.1 Nonlinear Cointegration . . . 66
5.2 Gaussian Process Regression . . . 68
5.3 GP Regression as A Nonlinear Cointegration Function . . . 73
5.4 Case Studies . . . 73
5.4.1 Case Study I: Linear Trend-Stationary Series Versus Quadratic Trend-Stationary Series . . . 74
5.4.2 Case Study II: the Benchmark Z24 Bridge . . . 79
5.5 Conclusions . . . 89

**6 A Regime-Switching Cointegration Approach 91**
6.1 Introduction . . . 91
6.2 A simulated spring-mass system . . . 92
6.3 A regime-switching cointegration method . . . 95
6.4 A brief summary of the proposed method . . . 98
6.5 An application to the SHM of the Z24 Bridge . . . 100
6.6 Discussions and conclusions . . . 105

**7 The TBATS Model for Heteroscedastic Cointegration 110**
7.1 A Motivating Example . . . 111
7.2 Exponential Smoothing and The TBATS Model . . . 114
7.2.1 Introduction . . . 114
7.2.2 TBATS Model Forms . . . 115
7.2.3 Innovations State Space Model Forms . . . 117
7.2.4 Parameter Estimation . . . 118
7.2.5 Model Selection . . . 119
7.2.6 Summary . . . 120
7.3 Case Studies . . . 120
7.3.1 Case Study I: A Cantilever Beam . . . 121
7.3.2 Case Study II: The NPL Bridge . . . 125

7.4 Conclusions . . . . . 132

**8 Conclusions and Future Work** **133**

8.1 Summaries . . . . . 133

8.2 Directions for Future Work . . . . . 137

8.3 Concluding Remarks . . . . . 139

**Bibliography** **140**

# Chapter 1

# Introduction to Structural Health Monitoring

Industry never sleeps. Important assets and infrastructure, such as power generators, aircrafts, wind turbines, roads and bridges, are so fundamental to society, that people always demand them to be well functioning both safely and constantly. However, in reality, damage, fatigue, degradation or corrosion are always developing inside materials and structures, and it is simply too costly to isolate them for testing and examinations. Many of these assets and infrastructures are near or already exceeding the end of their original design life spans. Consider the road bridges and railway bridges in the United Kingdom for example, as illustrated in Figure 1.1, a great portion of the bridges in the UK has already surpassed 100 years, whereas the standard design working life for bridges in the UK is usually 100 $\sim$ 120 years [1]. This is where the technique of *Structural Health Monitoring (SHM)* comes to the remedy. Intuitively, SHM systems are like doctors for structures that can provide diagnostic and even prognostic information about the health state of the structures through collecting and analysing sensor data collected from the structures, except that these "doctors" are on duty 24/7 throughout the years.

A fairly recent example comes from the Forth Road Bridge in Scotland, as pictured in Figure 1.2, which was opened in 1964 and was the largest suspension bridge in Europe at the time. Unfortunately, originally designed to last for 120 years, the bridge was forced to be fully closed for a few months in 2016 due to structural defects found in the bridge truss, which the engineers believed were caused by a seized pin

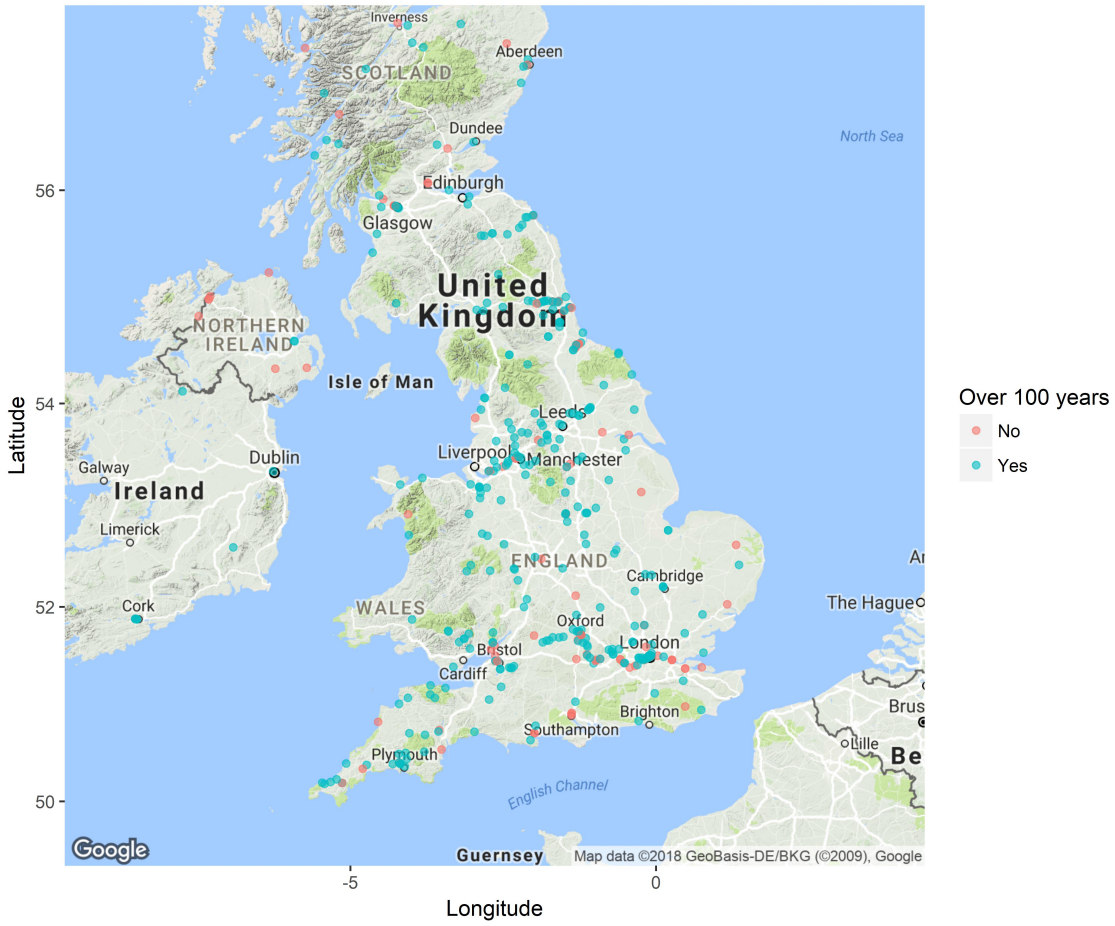


Figure 1.1: An illustration the ageing of some of the bridges (including road bridges, railway bridges and viaducts) in the UK.[1]

[2][3]. However, the good news is, a new bridge called the Queensferry Crossing Bridge, also pictured in Figure 1.2, has already started to service the public as a replacement for the Forth Road Bridge, and a full SHM system has been installed and is fully operational [4][5], in an effort to detect any kind of structural degradation as early as possible.

The term "SHM" embodies a multitude of techniques which are constantly evolving themselves, perhaps it is only feasible to provide a definition of the general framework for SHM. It normally involves implementing damage detection strategies for civil, aerospace and mechanical structures, which consists of data acquisition

[1]Data acquired from the Wikipedia web pages: 1. `https://en.wikipedia.org/wiki/List_of_bridges_in_the_United_Kingdom` 2. `https://en.wikipedia.org/wiki/List_of_railway_bridges_and_viaducts_in_the_United_Kingdom`

through sensors or sensor networks, damage-sensitive feature extraction, statistical or machine learning algorithms. Limited to the length of the thesis, it is formidable to give a full account on all the subjects related, so instead, this chapter will aim to provide a quick tour of the important topics around SHM, which includes a history overview of SHM, the data acquisition and sensing technology, damage-sensitive feature extraction and damage detection algorithms.

Figure 1.2: The Forth Road Bridge (front) alongside the Queensferry Crossing Bridge (back), image downloaded from https://www.theforthbridges.org/forth-road-bridge/.

## 1.1 Motivations for SHM

The application of SHM may provide various kinds of industry with enormous benefits, which can be either short-term or long-term [6].

In the short term, SHM can:

- detect the onset of damage as early as possible, in order to prevent catastrophic events caused by structural damage;
- aid to reduce time and cost of scheduled inspection;
- help to maximise the efficiency of operation and maintenance;
- minimise the risk of human error, if the whole process of SHM is automated.

In the long term, SHM has the potential to

- shift the maintenance strategy from time-based to condition-based, becoming more efficient;
- revolutionise the design philosophy, which is to integrate the concept of SHM into the whole life span of the structures.

In general, the practice of damage detection aims to answer the following five questions established by Rytter [7]:

1. **Detection**: is there any damage existing in the structure?
2. **Localisation**: where is the location of the damage?
3. **Classification**: what specific type of damage is present?
4. **Quantification**: how severe is the damage?
5. **Prognosis**: how long will the structure last before it cannot function safely any more?

## 1.2 Overview of Some Related Research Topics

There are a few closely related research fields, all centred around the task of finding damage/failure/novelty; some of them are overlapping with each other. It is desirable to first distinguish some of these research topics.

*Novelty detection* often refers to methods that are established under normal conditions, capable of classifying test data that are different from the training data in some respect. It has a very broad range of successful application areas, including medical diagnostics [8], malware detection [9], video surveillance [10], structural damage [11], etc. Novelty detection is very suitable for areas where data under abnormal conditions are relatively scarce compared to data under normal conditions. For a comprehensive review of this multidisciplinary research area, readers are encouraged to refer to [12].

*Condition monitoring (CM)* is a terminology mostly used in vibration analysis of rotating machinery [13], where 'rotating machinery'usually refers to machines like

turbines, gearboxes, reciprocating machinery, centrifugal machinery, etc. Accelerometers are often used to measure the dynamic response of these machines, i.e vibration signals, which contain the information about frequency components that are sensitive to structural damage. Fourier-based spectral analysis is widely used in CM [13]; wavelet analysis can also be useful as it analyses both time and frequency information [14]. Some other signal processing techniques include the Hilbert transform, the cepstrum analysis; one can refer to [15] for a systematic review. Condition monitoring has been probably one of the most successful and mature research fields that has been adopted widely. In comparison with SHM however, CM normally studies relatively small machinery that is operating in a restrained environment, whereas SHM aims at much larger structures (bridges, buildings, wind turbines for example), which are operating in an open and changing environment.

*Non-destructive Testing (NDT) or Non-destructive Evaluation (NDE)* is another emerging technology that has been widely employed in evaluating the health state of material, component or system without inducing any damage to them. Due to the rapid advances made by sensing technology, researchers have developed a full arsenal of methods tailored for specific sensing technology and the material to be inspected: acoustic emission [16], electromagnetic testing [17], microwave imaging [18], ultrasonic testing [19], the list goes on. Comparing to SHM, NDT is normally conducted in an off-line manner, subject to the working conditions of the instruments.

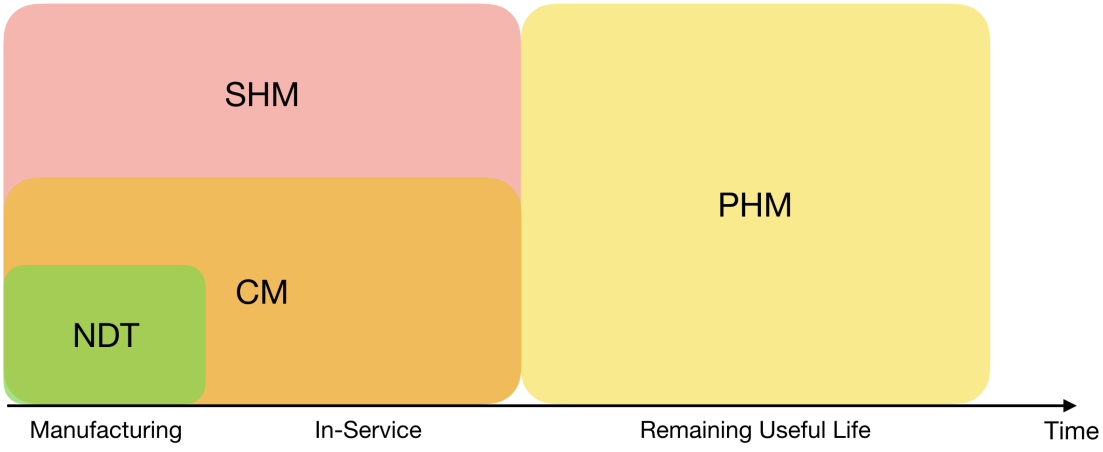


Figure 1.3: The relationship between SHM, NDT, CM and PHM.

*Prognostic Health Management (PHM)* has drawn increasing amounts of interest from both industry and academia; it is the study of system behaviour focusing on predicting how long the system will last before it fails to deliver its desired perfor-

mance. PHM has been studied extensively, particularly in the aerospace industry, where system failure might lead to catastrophic accidents and prohibitive economic loss. Potential applications of PHM are to support decision making for contingency mitigation, and to develop condition-based maintenance strategies. Physical models, data-driven models and hybrids of these two are extensively studied in PHM. A thorough review of this topic can be found in [20].

Figure 1.3 can approximately summarise the relationship of these terms, although there may be a few exceptions. NDT can be used during a manufacturing process to ensure the quality of the product; when the product is in service, CM can provide ongoing monitoring and evaluation of its performance; while SHM can be regarded as the general aim for these practices, and SHM can integrate all the available information from manufacturing to service life; PHM is concerned with forecasting the remaining useful life of the product.

## 1.3 Data Acquisition and Sensing Technology

How to accurately measure the property of a system is obviously one of the most fundamental and essential components for SHM. With the rapid development of sensor technology, there have been many new sensing technologies being developed that are suitable for the application of SHM. However, it is beyond the scope of the thesis to review all of them, only a few of them are selected here for illustration purposes.

#### Vibration Sensors

Vibration sensing has been arguably the most popular sensing technology in SHM applications, as dynamic response from structures encodes the information of dynamical properties such as natural frequency, damping ratio, which can be very sensitive to damage in the structure. To measure dynamic responses, strain gauges, displacement transducers and piezoelectric accelerometers are three commonly-used types of sensors, but generally, strain and displacement are relative measurements to some references, while accelerometers can provide absolute measurements of accelerations. Nowadays, accelerometers are being made more and more sophisticatedly, with on-board signal conditioning modules, multi-axis orientation, and high preci-

sion measurements [6].

### Guided Wave Sensing

As an active sensing technique, guided wave testing has quickly emerged as a very useful tool for damage detection, classification and localisation. Guided waves normally refer to the techniques which enforce stress waves to propagate through a path which is defined by material boundary conditions [21]. In the SHM setting, typically a high-frequency pulse signal is generated by an actuator, and then travels through the material, when it hits some structural discontinuity (which can be crack or delamination), the guided wave will be scattered in all directions. Two kinds of approaches are commonly used to decipher the information in the guided wave, pulse-echo and pitch-catch, depending on the locations of actuator and receiver sensors, the actuator and receiver are collocated in the former and in different positions for the latter.

Piezoelectric wafer transducers are the most widely-used sensors in guided wave SHM, which is due to the piezoelectric and inverse piezoelectric principles of this unique material. That is, when the piezoelectric material is under stress, an electric charge signal is generated on the surface of the material; conversely, when an electric filed is applied to the piezoelectric material, mechanical strain is generated in the material. These properties make piezoelectrics perfectly suitable for both actuators and sensors. Lead zirconate titanate (also known as PZT) and polyvinylidene fluoride (PVDF) based sensors are now probably the most commonly-adopted piezoelectric materials in guided wave SHM applications [22][23].

### Acoustic Emission

*Acoustic Emission (AE)* is a passive non-invasive monitoring and evaluation technique, which has several successful applications especially in bridge monitoring [24][25]. AE monitoring usually represents the method to detect potential flaws in structures by measuring high-frequency sound waves that propagate within structure, which are often emitted from defects in the structure. Generally speaking, there are two kinds of AE forms, primary AE and secondary AE, where primary AE are typically generated from the material of interest, while secondary AE refers to those generated from external sources [26].

Thanks to its passive nature, AE monitoring can be adopted as an *in situ* monitoring technique, which is hugely beneficial for the operation of structures; signal processing methods have improved greatly in recent years, detection and localisation algorithms are now available for SHM practices. However, AE monitoring is a highly application-specific technology, the variability of the types of structure and their operational conditions make it difficult for the wide adoption of this technique [26].

### Fibre-Optic Sensors

*Fibre-Optic Sensing* has been extensively exploited in recent decades for conducting SHM. Fibre-optic sensors have a few advantages that traditional mechanical-electrical sensors do not possess; for example, fibre-optic sensors are robust to electromagnetic interference and corrosion, they are also light-weight and economically affordable. These nice properties make them broadly used in measuring strain, stress and temperature in civil engineering [27]. Generally, a fibre-optic sensing system is composed of a light transmitter, an optical fibre, a receiver sensor, a modulator and a signal processing unit, they are normally mounted or embedded in a structure, when the strain of the structure varies, the optical fibre will deform its shape accordingly, thus the light travelling inside the optical fibre will change its property, which can be detected by signal processing and post processing [28]. Fiber Bragg Grating (FBG) sensors [29], Extrinsic Fabry-Perot Interferometric (EFPI) sensors [30], Optical Time-Domain Reflectometry (OTDR) sensors [31] are three of the mainstream fibre-optic sensors adopted in the market. For a systematic review on this technology, one can refer to [32] and [33].

### Summary

One can easily see from the sensing technologies listed above, SHM is quickly evolving with the advancement of sensing technology; better tools always lead to better diagnosis. However, the list above is far from exhaustive and represents only a fraction of all the available sensing technologies; other useful measurement methods used in the SHM community include: corrosion sensors [34], wireless sensor network (WSN) [35], (embedded) magnetostrictive sensors [36], and even video-based measurement [37].

## 1.4 Damage-Sensitive Feature Extraction

Once data have been collected from structures using sensors, the next question becomes how to make use of them and ultimately make decisions about the health state of the structure. Damage-sensitive feature extraction is a vital step of SHM to answer this question. According to the fourth axiom of SHM concluded in [38], damage cannot directly be measured by sensors, feature extraction is a necessary step for converting sensor data into damage information. In the literature, feature extraction is often accomplished by fitting either a physics-based model or a data-based model to the measurement data from sensors.

#### Physics-based features

In terms of physics-based models, modal properties are probably the most successful features used in SHM. Basic modal properties, including resonance frequencies and mode shapes, can work as characteristics of a structure, such that when damage alters the properties of a structure, these modal properties will also change accordingly. With the input and output data readily measured, modal analysis can then be applied to these data using frequency response functions or impulse response functions, these basic modal properties can then be easily extracted. Sometimes, input data cannot be acquired, and associated output-only modal analysis methods have been developed [39], although they are not guaranteed to be able to identify all the frequency band due to unknown input exciting sources [6].

Despite their practical use in engineering applications, extracting modal properties has some fundamental challenges to overcome. Firstly, damage is often known as a local phenomenon, which does not necessarily have a significant reflection on the low-frequency response. The other difficulty comes from the basic assumptions of modal analysis: that the structure is linear and invariant with time, and shows reciprocity [6]. These assumptions may be violated when there is onset of damage in the structure, for example, a damaged structure can become a nonlinear one, making the linear parametric model fitted to the data immediately invalid; any modal parameters estimated from them are thus inaccurate.

Other features derived from modal properties are also available in the literature: mode shape curvature [40], structural flexibility [41], modal strain energy [42], etc.

### Data-based features

In general, data-based methods are aiming to lower the dimension of raw measurement data, which are often prohibitive to deal with directly, to condensed features that still maintain sensitivity to damage. Summary statistics like the mean, variance, skewness, kurtosis are some of the common choices for damage-sensitive features. Fourier-based algorithms have also proved to be useful for feature extraction. Fast Fourier transform (FFT) and power spectral density (PSD) function are frequently used to extract the system resonance frequencies, which can then be used as a low-dimensional feature vector. For qualitative comparison between two signals, some of the time-domain and frequency-domain methods can be adopted, for example the coherence function, the PSD and cross-spectral density. Moreover, features can also be extracted from the time series models. The family of autoregressive moving average (ARMA) models can be fitted to the measurement time series, the ARMA model is able to characterise how time series evolve dynamically over time. The estimated ARMA model coefficients are treated as damage-sensitive features, applications in SHM can be seen in [43][44][45].

## 1.5 Damage Detection Algorithms

At this point, data have been measured from structures, and meaningful features can also be extracted from measurements; the next challenge becomes to assess and make decisions about the health state of a structure. This decision making process is well fitted in the discipline of *statistical pattern recognition*. According to Rytter's hierarchy as stated previously, the first level of decision making is to ascertain whether damage has occurred; the higher levels for SHM include localisation of damage, and classification of damage types. These can all possibly be addressed by statistical pattern recognition, which can be largely classified into two methods, supervised learning and unsupervised learning.

### Supervised Learning

Supervised learning is a class of machine learning algorithms that is capable of learning a function mapping inputs to outputs, based on annotated training input-output pairs. In the context of SHM, supervised learning is essential for damage

localisation and classification.

The Artificial Neural Network (ANN) is an excellent framework for fitting nonlinear functions, making it an ideal choice for performing damage localisation [46] and damage classification [47][48] in SHM; support vector machines are also widely adopted in the same tasks [49][50]; other algorithms include decision tree based methods [51], hidden Markov models [52].

However in actual practices of SHM, it is often a luxury to have labelled damage data for training a supervised learning algorithm, as obviously in most cases, it is highly uneconomic and unacceptable to perform a damage test on a real operational structure. A potential solution has been proposed by researchers; that is to develop a high-fidelity digital model - digital twin - working as a proxy for real physical systems, and able to generate high-quality labelled annotated data [53].

### Unsupervised Learning/Novelty Detection

As mentioned above, due to the lack of labelled data, unsupervised learning algorithms have been the mainstay in most SHM applications. In the context of damage detection, unsupervised learning can be seen as a two-class classifier, which separates data with damage from those data in normal conditions. This framework is also known as novelty detection, which has been briefly reviewed in Section 1.2.

'Outlier analysis'refers to methods to calculate the discordance between data points and a baseline model, if the discordance exceeds some threshold, then these data points are marked as outliers. Various applications can be found in the SHM literature [54][55], where different assumptions about the baseline model and different types of discordance metrics are used.

Statistical process control (SPC) is also widely used in SHM to detect damage. The premise for adopting SPC in SHM is that when the system is under normal conditions, its statistical properties including the mean, the variance and possibly others, should remain largely stationary; when damage occurs however, these statistical properties will consequently undergo some changes; when they surpass the control limits, a damage alarm can be signalled. Different types of control charts are available in the literature, tailored to monitoring certain statistics. Some examples include the X-bar chart for the mean [56], the S control chart for the variance [57], the CUSUM chart for change detection [58].

However, one important remark at this point is that often extracted features are heavily affected by the confounding influence of environmental and operational variations; the structure may have even larger responses to the variations caused by temperature than the variations caused by damage. This problem has be be addressed before any sensible decision can be made. In fact, the work of the whole thesis is building around this issue. The following chapters will attempt to review the current literature on this issue, and propose new algorithms to effectively solve the problem.

## 1.6 Scope of the Thesis

This thesis is structured as follows:

- Chapter 2 reviews the special topic of the issue of environmental and operational variations, and also presents a literature review of machine learning methods and time series methods.
- Chapter 3 gives an overview of the benchmark study of the Z24 Bridge, as it is repeatedly utilised as case studies later in Chapter 5 and Chapter 6. The experimental setup and system identification of the Z24 Bridge are reviewed, also a short review of recent research efforts on this bridge is given.
- Chapter 4 introduces some of the basic theory for nonstationary time series: the unit root test and cointegration; two kinds of cointegration framework are reviewed in detail; in addition, a review on the cointegration method for SHM is provided.
- Chapter 5 proposes a nonlinear cointegration method based on Gaussian process (GP) regression; the basics of GP regression is presented, and the detailed procedures to perform the proposed methods are also demonstrated. The proposed methods are tested with two case studies, one synthetic dataset and the Z24 Bridge data.
- Chapter 6 introduces a regime-switching cointegration approach, which is a nonlinear cointegration method. The timing for switching regimes is controlled by external variable, which is learnt by using the ADF statistic. Proposed methods are illustrated with case studies, a synthetic dataset and the Z24

Bridge.

- Chapter 7 explores how to apply cointegration methods on a heteroscedastic dataset. The proposed method is to first apply the TBATS model to decompose the original signal into different components, and then build a cointegration model on the long-term components. The method is validated with a simulation study and also the real data from the NPL Bridge.
- Chapter 8 summarises the findings of the thesis and discusses some of the future directions for this research work.

# Chapter 2

# Literature Review on Environmental and Operational Variations

As previously alluded to, arguably the greatest challenge obstructing SHM transitioning from a laboratory technology to commercial application comes from the effect of *environmental and operational variations (EOVs)*. Once the damage-sensitive features have been extracted from data, the next step is to find the underlying relationship between these features and damage information. Unfortunately in many cases, the more sensitive the features are to damages, the more sensitive they are to the EOVs [6]. Addressing the effects of EOVs is the central focus of this thesis, therefore it is sensible to review some of the attempts made by researchers, especially the articles published after the comprehensive review done by Sohn in 2007 [59]. This chapter will mainly focus on machine learning and time series methods, as they are closely related to the methods to be presented in later chapters.

## 2.1 Sources of EOVs

### Temperature

Temperature affects almost all structures, no matter whether they are in the laboratory environment or in a real world environment. Many properties of materials are temperature dependent; for example, the Young's modulus and the mass densities, which sometimes can lead to the formation of thermal stress inside structures, causing elastic deformation and even change of boundary conditions. For example, it was observed in the modal testing experiments on the Alamosa Canyon Bridge that the modal frequency can vary up to 5% in just 24 hours of temperature variations [60]. Also, Xu et al. [61] discovered that the displacement of the bridge deck was linearly related to the changes of ambient temperature, after conducting a six-year monitoring on the Tsing Ma Bridge in Hong Kong, which is illustrated in Figure 2.1. Similarly, in [62], Moser and Moaveni found that the identified natural frequencies of the Dowling Hall Footbridge varied by 4% to 8% in a 16-week time span, where in the same period, temperature fluctuated between -14 °C and 39 °C.

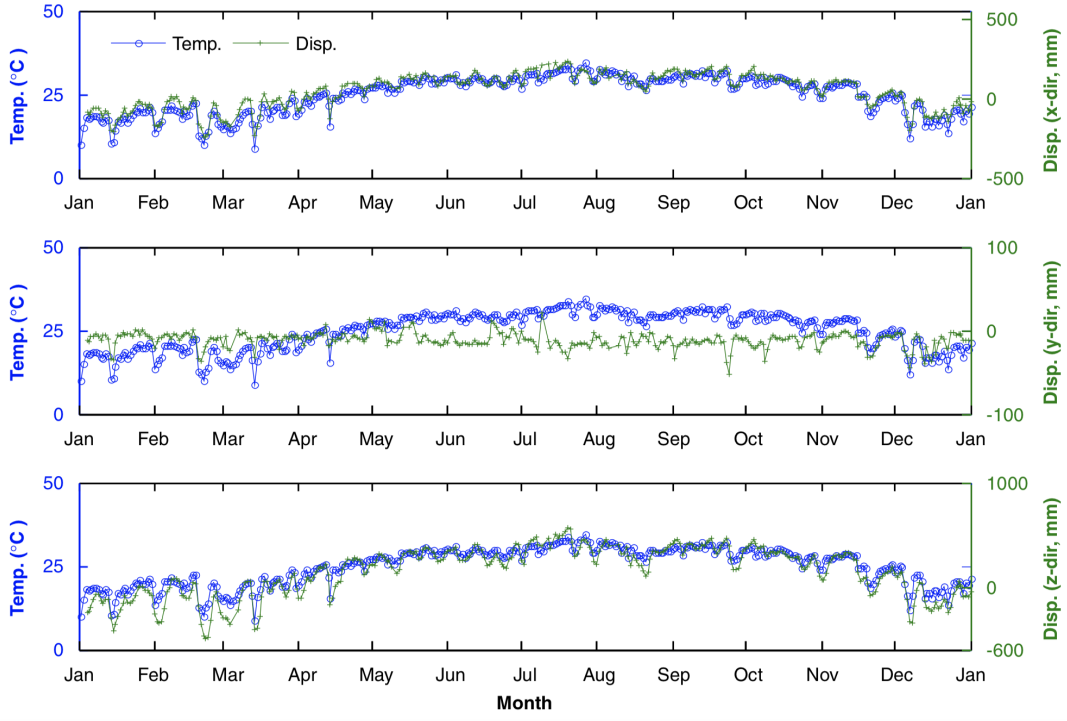


Figure 2.1: Comparison of the ambient temperature and the three-direction displacements of the Tsing Ma Bridge deck in 2005 [61].

However, the field measurements of temperature are not always straightforward, especially for large-scale structures. While investigating the thermal effects on the Zhenjiang Bay Bridge (a cable-stayed bridge with a 480m main span) in China, Cao et al. discovered that temperature distributed differently in different parts of the bridge, and that the temperature in the concrete was 5∼6 hours lagged from the ambient air temperature, which is illustrated in Figure 2.2 [63]. Also in the Tamar Bridge in the UK, the monitoring campaign observed that the identified temperature of the structure was 10 to 60 minutes delayed to the air temperature, depending on which part of the bridge was measured [64].

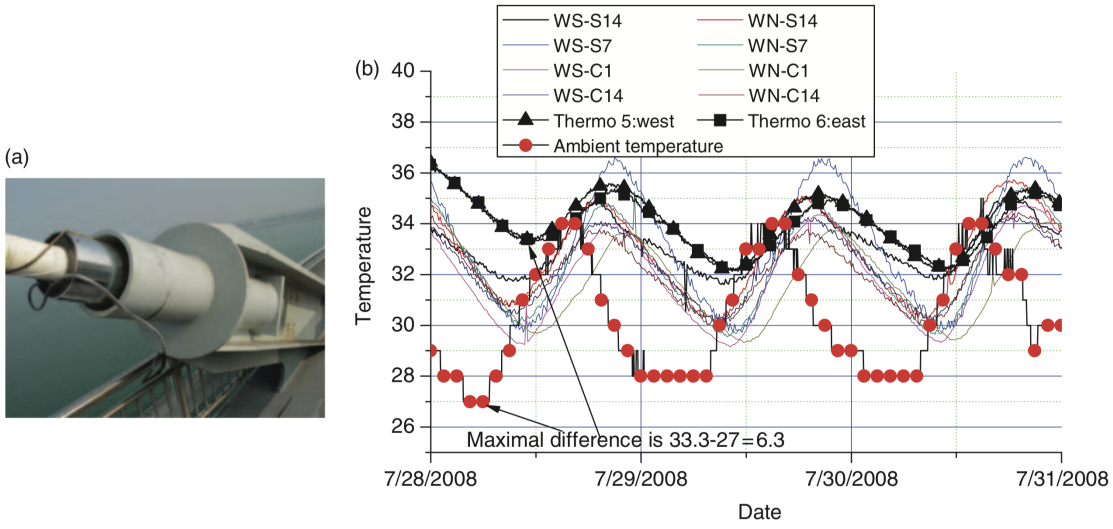


Figure 2.2: Ambient air temperature VS temperature measured in different parts of the Zhanjiang Bay Bridge: (a) the thermal sensor used; (b) temperature measured over a three-day period [63].

The change in temperature can sometimes vary the properties of materials as well. Watson and Rajapakse [65] investigated how the material properties of pavements varied with the temperature; the study showed that the stiffness of the asphalt layer increased dramatically in the sub-zero regime, while it showed much smaller decrease in the above-zero regime. The findings were later validated in a bigger structure, bridges: in Moser and Movaveni's research on the Dowling Hall Footbridge [62], the modal frequency of the bridge saw a significant rise when the temperature dropped below 0°C; a very analogous condition can be observed in the Z24 Bridge[66], which will be extensively reviewed and studied in this thesis.

The effect of temperature is also vital for guided-wave SHM [67], impedance-based SHM [68], fibre-optic sensing [69], and so forth, temperature affects almost all the

techniques in SHM studies.

### Humidity

Humidity is a subtle environmental factor which normally does not vary significantly, but it is certainly an important one that cannot be neglected when performing SHM practices. To find out how humidity may affect the dynamic behaviour of structures, Xia et al. conducted an experiment on a reinforcement concrete slab; they concluded that as the humidity increased, the concrete absorbed more water and thus increased its mass, its natural frequencies increased as a consequence [70]. Another example comes from the condition monitoring of gas turbines, where a twin shaft industrial gas turbine was tested for performance monitoring; Mathioudakis and Tsalavoutas [71] found that the lack of humidity measurements may cause a significant increase in the uncertainty bands of the measured quantities, the situation may get worse if the relative humidity increased. Their observations also confirmed that the variations caused by humidity changes may actually be at the same level of the variations caused by faults.

### Wind

Wind-induced vibration is a critical factor for the design and maintenance of tall and slender structures like wind turbines, skyscrapers, and long-span bridges. The energy that wind-induced vibration can input to structures may excite the fundamental modes of structures, causing the structure to fatigue or fail. Li et al. [72] monitored the wind effect of a super tall building (370m) located in Hong Kong during a typhoon event. The wind speeds, wind direction, and the dynamic responses of the building were continuously collected. After spectral analysis, it was discovered that the first and second natural modes of the building had been excited by the typhoon, and the values of the first two modes were about 20% different from the original design. A suspension bridge in Japan was tested by Mahmoud et al. [73]; they found that the natural frequencies, mode shapes and damping ratios were all related to the variations of the ambient wind [74]. Similar findings can also be seen in **??**, where Zhou et al. concluded that, apart from temperature, wind was another important factor to explain the variations of the modal properties of a bridge. Cross et al. [75] observed that the modal frequencies of the Tamar Bridge in the UK were

not significantly related to wind speed when the wind speed was relatively slow, but when the wind hit the bridge with speeds above 25 mph, the modal frequencies showed a clear relationship with the wind speed.

### Boundary Conditions

Boundary conditions of structure are places where the structure interacts with the external environment through external forces or constraints on displacements. Boundary condition may change over time, implying that it may have significant influence on the dynamic response of the structure. Quek et al. [76] performed a numerical study on a beam, and examined how their damage detection algorithm worked under different boundary conditions and different crack characteristics. Two kinds of boundary conditions were simulated: simply-supported and fixed, they found that the damage-sensitive features were relying on the type of boundary condition, that the simply-supported case was about one-third of the fixed case. Also, in the context of impedance-based SHM, boundary conditions can be a critical factor for damage detection, for example in [77], Park and Inman used impedance-based technique to detect damage (loosening bolts) in a scaled-down steel bridge section, the experiment was designed for three different boundary conditions to mimic real-life variations. As illustrated in Figure 2.3, responses from two PZT sensors are plotted; the first 14 bars for each PZT sensor represents 14 different boundary conditions, the following three bars are from damage scenarios. As one can see, especially for PZT 1, the changes of damage metric that are caused by the boundary conditions are close to the magnitude of the changes caused by Damage 1 and Damage 2.

### Operational Conditions

Operational conditions in SHM can be considered to be a broad terminology that may include factors like traffic loading, flight conditions, operating speed and payloads, which may vary with time, resulting in significant influences on the response and dynamic properties of interested structures. In his PhD thesis [78], Gong presented a numerical study on how vehicles loads may interact with the dynamic properties of long-span bridges. He concluded that traffic load may have positive or negative impact on the dynamic response of bridges, and the impact could result in

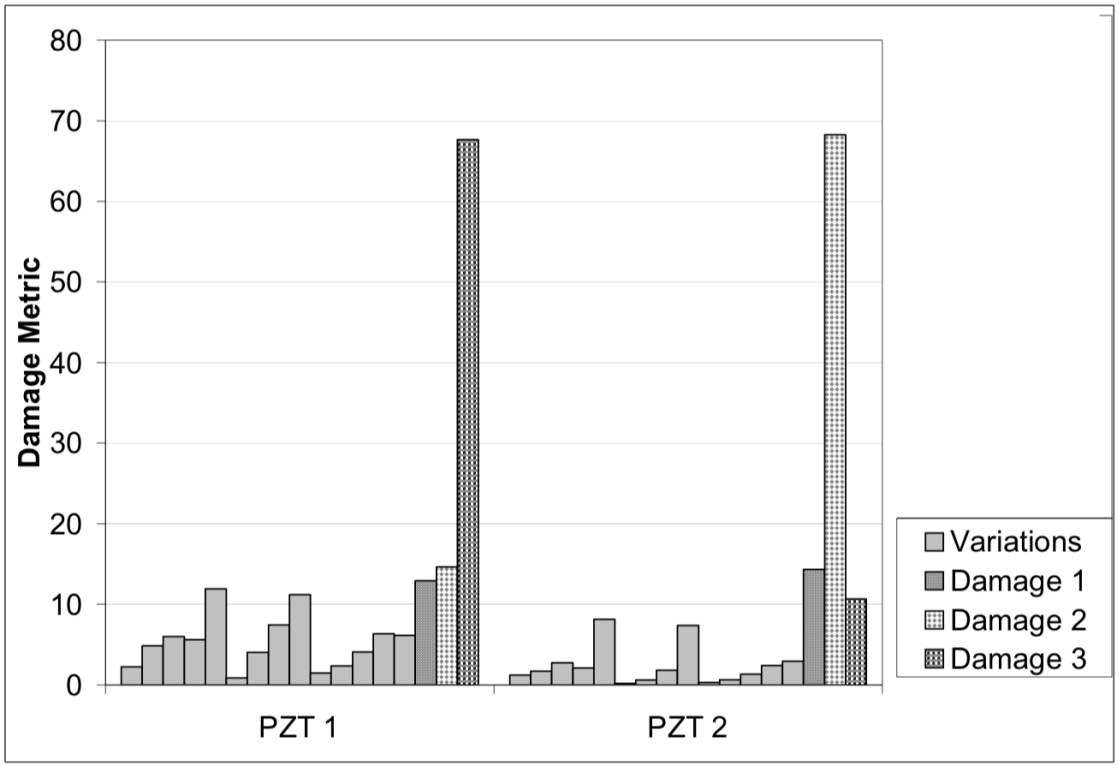


Figure 2.3: The variations of the damage metric under different boundary conditions in comparison with the damage metric under damage conditions [77].

significant variations in the response. In general, long-span bridges were more pronounced to traffic loadings than short-span bridges. Besides, the dynamic response of bridges tended to increase when vehicle speed increased. The findings from Gong were quite consistent with the experimental study on the Tamar Bridge; Westgate et al. [79] found that the modal properties of the Tamar Bridge were dependent on the level and spatial distribution of the traffic loads; also, the effect of traffic loads had a different role in different dynamic modes, as temperature appeared to be more dominant in some modes than traffic loads. Similar conclusions about the Tamar Bridge can also be found in [75].

For condition monitoring, operating conditions also play an important role, especially for gas turbines and aircraft engine monitoring. For example, the vibration analysis during the start-up and shut-down periods of an aircraft engine is very crucial for it safety and reliability, as it may frequently repeat the start-up and shut-down process. Therefore, transient analysis of the dynamic properties becomes necessary for damage detection, for reviews and application studies, one can refer

to [80][81][82].

## 2.2 Machine Learning Methods

The process to distinguish changes caused by damage from those caused by EOVs is called *data normalisation*. However, there is no panacea for data normalisation in SHM, most methods available are problem-specific. In this section and the following section, machine learning and time series methods for data normalisation will be briefly reviewed.

### Neural Networks

Neural networks represent a large family of parametric methods that can perform nonlinear regression and classification tasks. When the measurements of EOVs are available to the researcher, then one can use a neural network model to fit the linear or nonlinear relationship between EOV variables and responses from structures. For example in [83], Ni et al. employed a two-layer back-propagation neural network (BPNN) model on 770 hour worth of monitoring data from the Ting Kau Bridge in Hong Kong. The model formed was a regression model with temperature measurements from multiple sensors as inputs and modal frequency as output. The whole dataset was divided into three parts for training, validation and testing respectively. The purpose of the study was to examine the generalisation ability of the BPNN, therefore the selection of training data needed to be carefully done. In the paper, a full cycle of temperature variation was utilised to form the training dataset. The number of hidden nodes was determined optimally using the validation dataset. They had also proposed to train the BPNN with tricks including early stopping and Bayesian regularisation, in an attempt to improve the generalisation capability. Once a proper BPNN model was trained, the model was used to make predictions of modal frequency with temperature data as inputs; once the prediction deviated from real measurements, then one could say the status of the bridge had changed. For the case study of the Ting Kau Bridge, the BPNN model can produce quite accurate predictions, and the Bayesian regularisation helped to improve the performance of the BPNN on the test dataset.

What if the measurements of EOVs were not easy to obtain? The solution proposed

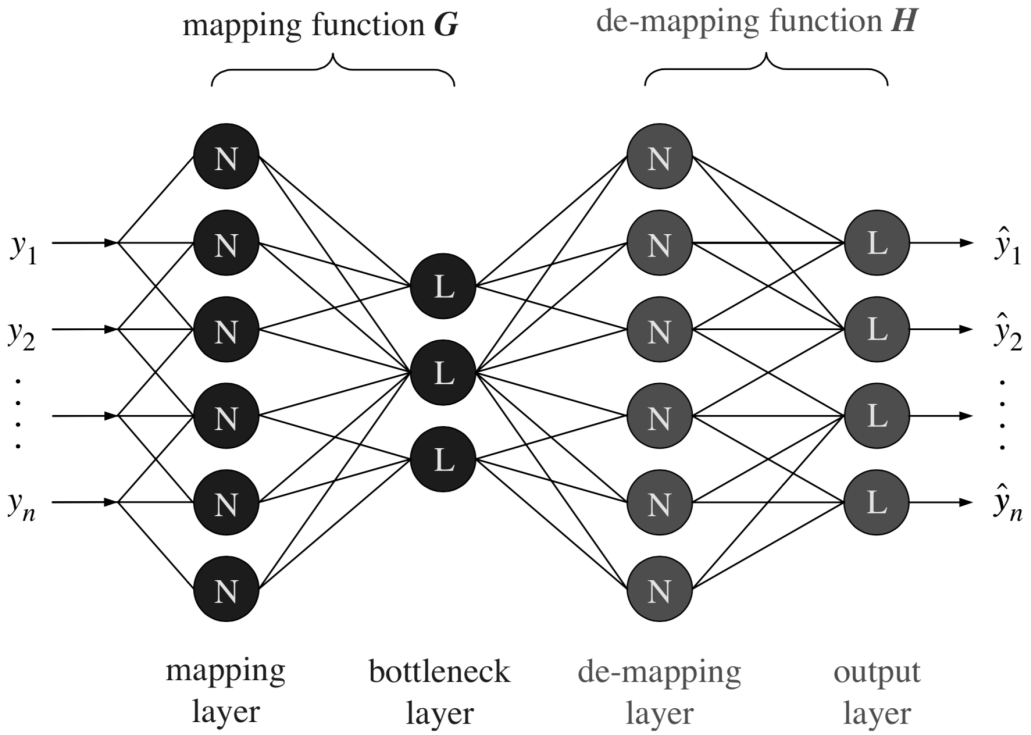


Figure 2.4: The schematic representation of an auto-associative neural network [47].

by Sohn et al. [47] was to train an auto-associative neural network (AANN) model. An auto-associative neural network is different from a conventional neural network, the above BPNN for example, that the target outputs are simply its inputs, as shown in Figure 2.4. An AANN normally consists of five layers: mapping, bottleneck, de-mapping and output layer namely. The bottleneck layer, usually contains fewer nodes than the input layer, and works as a concentration function in order to extract the most informative features from the inputs. The idea of employing AANN to the data normalisation in SHM is based on the assumption that the underlying dependency on EOVs can be captured by the nonlinear mapping functions trained in AANN; once the structure experiences damage, the prediction error produced by AANN will be expected to grow as a result, which can be regarded as a damage indicator. In [47], they first extracted features from measurement data using an autoregressive and autoregressive with exogenous inputs (AR-ARX) model, then the estimated coefficients in the model were used to train the AANN model. More recently, Dervilis et al. [84] proposed to improve the robustness and efficiency of AANN by adopting an auto-association with Radial Basis Function (RBF). The main difference between a traditional multi-layer perceptron (MLP) network and

an RBF network is that instead of representing the nonlinear transfer function with the scalar products of the input vector and the weight vector, the RBF network adopts a nonlinear function of the distance (Euclidean distance in this case) between them, which is hugely advantageous because an RBF network does not require a cumbersome nonlinear optimisation for the model parameters. The RBF network was examined with an experimental case study to detect damage in a wind turbine, and was proved to be an fast online damage detection algorithm.

### Singular Value Decomposition

Singular Value Decomposition (SVD) has been used as a data normalisation method in SHM so as to distinguish between changes caused by EOVs and changes caused by damage [85]. The concept was based on the premise that once one had assembled a feature matrix under normal conditions, the rank of the matrix was supposed to remain constant if the structure stayed intact; when new data was observed, the new feature vector was concatenated to the feature matrix, if there was the onset of damage, the rank of the new matrix would increase by 1, otherwise, the rank stayed constant. This method works relatively well if the features are properly selected, and the damage feature is orthogonal to the feature space expanded by the baseline feature vectors. Later, Vanlanduit et al. proposed a more robust SVD method to deal with EOVs [86]. In the case where data under the intact condition is available, the SVD method can be trained appropriately, but when there is an outlier in the data or when the damage data and normal data are actually mixed together, then the SVD method would tend to fail. Vanlanduit et al. proposed a robust SVD method to find the feature matrix representing the underlying normal condition, by applying an exhaustive search for the singular value decomposition with the smallest cost function.

A different direction of using SVD was proposed by Ruocci et al. [87], where the aim was to assess damage of a pre-stressed beam. The interpretation in [87] was that the variability from EOVs can be mostly expressed by the singular value matrix, and the contributions were ranked by the singular values. In their case study, Ruocci et al. found that the first singular value could account for 99.8% of the variability, thus they removed the first singular value, as they believed most of the variations were from EOVs. The remaining three singular value were then used for damage detection.

### Principal Component Analysis

Principal component analysis (PCA) is a statistical method for dimension reduction, a set of $N-$dimensional variables is orthogonally projected into a new set of uncorrelated $p-$dimensional ($p < N$) variables, which are called the principal components. Traditionally, in a damage detection context, PCA has been used as a feature extraction method; for example in [88], Zang and Imregun used the principal components that accounted for most of the variations to reconstruct the frequency response function (FRF), and then applied a back propagation neural network to train these features under normal conditions. However in order to eliminate the effect of EOVs, PCA needs to be applied differently. Cross et al. attempted to find features that were sensitive to damage but insensitive to temperature variations in [89]; PCA was applied to the training data first, and then the higher principal components that could explain the maximum variance were discarded, based on the assumption that temperature variations were accounting for most of the variance in the data. Therefore, the space that these minor components projected to could represent the feature space under the normal conditions, when damage happened, the projected minor components would deviate from the baseline space, which could be captured using a proper distance metric. The case study used in [89] was to detect damage through Lamb waves propagating within a composite plate. PCA was applied to 50 spectral lines to obtain 20 principal components. Only the 10 principal components, which only explained 0.005% of the variance, were used for constructing a new feature; the result is shown in Figure 2.5. There are three sections in the plot separated by two vertical lines; temperature is steady in the first section, and cyclic in the second, the last section introduces damage to the plate. The minor component projection is not influenced by the temperature variation in the second section, and damage indication is clear and efficient. Also in [89], the PCA method and a few other novelty detection methods were reviewed and compared with the cointegration method, which is the main theme of this thesis.

### Gaussian Processes

The Gaussian process (GP) is a Bayesian nonparametric model that can perform both regression and classification tasks. Due to its excellent performance in nonlinear regression, in the areas of machine learning and statistics, GP regression has been widely adopted for prediction, interpolation, optimisation and uncertainty quantifi-

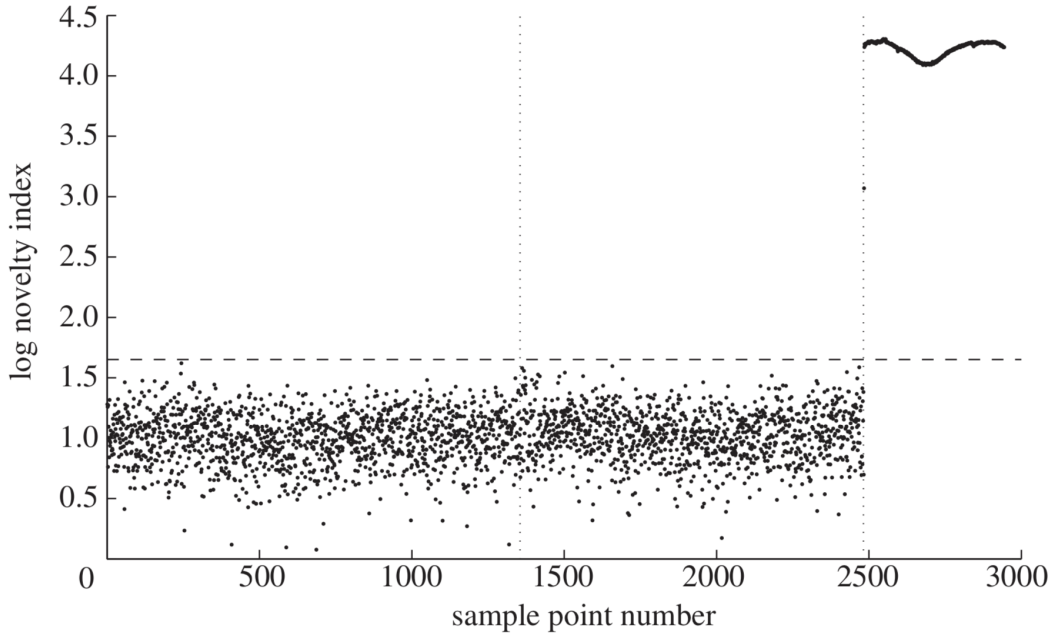


Figure 2.5: Results of damage detection using the minor components from PCA [89].

cation. More technical details will be reviewed in Section 5.2, where GP regression is hybridised with cointegration. However, for the sake of this literature review, some of the applications of GPs in SHM are reviewed first.

As mentioned above, GP regression is an excellent nonlinear regression framework; due to its Bayesian nature, it can produce a probabilistic prediction rather than a single value prediction, which is very advantageous for quantifying the uncertainty of model predictions. For example in Chapter 5.2 of [90], GP regression was employed to model the relationship between environmental variables (temperature, wind, traffic) and the natural frequencies of the Tamar Bridge. The changes in the natural frequencies were mostly caused by EOVs, which can be accurately modelled by a GP regression, the model error could then be used as a damage indicator. GP is normally characterised by its mean function and covariance function, most of which are functions of distances in the input domain; as such, most of the GP are actually stationary processes. When dealing with nonstationary processes however, one good idea is to combine the idea of Classification and Regression Trees (CART) with the GP. Gramacy and Lee [91] have established the method of Treed Gaussian Process (TGP); the idea is to partition the input domain into different regimes (leaves) using a Bayesian CART algorithm, and the specifications of GP are different in each

regime. The TGP model has been adopted to the Tamar Bridge and the Z24 Bridge in [92], where the switching behaviour of the interested structure were modelled. The GP can also be extended to the heteroscedastic context (the variance of the noise is time dependent); see for example [93].

#### Kernel Methods

Kernel-based methods, often based on support vector machines (SVMs), have been widely used for classification and regression especially in the context of supervised learning, applications in SHM can be seen in [94] and [95]. However in the context of EOVs, unsupervised learning methods are more favourable as labelled damage data are normally not easy to obtain. To review unsupervised kernel-based methods in SHM, it suffices to refer to a recent article by Santos et al. [96], where four kinds of unsupervised kernel methods were used for damage detection under changing environmental and operational variations. The four methods were: the one-class SVM, support vector data description (SVDD), kernel principal component analysis (KPCA) and greedy kernel principal component analysis (GKPCA). These four algorithms are all concerned with projecting the original data into a higher-dimensional space, and the SVDD and SVM manipulate data in this high-dimensional space, whereas the KPCA and GKPCA map the high-dimensional features back into the original space for damage detection.

## 2.3 Time Series Methods

Naturally, sensor data can be treated as time series, as they are often acquired and recorded in equidistant time intervals. Therefore, many of the mature time series modelling methods can be readily used in the context of SHM. The review presented here intends to gain some insights about how to understand the effect of EOVs from a time series perspective. However, under the umbrella of time series, there is a very broad range of methods, and many of them are overlapping with some of the machine learning methods just reviewed. Thus in this section, some of the popular time series models suitable for addressing EOV issues are reviewed.

### ARMA Models

The Autoregressive Moving Average (ARMA) model is perhaps the most classical stationary time series model in the time series field. Before finding the link between ARMA models and SHM, it is worthwhile to briefly review the form of an ARMA model. Consider a time series $x_t$, it can be referred to as an ARMA(p,q) model, if $x_t$ has the following form:

$$x_t = \sum_{i=1}^{p} \phi_i x_{t-i} + \sum_{j=1}^{q} \theta_j \epsilon_{t-j} + \epsilon_t + c \tag{2.1}$$

where $x_t$ is expressed as a sum of $p$ autoregressive terms $x_{t-i}$, $q$ moving average term $\epsilon_{t-j}$, a Gaussian noise term $\epsilon_t$ and a constant term $c$; $\phi_i$ and $\theta_j$ are the coefficients for the autoregressive terms and the moving average terms respectively. To determine the orders $p$ and $q$, one can either use the autocorrelation function and partial autocorrelation function or use the Akaike Information Criteria (AIC) [97]. ARMA model can parsimoniously capture the dynamical behaviour of a time series, therefore the coefficients of ARMA models have been widely used in SHM as features. For example in [43], Carden and Brownjohn trained an ARMA model with measurement data from the Malaysia-Singapore Second Link Bridge and the Z24 Bridge; the ARMA coefficients were used to train a damage classifier in an unsupervised manner. The method worked relatively well for the Singaporean bridge, but did not classify some of the damage in the Z24 Bridge case, probably because of the nonlinear behaviour of the latter bridge.

To improve the performance of the ARMA model, Chen and Yu [98] attempted to explicitly model the residual error with a Generalised Autoregressive conditional heteroscedasticity (GARCH) model. The idea of a GARCH model is straightforward; it assumes the conditional variance of a time series follows an ARMA process [99]. The ARMA-GARCH algorithm proposed worked as follows: first a baseline ARMA model was fitted to the measured acceleration time series; then if the residual series presented heteroscedasticity, then a GARCH model would be used for the residual series; the fitted GARCH model was then used to form damage sensitive features. An experimental study was then presented, which was a three-story building structure from the Los Alamos Laboratory (LANL); the ARMA-GARCH model could outperform the ARMA model in terms of damage sensitivity, and the new framework was also robust to the changes in the environmental and operational

conditions.

Sohn and Farrar proposed an unsupervised damage diagnosis method based on a AR-ARX (AR with exogenous input) model [100]. The experiments were conducted under different types of environmental and operational conditions; to normalise the data, they first started to build a "pool "of signals that contained various system responses under normal states but in different EOVs. In their proposed algorithms, an autoregressive (AR) model was first fitted to all the signals in the pool to form a so-called reference database. Once one received a new measurement signal, an AR model was fitted, then the closest AR model needed to be selected as a reference model, based on a difference metric. Then, a prediction model (a two-stage method combining an AR model and an ARX model) was developed, in an attempt to reconstruct the signal using the reference model. The prediction error between the original signal and the reconstructed signal was used as a damage-sensitive feature. The proposed method was validated on a multi-degree-of-freedom mass-spring system, the residual series could be used to detect the onset of damage, while immune to the changes caused by EOVs.

Another way of extending the ARMA model is to extend the univariate model into a multivariate context - that is the vector ARMA (VARMA) model or vector AR (VAR) model. One advantage of adopting vector variants of the ARMA model is that it can possibly incorporate the spatial information of the measured signals, implying that a VAR or VARMA model can potentially be used to localise damage. For instance, Bodeux and Golinval [101] used a VARMA model to fit to the vibration response from the Steel-Quake structure, and used the natural frequencies derived from the VARMA model for damage detection purposes. Mosavi et al. [102] proposed a damage detection and localisation algorithm in steel beams under ambient vibrations. The VAR model was fitted to the multiple time series of acceleration measurements, from a number of accelerometers deployed on the beam, so as to model the spatial information about the damage. The damage sensitive features were derived from the coefficient matrix in the VAR model, and the Mahalanobis distance was used as a distance metric for identifying outlier/damage from the data. They concluded that those sensors with the largest Mahalanobis distances were identified as closest sensors to the damage locations. Similar research work can be seen in [103], where a functionally-pooled VAR model was used to extract damage sensitive features.

More recently, Liu et al. [104] investigated the switching VAR model (SVAR) for

robust damage detection under various EOVs. The concept of SVAR is to combine a Markov-switching model with a VAR model. A Markov process refers to a process whose current observation is only dependent on the recent observations, it is of order 1 if it is only correlated to the last observation, of order $p$, if related to the past $p$ observation(s). A schematic representation of the SVAR model is shown in Figure 2.6, where the hidden state variable $s_t$ follows a first-order Markov process, the observation variable $x_t$ is an AR(2) process, which is dependent both on the hidden state variable $s_t$ and the previous two observations. The hidden state $s_t$ was designed to model the phenomenon of the regime-switching behaviour of some structures under the influence of EOVs, and within each regime, there lived a different AR model that could capture the dynamic behaviour of the interested structure in that regime. It is also worth pointing out that this SVAR model did not necessarily require the measurements of EOVs, however if the EOVs were available, it would greatly ease the estimation of the parameters. In the case where the EOV measurements were not available, the model parameters were learnt through a expectation maximisation (EM) algorithm, which is an iterative learning algorithm converging on the local maximum likelihood [105]. The proposed method was examined with a simulated time series and a laboratory experimental study.

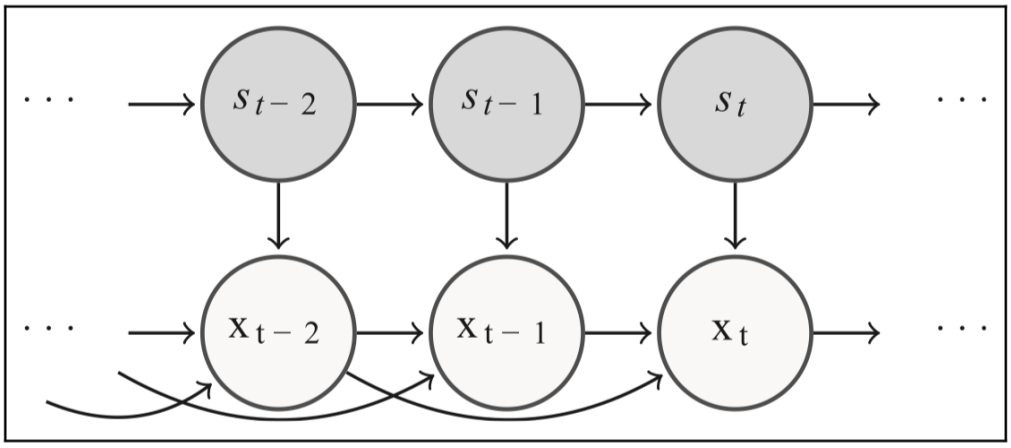


Figure 2.6: A graphical representation of the SVAR model, $s_t$ stands for the hidden state variable, $x_t$ represents the observation. [104].

### State Space Models

State space models subsume a large family of sequential models which are capable of unveiling the underlying dynamic evolution of the observing variables measured over time. Hidden Markov Models (HMMs) and Linear Dynamical Systems (LDSs) are the two most important state space models; they are both based on the same premise that noisy measurements can be made from a set of hidden state variables which evolve with Markovian dynamics, as depicted in Figure 2.7. $p(s_t|s_{t-1})$ is often termed as a transition probability distribution, and $p(x_t|s_t)$ is an emission distribution. When the hidden state variable is assumed to be a discrete variable, the model in Figure 2.7 is an HMM; if the state variable is continuous, it represents an LDS model. Specially, when the transition and emission distribution are assumed to be Gaussian, then it becomes the well-known Kalman filter. The filtering and smoothing of state space models are normally achieved using the backward-forward propagation algorithm and Rauch-Tung-Streibel smoothing algorithm [106], which are already well-studied in the literature. For an unifying review on inference algorithms of HMM and LDS, one can refer to [107]; for parameter learning algorithms, one can refer to [105]. For a thorough treatment of the state space model and its variants, one can refer to Part IV in [106].

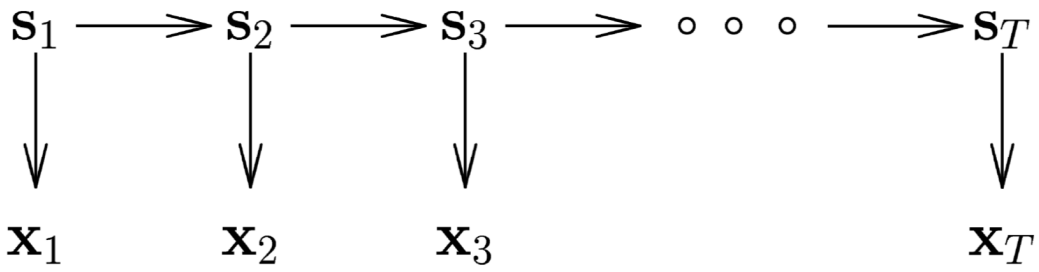


Figure 2.7: A diagram plot for a state space model. [107].

Ocak and Loparo developed a fault detection algorithm with HMMs using vibration signals from a bearing [108]. They first extracted features - coefficients of linear autoregressive function in this case - from vibration signals collected under normal conditions; then an HMM was trained to obtain the most probable sequence of states under normal conditions; the fault detection was accomplished by comparing the likelihood of a newly-observed signal with the trained baseline signal, if it stayed below a pre-determined threshold, then the bearing was undamaged, otherwise it was damaged. Miao and Makis [109] presented a similar study, where the

most probable HMM was also used to identify damage for rotating machinery, except that the damage-sensitive feature they used was based on the wavelet modulus maxima distribution derived from vibration signals. In a supervised learning manner, Lin and Makis recently investigated a condition-based maintenance policy and early fault detection algorithm, where a three-state HMM was employed to form a reference baseline model [110]. The three states consisted of healthy, warning and failure, which are trained with labelled vibration signals from a gearbox. The other contributions of the paper were to develop a residual life prediction algorithm and a Bayesian optimal decision making process.

Kalman filters, on the other hand, have been widely used for the task of system identification, based on which further damage detection algorithms can be developed. Yang et al. [111] used a nonlinear Kalman filter - an extended Kalman filter (EKF) - to adaptively track the change of system parameters, which were used for damage detection. The EKF framework was suitable for systems exhibiting abrupt changes in the parameters. Similarly in [112], the EKF was used to identify system parameters of a highway bridge which were changing because of the variations in temperature. The EKF method was used in conjunction with the neural network, for creating a baseline model which is capable of detecting damage.

If the state space model has nonlinear transition and emission functions, and its noise is also non-Gaussian, then the particle filter (PF) or sequential Monte Carlo (SMC) comes to the rescue. PF employs a generic mutation selection sampling method, using a series of particles (samples) to approximate the posterior distribution of a random process. One can refer to [113] for an overview on PF. In the context of SHM however, Chatzi and Smyth [114] have developed a PF with mutation (MPF) scheme to improve the sampling efficiency; the proposed MPF was examined with a nonlinear system identification case study, and the variations of the system parameters were accurately captured. Also in [115], Chen et al. combined Lamb waves with the particle filter, in order to predict crack growth.

### Mixture Models

Mixture models are models consisting of a mixture of components, each component can be represented by a certain parametric form. When these components are Gaussian distributions, then it is termed a Gaussian mixture model (GMM). Mixture models are generally good at modelling multi-modal data, and are suitable for

clustering and classification. Banerjee et al. [116] used a GMM as a damage classifier, based on features extracted from a newly-proposed discrete-time energy model. In terms of the damage detection under the effects of EOVs, Qiu et al. developed an online updating GMM algorithm to address this issue [117]. Their damage detection method was based on a piezoelectric transducer and Lamb waves. Features were first extracted from Lamb wave signals, and reduced to only two dimensions using PCA; a GMM was then fitted to the features under undamaged conditions in order to construct a baseline GMM. They also proposed an online updating algorithm for estimating a new GMM in real time. Lastly, damage quantification was performed by comparing the newly estimated GMMs with the baseline GMM, using two kinds of distance metrics - Mahalanobis distance and Kullback-Liebler divergence. The proposed framework was tested for damage quantification of edge crack growth in an aircraft wing spar, which was subjected to time-varying boundary conditions. Similar research can also be seen in [118].

## 2.4 Summary

The current chapter provides an overview of the important developments in the structural health monitoring literature, with an emphasis on the effect of environmental and operational variations. First, the main sources of EOVs are reviewed, and each source of EOV is also accompanied with examples in the research field. The next two sections are concerned with a literature review of data normalisation in SHM; it is intended to primarily focus on two big categories of methods, namely machine learning and time series methods, for the reason that the methods proposed later in this thesis can also largely fall into these two categories.

One can see a clear trend from the literature in SHM, that this research field is increasingly drawing attentions from engineering practitioners, SHM is quickly transferring from a laboratory technique to real-world commercial applications. Therefore, in this thesis, the author will not only focus on developing novel algorithms to address the effect of EOVs, but also will attempt to validate the applicability of the algorithms proposed on real engineering dataset.

From the articles listed above, it is probably safe to conclude that the research in SHM is rather interdisciplinary, and algorithms have to be carefully designed to specific problems. Admittedly, limited to the author's knowledge, the review

provided here is rather biased and can only touch some of the basics on these topics. Moreover, with the rapid developments in data science, sensing technology and cloud computing, research in SHM is almost certain to evolve with these emerging technologies, and more powerful and efficient algorithms will be seen in the field.

# Chapter 3

# The Z24 Bridge Benchmark

The Z24 Bridge is now a well-studied benchmark in the community of SHM, many research papers related to the Z24 Bridge have been published. This chapter will review some of the unique properties of this bridge which have attracted much research interest; also, some of the research articles are reviewed. As in the later chapters of this thesis, the Z24 Bridge will be used in case studies; thus the aim of this chapter is also to provide some references for comparison between the existing methodologies and the author's proposed methods.

## 3.1 Overview of SHM of the Z24 Bridge

The Z24 Bridge was built in 1963; it was designed to connect Koppigen and Utzenstorf in Switzerland, overpassing the A1 Bern-Zürich Motorway. The bridge structure was a classical post-tensioned concrete box-girder bridge, consisting of three spans (30m main span and two 14m side spans), as illustrated in Figure 3.1. The main piers were made of concrete diaphragms, which were clamped into the bridge girder. Both ends of the deck were extended in order to protect the anchor heads [119].

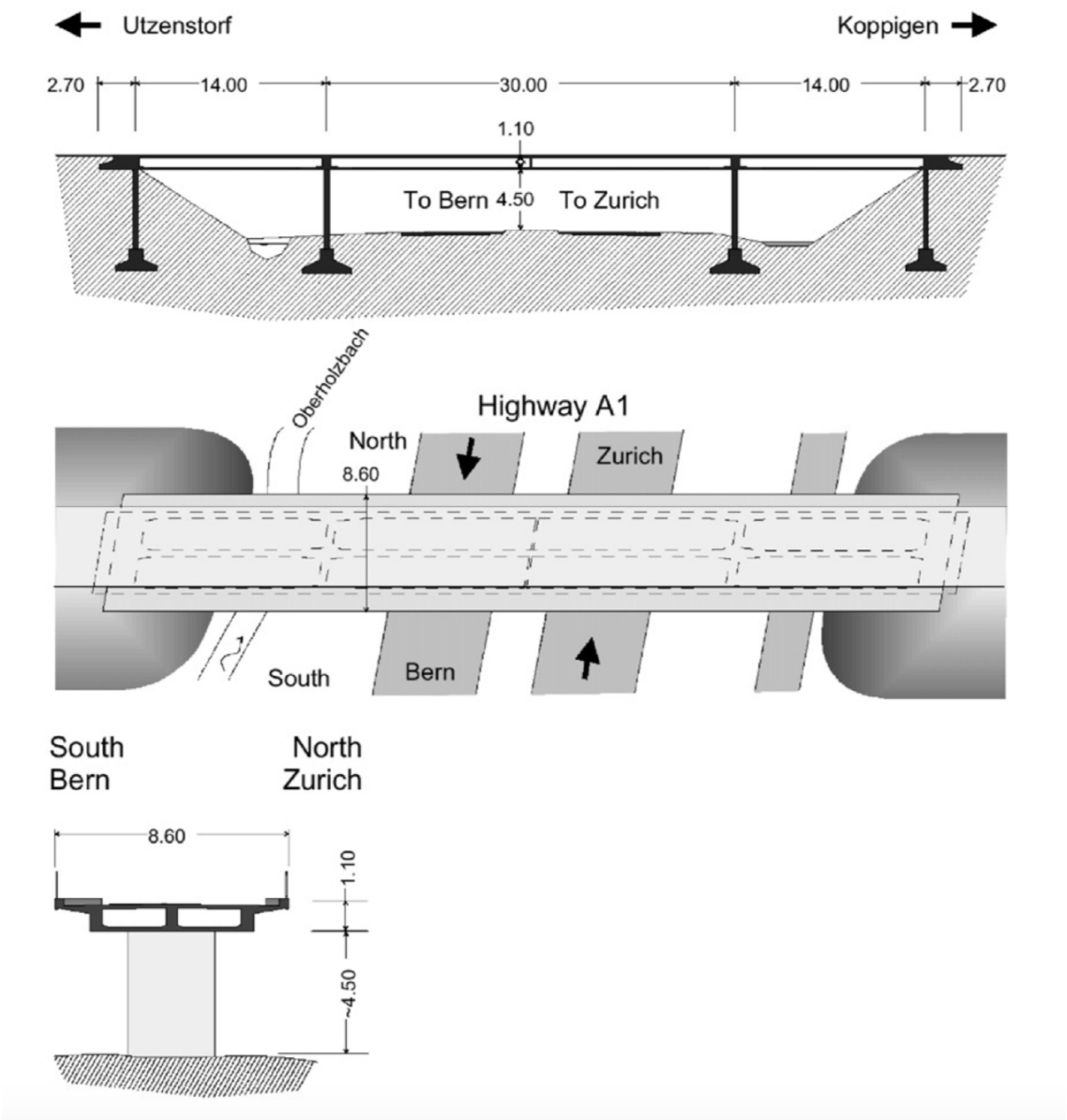


Figure 3.1: Front view, top view and cross-section of the Z24 Bridge [119].

### Test Setup

The bridge was scheduled to be demolished in the end of 1998 to allow the construction of a new railway track adjacent to the motorway, albeit in relative good conditions. The monitoring campaign continuously monitored the bridge for about one year, from $11^{th}$ November 1997 to $11^{th}$ September 1998. To identify its dynamical characteristics, the Z24 Bridge was heavily instrumented with both accelerometers

and environmental sensors (temperature, humidity, wind speed, wind direction). In order to accurately measure the mode shapes, nine setups of accelerometers were placed on the deck of the bridge, along three parallel lines, two sidelines and one central line, as shown in Figure 3.2.

In the later stage of the monitoring test, progressive damage scenarios were introduced to the bridge by the researchers. One can refer to Table 5.4 in Chapter 5. As damage detection is the priority task for the studies in this thesis, the first damage scenario is of particular interest, which was the settlement of the bridge pier. The pier settlement was conducted by gradually cutting the pier near the Koppigen side by 0.2m, 0.4m, 0.8m and 0.95m, and the pier was later restored. The lowering and lifting of the pier were done by six hydraulic jacks, as illustrated in Figure 3.3.

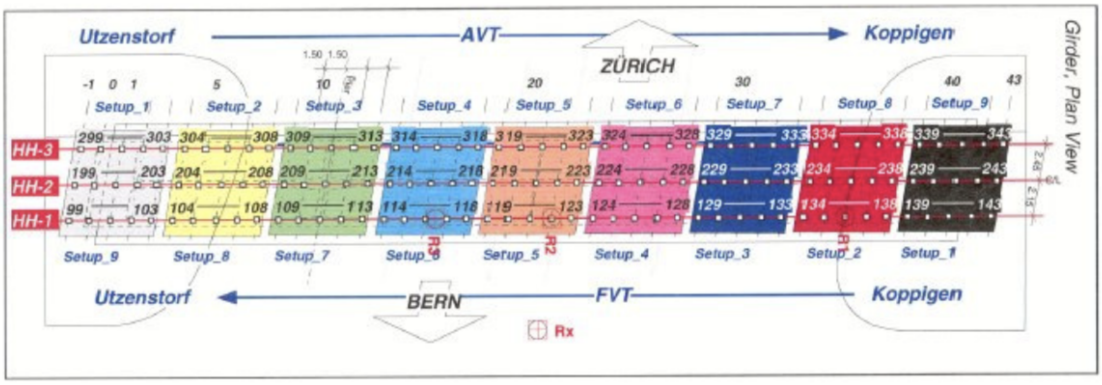


Figure 3.2: Measurement grid of the accelerometers placed on the bridge deck[119].

### System Identification

Dynamical properties of bridges are often deemed as damage sensitive features, as can be seen from the papers reviewed in the last chapter. Modal properties like natural frequencies, mode shapes and damping ratios have been identified for the Z24 Bridge for damage detection studies [58]. The stochastic subspace identification (SSI) was employed for system identification; the modal properties were identified from ambient vibrations, especially those coming from the traffic of the A1 motorway underneath the Z24 Bridge. To avoid repetition, the first four natural frequencies which were identified using SSI can be seen in Figure 5.6 in Chapter 5 and Figure **??** in Chapter 6. The identified mode shapes of the bridge are plotted in Figure 3.4, where the first is a bending mode, the second is a transverse mode, the third and

Figure 3.3: The hydraulic system used for settling the pier [119].

fourth are coupled torsion and bending modes.

### The Effect of EOVs

On observing Figure **??**, the time series of the first four natural frequencies are obviously nonstationary, especially when the temperature drops below freezing point, when the magnitude of natural frequency tends to increase significantly. Moreover, one can visualise the relationship between temperature and natural frequency, as in Figure 3.5; the natural frequency is a nonlinear function, or bilinear function to be precise, of the temperature, the natural frequency shows an obvious rise below 0 degree Celsius. According to Peeters and De Roeck [66], that may be explained the the stiffening of the asphalt layer of the bridge, causing the stiffness of the deck to increase. This example may showcase the effect of EOVS, temperature specifically in this case, can have a negative influence on the development of damage detection algorithms, the major challenge would be to distinguish the difference between a variation caused by EOVs and a change caused by real structural damage.

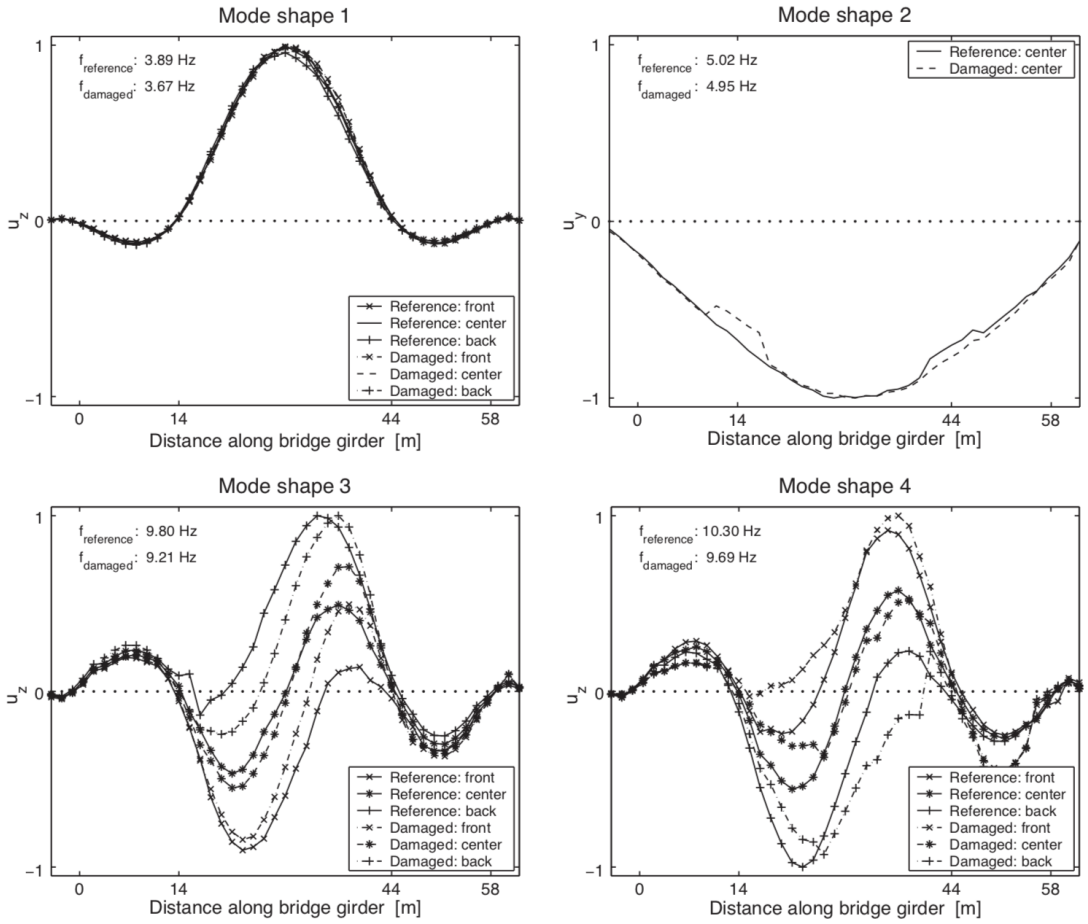


Figure 3.4: The identified modal frequencies and mode shapes of the Z24 Bridge before and after damage [120].

## 3.2 Damage Detection Algorithms

To overcome the issue of EOVs of the Z24 Bridge, many research articles have been produced in the SHM community. This section will review some of the recent damage algorithms developed for the Z24 Bridge benchmark.

Reviewed in the last chapter, the machine learning methods to tackle the issue of EOVs are mainly in two categories, supervised learning and unsupervised learning; likewise in the literature of the Z24 Bridge.

Temperature measurements are available in this benchmark study, thus most of the supervised learning methods applied are to find the regression relationship between dynamic properties and temperature. For example, Worden and Cross [92]

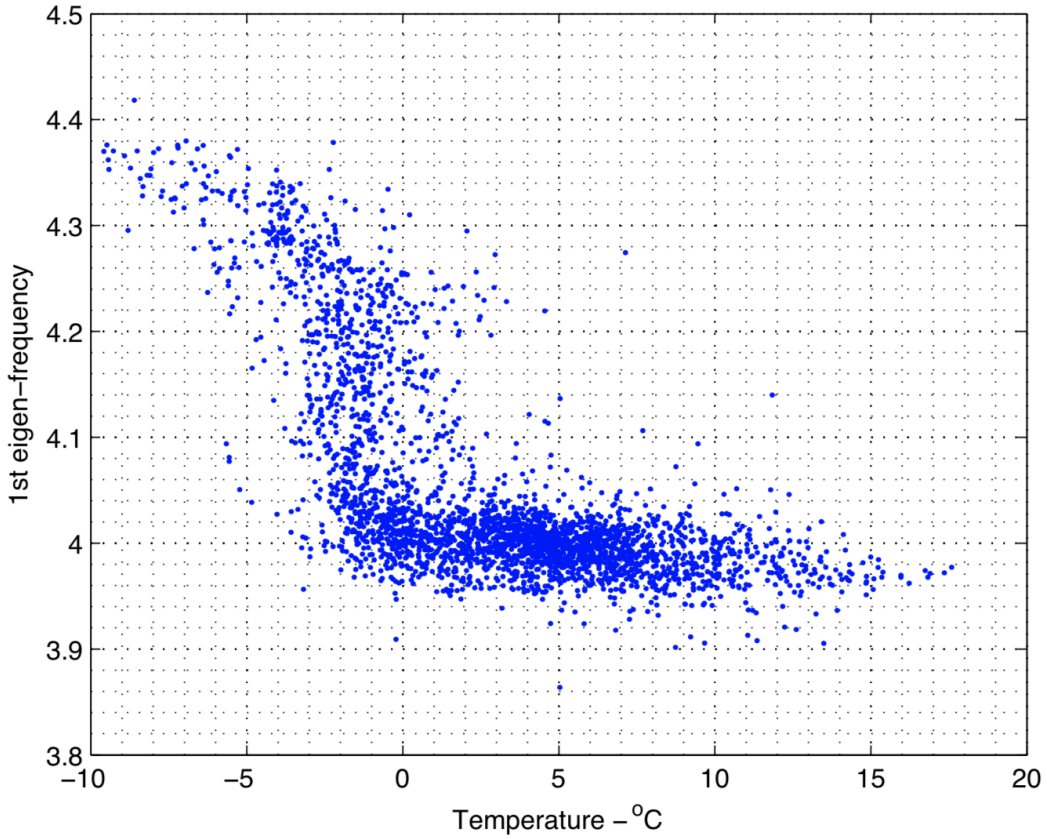


Figure 3.5: The bilinear relationship between the first natural frequency and temperature.

trained a Gaussian process regression and a Treed Gaussian process regression to the Z24 data (previously reviewed in Section 2.2). Baldacchino et al. [121] presented a variational Bayesian mixture of experts model for this nonlinear mapping problem. Mixture of experts (MoE) models can be expressed as the following: $y = \sum_{i=1}^{M} g_i(\mathbf{x}, \pi_i, \theta_i) f_i(\mathbf{x}, \mathbf{w}_i)$, where $\mathbf{x}$ represents the input vector and $y$ is the output target, temperature time series and the natural frequency time series respectively in this case; $g_i(\sim)$ and $f_i(\sim)$ are the $i^{th}$ gating function and expert function respectively; $M$ is the number of experts. The gating function used in the paper was a normalised Gaussian function, making the gating a Gaussian mixture model (GMM). The expert function was expressed as a linear input vector, although they could take on higher-order polynomial form. MoE models can partition the input domain into separate regions, where each region is represented by a different expert. To perform inference and model selection, Baldacchino et al. adopted a variational Bayesian expectation maximisation (VBEM) algorithm for maximum likelihood es-

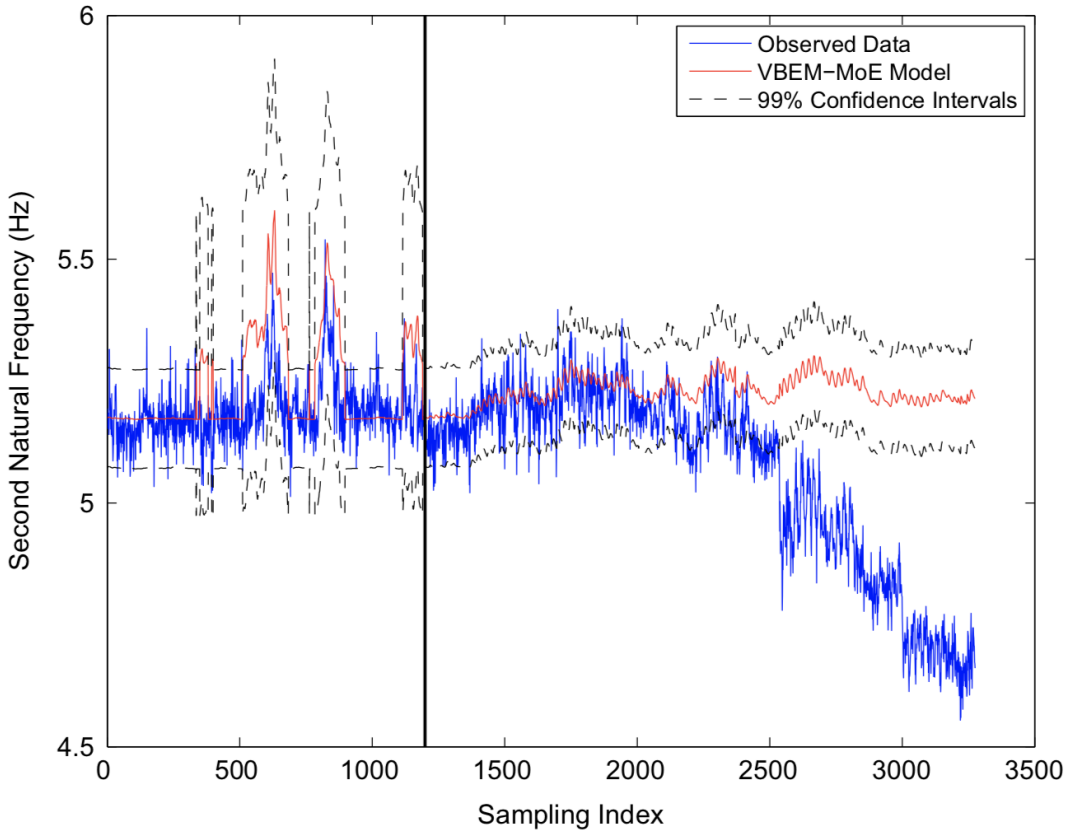


Figure 3.6: Red line is the second natural frequency of the Z24 Bridge; blue line is the prediction from the VBEM MoE model with three experts; the black lines are the 99% confidence intervals [121].

timates. As for the case study of the Z24 Bridge, a MoE model with three experts were employed, the input domain (temperature) was split into three regions, below 0.42°C, between 0.42°C and 13.4°C, and above 13.4°C. Interestingly, the TGP paper [92] and the work presented later in Chapter 6 have both introduced split points in temperature, TGP had two split points both near 3°C, whereas Chapter 6 splits at one point (0.98°C) or at two points (2.36°C and 3.95°C). The fitting and prediction performance of MoE model can be seen in Figure 3.6, where the blue line is the identified second natural frequency time series of the Z24 Bridge, the red line is the prediction from the VBEM MoE model with three experts, and the black lines represent the 99% confidence interval. The fit is reasonably good and the damage is detected where the blue line goes beyond the black line.

Spiridonakos and Chatzi [122] introduced a novel damage detection framework using the combination of a polynomial chaos expansion (PCE) and independent compo-

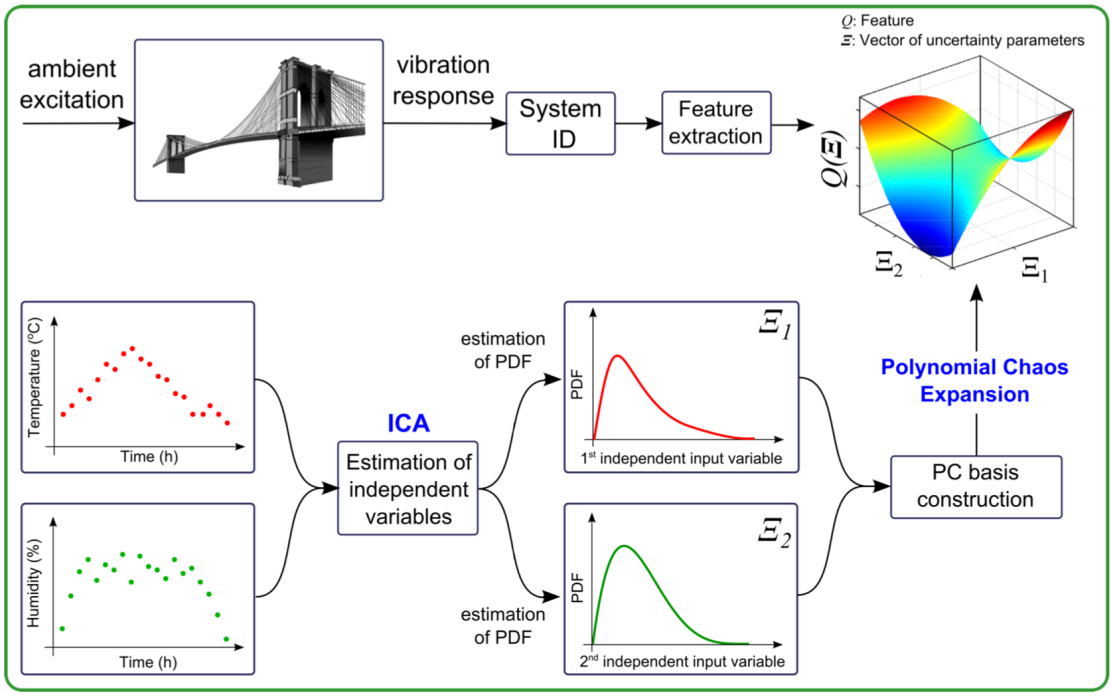


Figure 3.7: Schematic diagram of the proposed PCE method [122].

nent analysis (ICA). The key concept herein is to express the dynamic property variable, natural frequency in this case, as an expansion in polynomial chaos (PC) basis functions, which are orthogonal to the probability space spanned by the input variables, temperature in this case. The PCE can be expressed in the following form: $Y = S(\boldsymbol{\Xi}) = \sum_{d(j)} \theta_j \phi_{d(j)}(\boldsymbol{\Xi})$, where $\boldsymbol{\Xi}$ denotes the input random variable, different temperature sensor measurements herein; $Y$ denotes the output variable, the natural frequencies in this case; $\theta_j$ are the undetermined coefficients, $\phi_{d(j)}(\boldsymbol{\Xi})$ are the PC functions, which are orthogonal with respect to the probability distribution of the input variables $P(\boldsymbol{\Xi})$. The PC basis function was selected as the Legendre polynomial function, because it was associated with the uniform distribution which the input variables were transformed into. However before the PCE could be done, the ICA algorithm needed to be applied to the temperature measurements, which are highly correlated, in order to obtain the most informative and independent input variables. The full procedures of their proposed method are illustrated in Figure 3.7. As for the Z24 case study, they reconstructed the first four natural frequency time series using the PCE model; the fitting was quite good, the standard deviations of the expansion error ranged from 0.027Hz to 0.13Hz. For the second natural frequency series, one can see in Figure 3.8, the residual series maintains stationarity before damage, meaning the effect of EOVs have been effectively eliminated; when

damage is introduced (black vertical line), the residual series indicates a prompt abnormal trend.

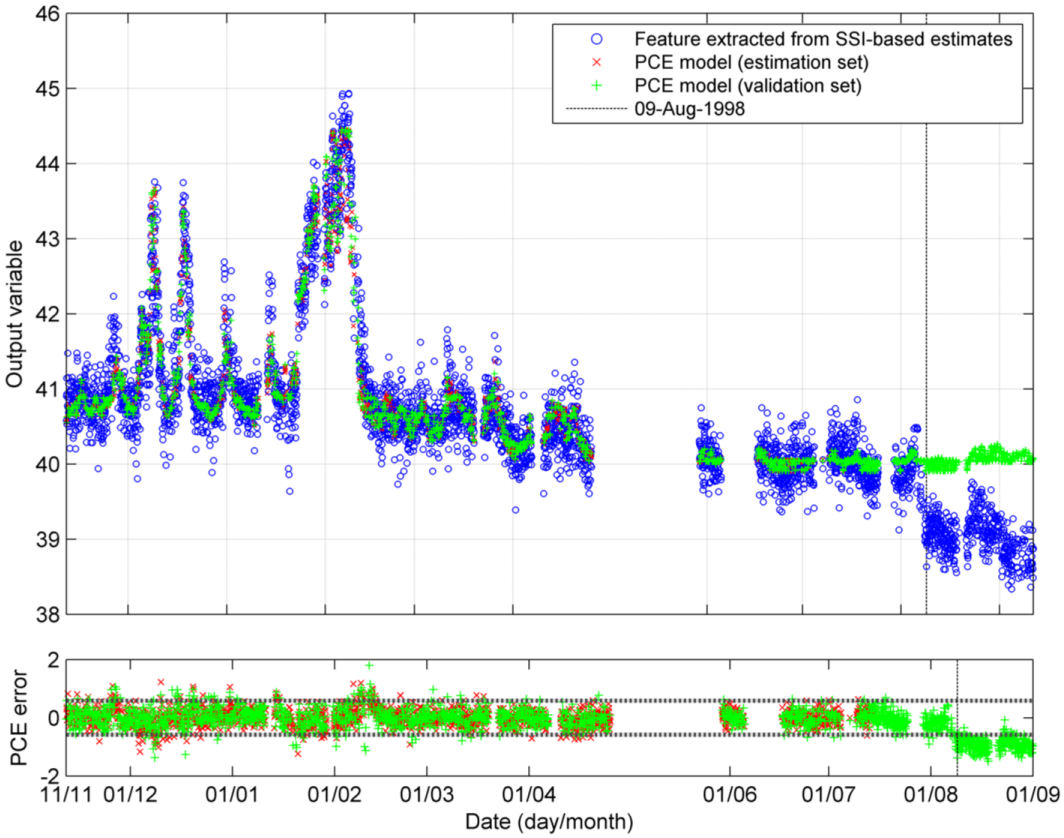


Figure 3.8: Upper plot: the estimated series using a PCE model (red and green) in comparison with the real series of the second natural frequency (blue) [122].

To gain insights into the meanings of outliers in the dataset, Dervilis et al. [123] proposed a robust analysis method to explore the EOV conditions in SHM data. The method used a combination of the least trimmed squares (LTS) regression and the minimum covariance determinant (MCD), which could ultimately distinguish the difference between leverage points and outliers, aiming to understand the effects from EOVs. The MCD method was designed to find the optimal subset of observations whose covariance matrix had the lowest possible determinant, such that the newly-obtained subset could be immune to the effect of outliers. The LTS estimator was used to classify the types of points: good or bad leverage points, or outliers. The results could be presented in a 2D map, as illustrated in Figure 3.9, where different regions represent different types of points; regions one and five are outliers, regions two and six are bad leverage points, region three is normal points, and region four is

good leverage points. Correspondingly in the plot of the LTS residual versus MCD index of the second natural frequency, most of the points fall into the third and fourth region; the green points however, represent those points in freezing temperatures, and are classified as outlier points in the first region, whereas the points caused by damage fall into the sixth region. This visualisation is obviously beneficial for further decision making, one can develop a more robust algorithm unaffected from the effect of EOVs.

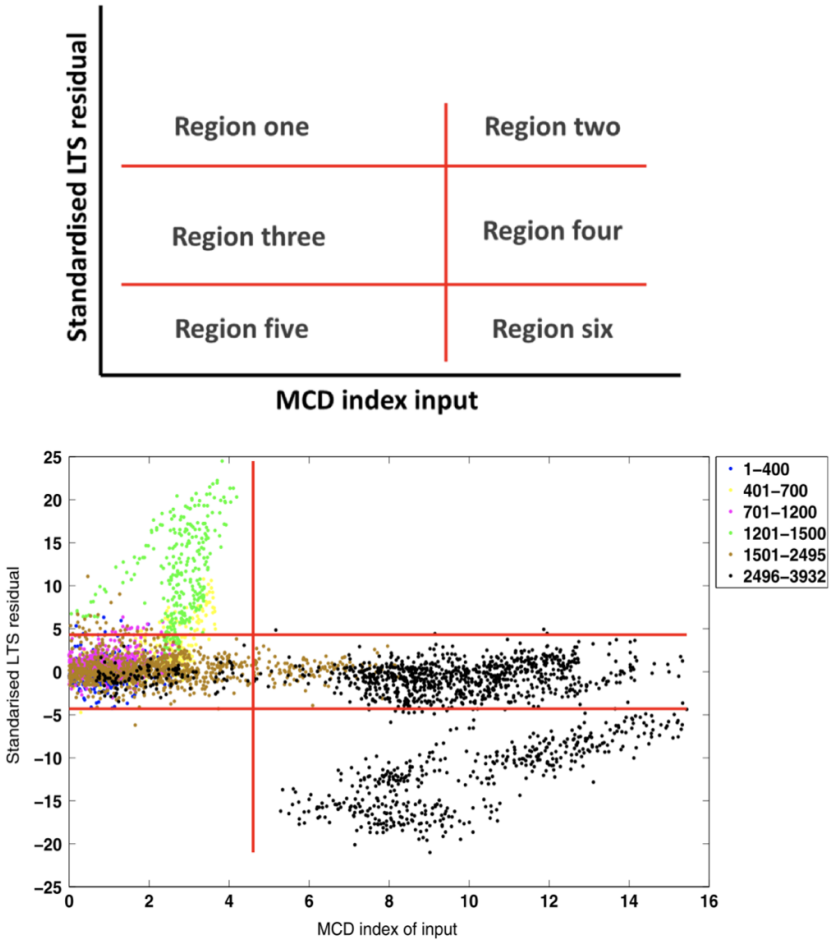


Figure 3.9: LTS residual outlier map (upper); LTS residual plotted against MCD for regression between temperature and the second natural frequency of the Z24 Bridge (lower) [123].

## 3.3 Summary

This chapter reviews SHM studies of the Z24 Bridge, which has been an unique benchmark in the research community. The monitoring practices and the progressive damage implementation are reviewed, the system identification studies further reveal that this bridge inherited a nonlinear effect from the environmental conditions. This chapter has also reviewed some of the latest efforts to model the behaviour of this bridge, which provides a reference for later chapters of this thesis.

# Chapter 4

# Cointegration Overview

*Cointegration* has emerged as an efficient modelling approach to deal with environmental and operational variations in structural health monitoring in recent studies [124][57]. This chapter will outline the key aspects of the cointegration theory, including the motivations for using cointegration in a engineering context, statistical tests for nonstationary time series, different frameworks to implement cointegration analysis and a literature review on cointegration methods in the domain of SHM.

## 4.1 Why Cointegration

As a routine method for dealing with nonstationary time series in econometric studies, cointegration is now widely used in statistical arbitrage, macroeconomic analysis, and fiscal policy research. However, what is the link between an econometric method and structural health monitoring? The answer is the existence of stochastic common trends.

Consider Figure 4.1 for example; the upper panel shows two normalised price indices (heating oil and crude oil in the US) during a certain time period; the lower panel exhibits two time series of two hanger displacements of the Tamar Bridge measured during a certain time history [75]. By visual inspection of these two images, two common characteristics can be observed immediately: each pair of time series is nonstationary; each pair shares some long-term common trend. These characteristics are not hard to understand, that economic time series are simultaneously affected

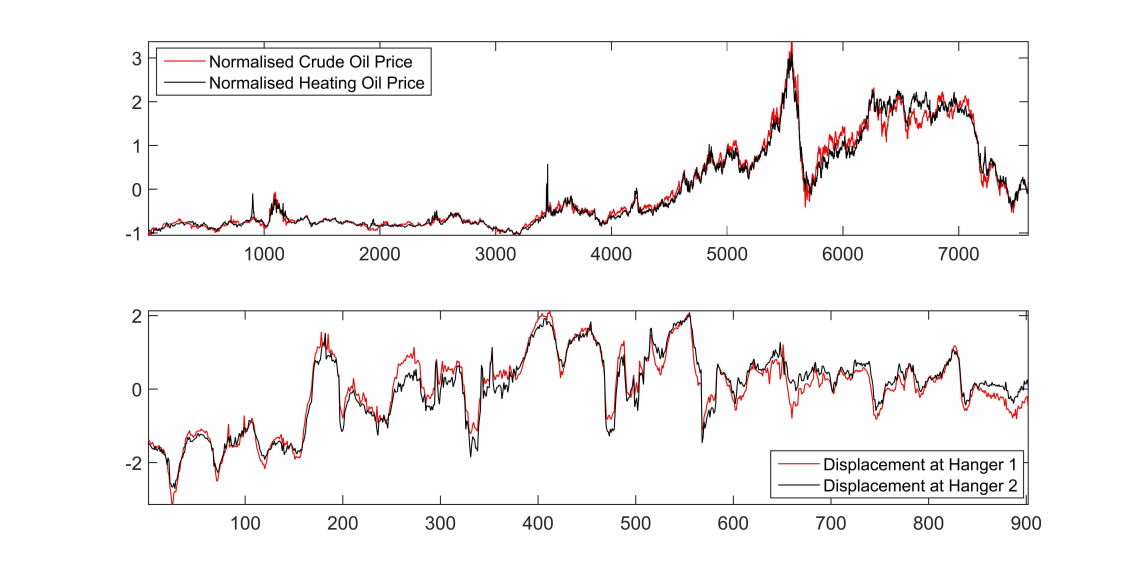


Figure 4.1: Upper panel: normalised price index of crude oil price and household heating oil price of US; Lower panel: normalised series of displacement measurements from the Tamar Bridge.

by markets, monetary policies etc., while the displacement of each bridge hanger is significantly influenced by temperature, traffic etc., or in the terminology of this thesis - Environmental and Operational Variations (EOVs). Nonstationary series are said to be *cointegrated* if there exists a linear combination of them that is stationary.

Denote the two time series in the upper panel of Figure 4.1 by $x_t$ and $y_t$ ; they can be found to be cointegrated if some linear combination of them:

$$\varepsilon_t = x_t + \alpha y_t \tag{4.1}$$

is stationary (confirmed by performing a stationarity hypothesis test, which will be reviewed shortly). The residual series for the oil price series and the displacement series are plotted in Figure 4.2, which shows that the residual series are purged of common trends and become largely stationary. Once the underlying equilibrium between the displacement series is built, the stationary residual series can serve as a damage indicator that is immune to EOVs. It is worth noting at this point that the cointegrated residual series of the oil series seems to behave differently before and after approximately point 5000. This interesting phenomenon can be seen as a regime change in the market, which will be elaborated more in the latter part of this thesis.

In conclusion, cointegration can be regarded as a data normalisation procedure [6]

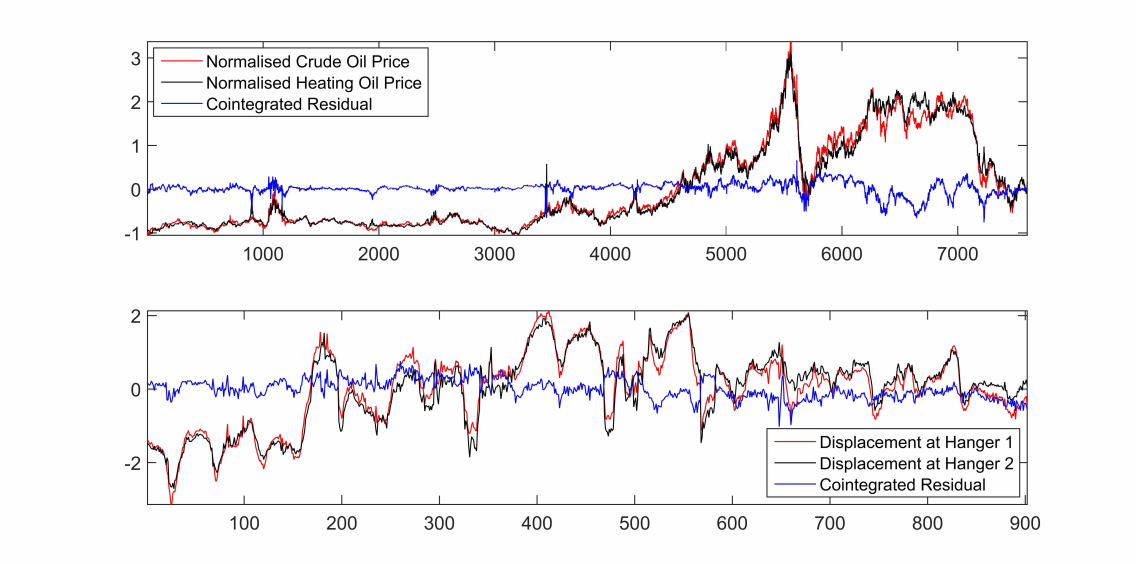


Figure 4.2: Cointegrated residual series plotted with normalised price index of crude oil price and household heating oil price of US.

for structural health monitoring, aiming to establish a normal or undamaged baseline feature for structures, based on which anomaly detection algorithms can be developed. Conventionally, regression-based methods are employed to deal with EOVs. Distinct from these methods, cointegration models the endogenous relationship of variables, instead of the correlating/causal relationships between systems and variables. This makes cointegration naturally advantageous, for the fact that the ground truths of exogenous variables are not always easy to obtain. Before reviewing the recent literature of cointegration in SHM, this chapter will first attempt to cover the basic theories and implementing procedures for cointegration.

## 4.2 Nonstationary Time Series and Unit Roots

### 4.2.1 Nonstationarity

A time series can be regarded as a stationary one if its statistical properties like the mean, variance and autocorrelation, etc. stay constant over time. In other words, a stationary time series can be treated as samples from the same probabilistic distribution. On the contrary, nonstationary time series are those time series whose statistical properties are time dependent.

Most of the classical time series modelling approaches, including ARMA modelling, spectral analysis etc., are based on the assumption of stationarity [97]. This assumption has a few advantages:

Firstly, stationary time series are relatively predictable, in the sense that their statistical properties will always revert to certain values, no matter what their current values are. Therefore, many time series modelling methods will convert a nonstationary time series into a stationary one using some kind of mathematical transformation, prior to further statistical analysis. The popular ARIMA model is one of these methods; one can stationarise a nonstationary time series via differencing (once or multiple times wherever necessary), then the conventional ARMA model can be fitted to the differenced stationary series.

Secondly, a time series can be well characterised by its sample mean, sample variance and other statistical variables if and only if this time series is stationary. It is easy to see that the sample statistics of a nonstationary time series are time varying, which implies no meaningful insights into its future behaviours. Therefore, one needs to be cautious when doing regression analysis with nonstationary variables. Because the estimates of the mean and variance of the nonstationary variables cannot be trusted, neither can their correlations, such that any statistical evidence suggesting linear relationships between independent nonstationary variables may be spurious.

### 4.2.2 Trend-Stationary VS Difference-Stationary Time Series

Most nonstationary time series have some kind of trend, either deterministic or stochastic. Two kinds of nonstationary time series models are popular in the econometrics literature, namely trend stationary and difference stationary time series. Next, this section will illustrate the difference between these two kinds of models, and why this is important to implement a statistical test to distinguish them.

#### Trend-Stationary Time Series

Consider a univariate time series $x_t, \{t = 1, 2, ...N\}$, which can be written as a stationary AR(1) model with a deterministic linear trend:

$$x_t = \theta x_{t-1} + \delta + \gamma t + \epsilon_t \tag{4.2}$$

where $|\theta| < 1$, $x_0$ is the initial value for $x_t$, $\gamma t$ is the linear trend term, $\delta$ is a constant, and $\epsilon_t$ is *i.i.d.* Gaussian noise: $\epsilon_t \sim \mathcal{N}(0, \sigma^2)$. One can convert (2.2) into a moving average (MA) representation:

$$\begin{aligned} x_t &= \theta^N x_0 + (\theta^{N-1}\gamma + ... + \theta\gamma)t + \{\delta + (\theta\delta - \theta\gamma) + ... + [\theta^{N-1}\delta - (N-1)\theta^{N-1}\gamma]\} + \\ &\quad \epsilon_t + \theta\epsilon_{t-1} + ... + \theta^{N-1}\epsilon_1 \\ &= \theta^N x_0 + \mu t + \mu_0 + \epsilon_t + \theta\epsilon_{t-1} + ... + \theta^{N-1}\epsilon_1 \end{aligned} \tag{4.3}$$

where $\mu = \theta^{N-1}\gamma + ... + \theta\gamma$ is the coefficient of the linear trend term, $\mu_0 = \{\delta + (\theta\delta - \theta\gamma) + ... + [\theta^{N-1}\delta - (N-1)\theta^{N-1}\gamma]\}$ is a constant. Therefore, one can find the mean of $x_t$ is:

$$E(x_t) = \theta^N x_0 + \mu t + \mu_0 \tag{4.4}$$

given that $|\theta| < 1$, thus $E(x_t)$ will converge to $\mu t + \mu_0$ as $N$ approaches $+\infty$, which is a linear trend plus a constant term. As for the variance of $x_t$:

$$\begin{aligned} E[x_t - E(x_t)]^2 &= E[\epsilon_t + \theta\epsilon_{t-1} + ... + \theta^{N-1}\epsilon_1]^2 \\ &= \sigma^2 + \theta^2\sigma^2 + \theta^4\sigma^2 + ... + \theta^{2N-2}\sigma^2 \\ &= \frac{\sigma^2}{1-\theta^2} \end{aligned} \tag{4.5}$$

which does not vary with time. $x_t$ is obviously nonstationary as its mean grows with time, however apart from the linear trend term, the remaining components are stationary, therefore series like $x_t$ are called *trend-stationary time series (processes)*.

The most important property of trend-stationary time series is *mean reverting*. As can be seen from the derivation of the mean in (4.3) and (4.4), the stochastic component of its mean is stationary, which means that any short-term deviations from the mean will gradually converge to its expected mean. Naturally, in practice, one would normally de-trend a trend-stationary process *a priori*, with time series decomposition or mathematical transformation techniques, before conducting any subsequent analysis.

**Difference-Stationary Time Series**

Consider a univariate time series $x_t, \{t = 1, 2, ...N\}$, which has the following AR(1) form:

$$\begin{aligned} x_t &= x_{t-1} + \delta + \epsilon_t \quad or \\ \Delta x_t &= \delta + \epsilon_t \end{aligned} \tag{4.6}$$

where $x_0$ is the initial value for $x_t$, $\delta$ is a constant, $\epsilon_t$ is *i.i.d.* Gaussian noise: $\epsilon_t \sim \mathcal{N}(0, \sigma^2)$, and $\Delta$ is a differencing operator such that $\Delta x_t = x_t - x_{t-1}$.

Note that $\Delta x_t$ is a stationary process, therefore $x_t$ is called a *difference-stationary time series (process)*, or a *unit root process*. If a series is nonstationary while its first difference is not, then it can be said to be *integrated of order 1*, or denoted as $I(1)$; if it requires $d$ times differencing to achieve stationarity, then the series is integrated of order $d$ or $I(d)$. In the context of SHM, it is not common to observe time series integrated of 2 or more, a detailed discussion on this can be found in [125]. Therefore, nonstationary series are treated as $I(1)$ processes in this thesis, if not explicitly stated otherwise.

One can re-formulate (4.6) in an MA representation as follows:

$$x_t = x_0 + N\delta + \epsilon_t + \epsilon_{t-1} + ... + \epsilon_1 \tag{4.7}$$

hence, the mean of $x_t$ is:

$$E(x_t) = x_0 + N\delta \tag{4.8}$$

and the variance of $x_t$ is:

$$\begin{aligned} E[x_t - E(x_t)]^2 &= E[(x_0 + N\delta + \epsilon_t + \epsilon_{t-1} + ... + \epsilon_1) - (x_0 + N\delta)]^2 \\ &= E(\epsilon_t + \epsilon_{t-1} + ... + \epsilon_1)^2 \\ &= N\sigma^2 \end{aligned} \tag{4.9}$$

As the mean and variance of $x_t$ both grow with time, $x_t$ is obviously nonstationary.

However, difference-stationary series are different from trend-stationary series in a few aspects: Firstly, one can notice in (4.8), the effect of the initial value stays in the mean, while the mean of trend-stationary series is not dependent on its initial value. Secondly, from the MA representations in (4.7), one can notice that the noise term $\epsilon_t$ has accumulated to a random walk process, which implies a stochastic trend is embedded in a unit root process, while for the trend-stationary process in (4.3), the effect of $\epsilon_t$ quickly decays as the time lag increases; Thirdly, the variance of a unit root process is increasing with time, but the variance of a trend-stationary process is time-invariant.

Because of all these differences, unit root processes are normally differenced, once or multiple times if necessary, to a stationary one, and then fitted with ARMA

models; these are the basic procedures of fitting an *ARIMA* (Autoregressive Integrated Moving Average) model. Also, because the trend in the unit root process is stochastic, this implies that de-trending a unit root process probably will not produce a stationary residual. Therefore, it is crucial to distinguish unit root processes from trend-stationary processes, before performing any subsequent procedures, detrending or differencing. However in practice, these two kinds of processes are not always easy to discriminate. The key to this question is through performing statistical tests for unit roots.

## 4.3 Statistical Tests for Unit Roots

As illustrated in the last section, unit root processes may explain a crucial share of all the nonstationarities observed in real time series. To test the presence of unit roots, econometricians have developed various statistical testing tools (a good survey of the ongoing research on unit roots can be found in [126] and [127]). The unit root test adopted in this thesis is perhaps the most commonly used, the Dickey-Fuller (DF) test. To illustrate how the DF test works, a natural starting point would be to impose a hypothesis test on the coefficient $\alpha$ of the simplest AR(1) model of the form:

$$x_t = \alpha x_{t-1} + \xi_t, \ (t = 1, 2, ...N) \tag{4.10}$$

where $\xi_t$ is a stationary process with zero mean and variance $\sigma^2$, $\alpha$ is a real number that determines the stationarity of $x_t$: if $|\alpha| < 1$, $x_t$ is stationary; if $|\alpha| > 1$, then $x_t$ is nonstationary, and its variance grows explosively with time; if $|\alpha| = 1$, then the variance of $x_t$ will be $t\sigma^2$, which will grow with time, such a process is a unit root process, or an $I(1)$ process.

Equation (4.10) can also be reformulated as:

$$\Delta x_t = (\alpha - 1)x_{t-1} + \xi_t = \pi x_{t-1} + \xi_t, \ (t = 1, 2, ...N) \tag{4.11}$$

where $\pi = \alpha - 1$. Based on this form, testing the null hypothesis $H_0 : \pi = 0$ is equivalent to testing the hypothesis $\alpha = 1$; the alternative hypothesis $H_1$ is $\pi < 0$. The test for the null is simply a $t$ test:

$$\hat{\tau} = \frac{\hat{\pi}}{se(\hat{\pi})} \tag{4.12}$$

where $\hat{\pi}$ is the least-squares estimate of $\pi$, and $se(\hat{\pi})$ is the standard error of $\hat{\pi}$. However, Dickey and Fuller investigated that under the null, the least-squares estimation $\hat{\pi}$ is not consistent with the true value, thus the usual $t$ test would be inappropriate for testing the null. They further investigated the asymptotic distribution of the $t-$statistic, and gave corrected tables based on Monte Carlo simulations [128][129].

One may notice that in (4.10) and (4.11), the disturbance term $\xi_t$ is a zero-mean stationary series, which is still a strong assumption for many cases. To allow potential serial correlation in the disturbance term, the augmented Dickey-Fuller (ADF) test was developed, which is based on the following form:

$$\Delta x_t = \pi x_{t-1} + \sum_{j=1}^{m} \gamma_j \Delta x_{t-j} + \varepsilon_t \tag{4.13}$$

where the $\gamma_j$ are the coefficients of the autoregressive terms, and $m$ is the lag number. In this regression, a sufficient number of lags should be included to achieve a white noise residual term $\varepsilon_t$; an information criteria is a common choice for determining the lag number. Clearly, the ADF test has greater robustness and flexibility than the DF test, thus it is most widely used in unit root testing [126].

Similarly to the previous, the null of the ADF test is $H_0 : \pi = 0$ with alternative: $H_1 : \pi < 0$. The $t-$statistic is the same form as in (4.12), critical values are given in [129]. The null hypothesis is rejected if $\hat{\tau}$ is smaller than the corresponding critical value, and accepted otherwise. The ADF test can also be easily extended by adding shift terms and/or trend terms:

$$\Delta x_t = \mu + \nu t + \pi x_{t-1} + \sum_{j=1}^{m} \gamma_j \Delta x_{t-j} + \varepsilon_t \tag{4.14}$$

where $\mu$ and $\nu t$ are the shift and trend terms respectively. Details of the model (4.14) and further extensions can be found in [126].

Having reviewed the fundamentals of unit root processes and their statistical tests, one can now ascertain the nonstationarity of a series through these procedures. In this thesis, the ADF test will not only be used to build cointegration models, but also the test statistic will be explored as a measure of the degree of stationarity, such that the best possible model form can be determined.

## 4.4 Cointegration

As illustrated in Section 4.1, cointegration is a powerful tool to understand nonstationary data: individual nonstationary time series might be difficult to predict, but a linear combination of them could be possibly predictable. To further explore and understand cointegration in mathematical context, two important cointegration estimation approaches will be reviewed and compared in this chapter, they will be the basic building blocks for the development of nonlinear cointegration approaches in the latter chapters.

### 4.4.1 Cointegration I: the Engle-Granger Approach

In fact, the example in (4.1) is a very special case for nonstationary time series. Assume the stationarity of $x_t$ and $y_t$ are in fact unknown, there are three possible scenarios: i) both are stationary, $I(0)$; ii) one of them is $I(1)$; iii) both of them are $I(1)$. For the first scenario, normal stationary modelling methods can be applied. For the second case, (4.1) will obviously result in a nonstationary $I(1)$ residual, no cointegration exists in this case. While for the last scenario, $x_t$ and $y_t$ are both $I(1)$ series, hence they both contain unit roots or stochastic trends, they can be expressed in the following form:

$$\begin{aligned} x_t &= (stochastic\ trend)_x + (stationary\ process)_x \\ y_t &= (stochastic\ trend)_y + (stationary\ process)_y \end{aligned} \tag{4.15}$$

In the more likely case, the *stochastic trend* terms in $x_t$ and $y_t$ are completely unrelated, $x_t + \alpha y_t$ will still produce a nonstationary residual; if and only if the stochastic trends are identical up to a scaling factor $\alpha$, i.e. $x_t$ and $y_t$ have a common trend, $(stochastic\ trend)_x + \alpha(stochastic\ trend_y)$ can then cancel out, such that a stationary residual $\varepsilon_t = x_t + \alpha y_t$ can be obtained. $x_t$ and $y_t$ are said to be cointegrated, and $(1, \alpha)'$ is called a cointegrating vector, where $'$ denotes the transpose of a vector.

Now the problem is to test and estimate the cointegrating vector. In their seminal paper [130], Engle and Granger proposed a simple framework for estimating and testing this long-run equilibrium relationship (cointegration), which consists of four steps:

1. As cointegration requires that all the variables involved are integrated to the same order, it is necessary to ascertain the order of integration of each variable. The ADF test examined in Section 4.3 can be applied here; there are three possible outcomes: i) the variables $x_t$ and $y_t$ are both $I(0)$, then the conventional regression methods can be used. ii) $x_t$ and $y_t$ are integrated to different orders, then one can conclude that there is no cointegration relationship between them. iii) both variables are integrated to the same order (usually $I(1)$ in SHM data), one can proceed to the second step.

2. Run a cointegrating regression $y_t = \alpha + \beta x_t + e_t$, using ordinary least squares (OLS) methods. One important note here is that because $x_t$ and $y_t$ are nonstationary, standard $t$ tests cannot be applied for inference. If $x_t$ and $y_t$ are proved to be not cointegrated in the subsequent analysis, then this regression is called a spurious regression; however, if $x_t$ and $y_t$ are cointegrated, then OLS can produce an unbiased and 'super-consistent'estimator $\hat{\beta}$ for the cointegrating coefficient $\beta$, which essentially means that the variance of the estimator $\hat{\beta}$ will reduce very rapidly as data sample size increases. The asymptotic properties of the estimator are beyond the scope of this thesis, interested readers can find a formal introduction and proof from [130] or [126].

3. From the second step, one can obtain an estimated residual series, denoted as $\hat{e}_t$. To check whether $x_t$ and $y_t$ are in fact cointegrated, one needs to determine the order of integration of the residual $\hat{e}_t$, with the ADF test for example. If $\hat{e}_t$ is found to be stationary, then $x_t$ and $y_t$ are cointegrated.

4. If there exists a cointegration relationship between variables, one can further establish an Error Correction Model (ECM) between $x_t$ and $y_t$, utilising the estimated $\hat{e}_t$ from step 3. The ECM has the following form:

$$\Delta y_t = \phi_0 + \sum_{j=1}^{p} \phi_j \Delta y_{t-j} + \sum_{k=0}^{q} \theta_k \Delta x_{t-k} + \alpha \hat{e}_{t-1} + \epsilon_t \tag{4.16}$$

where $\phi_0$ is a constant term, $\phi_j$ and $\theta_k$ are the coefficients of the lagged differenced terms, and $\alpha$ is the adjustment coefficient. What ECM represents is that the long-term error $\hat{e}_{t-1}$, inherited from the last time step will have a impact on the current short-term dynamics, the speed of adjustment is characterised by $\alpha$. Intuitively, if $y_t$ deviates from its long-term equilibrium with $x_t$ (cointegration), the large error will force the following $y_t$ to quickly adjust to the "norm". Additionally, one can

observe that every term in the ECM is stationary, indicating that any conventional hypothesis testing methods, for example the $t-$test, are therefore appropriate. The derivation of ECM from the AR model is omitted in this chapter, as the vector-form ECM and its derivations will be shortly examined in the next section.

The four steps reviewed above are the basics of the Engle-Granger (EG) approach, it is also called Engle-Granger two-stage method sometimes, which treats the first three steps as the first stage, the fourth step as the second stage. The EG approach is simple in its forms and easy to interpret, and has been excessively popular in econometrical and financial applications. In the context of structural health monitoring, cointegration is used as a data normalisation method, thus the stationary residual from the third step is of most interest, which can be used as a system health indicator. The ECM from step 4 depicts the dynamics of the cointegrating system, it can be used as a powerful tool for on-line time series prediction, which, however, is not explored in the context of SHM in this thesis, and is deferred to the author's future work.

Despite all the merits mentioned above, the EG approach has a few important drawbacks:

1. The choice of regression model forms is rather arbitrary, i.e. the EG approach does not provide a guide for selecting regressing target or regressor(s), one has to arbitrarily choose one particular variable and place it on the left-hand side of the equation. One can imagine that this problem can get even more complicated when multiple variables are involved. Nevertheless, with the help of the information criteria, for example, this issue might be mitigated.

2. Another important problem comes from the fact that the EG approach does not tell us how many possible cointegration relationships exist between variables, especially when there are more than two variables.

3. Additionally, when conducting the OLS regression in Step 2, the EG approach assumes $e_t$ to be a stationary and uncorrelated residual. However, in the following step, this assumption can be defied if the unit root test is accepted under the null hypothesis, where $e_t$ is in fact nonstationary [131].

All these problems can be well resolved using a maximum-likelihood based method - the Johansen procedures - which will be reviewed in the next section.

### 4.4.2 Cointegration II: the Johansen Procedures

The Johansen procedure offers an efficient framework that not only estimates multiple cointegrating vectors at the same time, but also produces a test statistic for determining the number of cointegrating vectors. In the SHM context, it is more of interest to estimate the cointegrating vectors than to perform tests on the number of cointegrating vectors, because it is the most stationary combination that one looks for to eliminate the EOV-induced nonstationary components in the data. For the sake of simplicity, this section will only give details of the estimation part of the procedure, readers who are interested in the cointegration statistical test can find reviews and details from [132].

To perform the Johansen procedure, one starts from a vector autoregressive (VAR) model, which has the form:

$$\mathbf{X}_t = \Phi_1 \mathbf{X}_{t-1} + \Phi_2 \mathbf{X}_{t-2} + ... + \Phi_p \mathbf{X}_{t-p} + \mathbf{u}_t = \sum_{j=1}^{p} \Phi_j \mathbf{X}_{t-j} + \mathbf{u}_t \tag{4.17}$$

where $\mathbf{X}_t$ is a $m-$dimensional vector time series, $\Phi_j$ is a $m \times m$ coefficient matrix, $\mathbf{u_t}$ is a $m-$dimensional vector Gaussian noise series, and the autoregressive order $p$ can be determined via information criteria. From a VAR($p$), there will always exist a corresponding vector error correction (VEC) model (by substituting $\mathbf{X}_t = \mathbf{X}_{t-1} + \Delta\mathbf{X}_t, \mathbf{X}_{t-1} = \mathbf{X}_{t-2} + \Delta\mathbf{X}_{t-1}, ..., \mathbf{X}_{t-p} = \mathbf{X}_{t-p-1} + \Delta\mathbf{X}_{t-p}$ into (4.17) and a few rearrangements), which has the following expression:

$$\Delta\mathbf{X}_t = \Pi\mathbf{X}_{t-1} + \sum_{j=1}^{p-1} \Psi_j \Delta\mathbf{X}_{t-j} + \mathbf{u}_t = AB^T\mathbf{X}_{t-1} + \sum_{j=1}^{p-1} \Psi_j \Delta\mathbf{X}_{t-j} + \mathbf{u}_t \tag{4.18}$$

where $\Pi = -(I - \Phi_1 - ... - \Phi_p)$, $\Psi_j = -(\Phi_{j+1} + ...\Phi_p)$, and $\mathbf{u_t}$ is a $m-$dimensional vector Gaussian noise series, $\mathbf{u}_t \sim \mathcal{N}(\mathbf{0}, \Omega)$. $A$ and $B$ are two $m \times r$ matrices, where $r$ is the rank of the matrix $\Pi$. Matrix $B$ is the cointegration vector matrix to be found, consisting of $r$ cointegrating vectors. Matrix $A$ is the adjustment matrix. Expression (4.18) is also referred to as the *Granger representation theorem*, which explicitly depicts the dynamics between the long run equilibrium (cointegration) and short term adjustments. Because $\Delta\mathbf{X}_t$, $\Delta\mathbf{X}_{t-j}$ and $\mathbf{u}_t$ are stationary, in order to make both sides of (4.18) equivalent, $\Pi\mathbf{X}_{t-1}$ has to be stationary as well. When the matrix $\Pi$ is full rank, $r = m$, $\mathbf{X}_t$ will be a stationary vector series, which violates the

pre-assumption of nonstationarity; When $\Pi$ is zero rank, then $\Pi = 0$, which means $\mathbf{X}_t$ has no cointegration. Consequently, matrix $\Pi$ has to be rank deficient such that $0 < r < m$ [126].

To find $B$, Johansen proposed a maximum likelihood method. One can first break the VEC regression in (4.18) into the following three smaller regressions:

$$\Delta \mathbf{X}_t = \sum_{j=1}^{p-1} C_j \Delta \mathbf{X}_{t-j} + \mathbf{r}_{0t} \tag{4.19}$$

$$\mathbf{X}_{t-1} = \sum_{j=1}^{p-1} D_j \Delta \mathbf{X}_{t-j} + \mathbf{r}_{1t} \tag{4.20}$$

$$\mathbf{r}_{0t} = \Pi \mathbf{r}_{1t} + \mathbf{u}_t = AB^T \mathbf{r}_{1t} + \mathbf{u}_t \tag{4.21}$$

where $A$ and $B$ are equivalent to those in (4.18). Based on the regression in (4.21) and the assumption that $\mathbf{u}_t$ is *iid* Gaussian noise $\mathbf{u}_t \sim \mathcal{N}(\mathbf{0}, \Omega)$, one can have the logarithm likelihood function:

$$\ln L(A, B, \Omega \mid \mathbf{X}_t) = -\frac{mN}{2} \ln(2\pi) - \frac{N}{2} ln\,|\Omega| - \frac{1}{2} \sum_{t=1}^{N} \mathbf{u}_t^T \Omega^{-1} \mathbf{u}_t \tag{4.22}$$

$$= -\frac{mN}{2} \ln(2\pi) - \frac{N}{2} \ln|\Omega| - \frac{1}{2} \sum_{t=1}^{N} (\mathbf{r}_{0t} - AB^T \mathbf{r}_{1t})^T \Omega^{-1} (\mathbf{r}_{0t} - AB^T \mathbf{r}_{1t}) \tag{4.23}$$

where $N$ is the sample size.

The next step is to find the parameters that maximise the log likelihood function (4.22) and to estimate the residuals $\mathbf{r}_{0t}$ and $\mathbf{r}_{1t}$. However, the details of derivation are omitted here, one can find the theory and proofs behind it in [132].

Finally, the optimisation problem turns into solving the following characteristic equation:

$$\left|\lambda_i S_{11} - S_{11} S_{10}^{-1} S_{01}\right| = 0 \tag{4.24}$$

where $S_{hk} = \frac{1}{N} \sum_{t=1}^{N} \mathbf{r}_{ht} \cdot \mathbf{r}_{kt}, (h, k = 0, 1)$. Assuming that $(\lambda_1, \lambda_2, ...\lambda_r)$ are the $r$ eigenvalues of equation (4.24), and they are arranged in the order $\lambda_1 \geq \lambda_2 \geq ... \geq \lambda_r$, then the corresponding eigenvectors $\mathbf{v}_1, \mathbf{v}_2, ..., \mathbf{v}_r$ can form the estimate of the

cointegrating vector matrix as follows:

$$\hat{B} = (\mathbf{v}_1, \mathbf{v}_2, ..., \mathbf{v}_r) \tag{4.25}$$

As the first cointegrating vector $\mathbf{v}_1$ corresponds to the largest eigenvalue $\lambda_1$, so it is natural to select $\mathbf{v}_1$ as the "most stationary" cointegrating vector, so as to make the stationary residual series.

So far, the background theory of cointegration has been reviewed. Although it is far from thorough, it is sufficient for the method that will be proposed in the subsequent chapters, which will largely be built around the theories above. As they are already relatively mature methods in the field of econometrics, the implementation of the unit root test and the Johansen procedure is fully integrated in various software platforms, such as Matlab (Econometric Toolbox), R and Eviews.

## 4.5 A Review of Cointegration Method on SHM

Since its first introduction to the field of SHM in 2011 [124], the cointegration method has attracted an increasing amount of attention from SHM researchers. Most of the related research work has fallen into two categories: firstly, to broaden the width of the applications of cointegration, for example, it has been successfully used in vibration-based SHM, Lamb-wave-based damage detection, wind turbine condition monitoring and so on. On the other hand, some efforts have been invested in exploiting the depth of this approach, by combining cointegration with other analysis methods, like wavelets and the Empirical Mode Decomposition for example. The work of this thesis is mainly focused on the second aspect, which is to further develop and strengthen the algorithms in nonlinear and heteroscedastic contexts. As this work will be thoroughly examined in the following chapters, the published papers [133][134][135][136] of the author(s) will therefore not be reviewed in this section.

In [124], Cross et al. linked the cointegration method from econometrics with the environmental trends observed in numerous SHM contexts for the first time; they also laid out the general framework for applying cointegration in the SHM context, and the efficient Johansen procedures were employed to estimate cointegration relationship. A simple multi-degree-of-freedom mass-spring system affected by a decreasing

temperature trend was simulated, to illustrate that dynamical properties of systems could be heavily influenced by temperature, and this influence could be deceiving for damage detection. The cointegration method could help to build a stationary residual, that was insensitive to temperature variations but still sensitive to damage. The second case study, the DAMASCOS project, was an experimental study, which was to measure the propagation of Lamb waves inside a composite plate under a cyclic temperature field. The features extracted from the Lamb wave signals were 50 spectral lines, which were essentially nonstationary, both in mean and covariance. Cointegration successfully established the normal condition indicator, a stationary residual, and efficiently detected the occurrence of damage when the residual series exceeded the confidence intervals. As an important development in addressing the EOVs in SHM, cointegration is proved to be simple in its forms, but powerful in its performance, it does not require measurements from the environment, which is vastly advantageous comparing with regression-based methods. The case studies employed in this paper, however, were either simulated or experimental, which were both highly deterministic environments. Besides, they also pointed out that training dataset needed to be carefully selected, such that a cointegration relationship could be accurately estimated, to avoid false positive indications.

In [125], Cross and Worden further validated the cointegration approach with a real world dataset, the displacement measurement data from the Tamar Bridge; they also re-examined the theoretical set-up for cointegration and discussed the general applicability of cointegration in the context of SHM. The dataset employed in this paper was the displacement measurements of the bridge hangers over two different time scales, a three-day period and a two-month period. Using cointegration, these displacement time series, obviously nonstationary in both cases, could be cointegrated to stationary residual series for both time scales. This proved that cointegration worked well as a data normalisation tool for real engineering data. They draw some analogies between econometric time series and SHM time series, that they may be regarded as a function of fluctuating external conditions, which are normally infeasible to quantify in both contexts. This was where the autoregressive (AR) model came into play; instead of modelling the external function, AR models reveal how the internal dynamics of time series evolves with time. The unit root process, which is based on the AR model, is used as a building block in cointegration modelling. They found that the increasing variance property of the unit root did not suit for most engineering variables, nonetheless, the unit root may well model the short-term behaviour of engineering variables, which were normally nonstationary. Therefore,

cointegration is naturally a good modelling framework to swiftly detect structural degradation over a short time period.

Studying the same benchmark dataset, from the DAMASCOS project, Cross et al. compared three different damage detection algorithms, namely outlier analysis, Principal Component Analysis (PCA) and cointegration, in [89]. Despite its popularity in SHM and condition monitoring, the outlier analysis method is not reliable to account for environmental variations. In this case study, the Mahalanobis distance was used as a measure for discordancy between sample points, but it had failed to classify environmental changes as normal conditions. PCA is normally used as a dimension reduction tool in many applications; however in this work, they took the opposite direction to extract the least principal or minor components from data, as an insensitive feature to environmental variations. They argue that the variance of the data mostly come from environmental variations, as the principal components can explain most of the variance, therefore discarding the principal components and keeping the minor components can be seen as a feature which is insensitive to environmental variations but sensitive to damage. They then compared cointegration with the PCA method, which are seemingly similar, both create a linear combination of the original variables. However, as the PCA algorithm finds principal components (or minor components in this case) by projecting the original variables onto orthogonal axes, which means that after the majority of the variance is explained by the principal components, it will become more restrictive to find orthogonal axes to find those minor components. Cointegration, on the contrary, is guaranteed to find the most stationary combination of the original variables, characterised by the cointegrating vectors using the Johansen procedures. In the their findings, cointegration was found to be superior than the other two methods, both in algorithm and performance.

Dao and Staszewski presented an interesting interaction between cointegration and wavelet/fractal signal processing [137]. The case study employed in this paper was the same benchmark dataset, the DAMASCOS project, as the previous two papers reviewed here. The signals they analysed were 20 Lamb wave responses propagated through a composite plate, subjected to different temperature and damage scenarios. Fractal signal processing was first used to understand the characteristics of the Lamb waves on different time scales, and the characteristics were quantified using logarithm variance at each time scale. Due to the influences of temperature, the characteristics from undamaged and damaged groups were not immediately separa-

ble. As these Lamb waves shared a common trend, they therefore applied cointegration before fractal signal processing. Taking a different direction, however, they utilised all of the cointegrating vectors estimated using the Johansen procedures (19 cointegrating vectors in this case), and performed fractal signal processing on all the cointegrated residuals, then estimated the log variance at each time scale. By applying these steps, the temperature effects were successfully eliminated, and the characteristics of damage could be observed easily. As is known that, cointegration is not unique in multivariate context, the method in this paper utilised all the possible cointegrating vectors to make full use of the Johansen procedures, a natural issue that may arise is the increase of computational cost, which gets even more intense when fractal signal processing is employed on every residual series. They also argued that after performing the ADF tests, the Lamb waves were found to be $I(0)$ series, thus they were integrated to the same order, which satisfies the condition of cointegration. According to the theory reviewed slightly earlier, cointegration is a property for nonstationary time series, i.e. cointegration only exists in series that are integrated to the order 1 or higher. $I(0)$ series, or stationary series, can be analysed using conventional time series modelling methods.

Worden et al. took steps even further by presenting an exploratory study into the connection between cointegration and multi-resolution analysis (MRA)/ wavelet [57]. In this paper, Worden et al. made an important argument that effects of environmental variations tended to manifest themselves on much longer time scales than those associated with the damage-sensitive signals, normally vibration-based signals. Based on this observation, MRA decomposition may therefore be applied to the raw signal first, such that components at different time scales could be extracted. Cointegration was used for all the components at the same time scale. As the damage information tended to manifest on the low-frequency/large-time-scale components, cointegration may therefore easily detect the changes in the structure. This provided the possibility of extracting the most nonstationary components from variables, and then constructing an enhanced cointegrating relationship. The idea was validated in two case studies, one simulated a multi-degree-of-freedom system and the DAMASCOS benchmark data, damage information was both visually evident, but different statistical process control tools are employed. The X-chart was used in the first case study in order to detect changes in the mean, while the S-bar chart was applied to expose changes in the variance. Despite the fact that the result in this study was very encouraging, the decomposed components from the MRA were mostly smooth. This may be contradicted a prerequisite of the Johansen procedure,

which requires the noise in the variables to be *iid*, and in this case the variables becomes "noise-free" after MRA decomposition. Therefore it required appropriate regularisation to the decomposed component, by adding a small amount of noise to them.

In the thread of multi-resolution analysis methods, [138] proposed to use the Empirical Mode Decomposition (EMD), a different MRA approach, to enhance the cointegration method. Antoniadou et al. chose the EMD method in an attempt to address some of the issues coming with the wavelet-based approach, for example the conditioning problem for the Johansen procedure, and also the selection of wavelet levels. This paper produced similar residual results with the previous research, the residuals had damage indication in variance changes at lower time scales, and mean shifts at higher time scales. The EMD decomposition addressed the issue of ill-conditioning, that it became unnecessary to add noise to decomposed signals before applying the Johansen procedures. However, the residual had unsatisfying early indications of damage. They suggested that this was caused by the off-line nature of the EMD method, that it processed data in batches, thus the EMD method needed to be further adapted to an on-line method to genuinely fix this issue.

Cross and Worden presented a study on a nonlinear cointegration approach in [139]. As cointegration is essentially a linear method, however in SHM, linearity is not always guaranteed. This paper started with two kinds of data generating processes, a deterministic linear trend model and a deterministic quadratic trend model. These two were apparently nonstationary, but the relationship between these two was nonlinear, therefore, cointegration was anticipated to be limited in this case. A nonlinear optimisation algorithm called Differential Evolution (DE) was utilised in this experiment to estimate the nonlinear relationship. The results turned out to be encouraging especially when a variance-based cost function is used in the DE algorithm, a stationary residual may be obtained. This article has pointed out a promising direction for nonlinear cointegration, that is to accurately model the nonlinear cointegrating relationship, which has led to some of the work in this thesis. Furthermore, the benchmark Z24 Bridge data was examined with a cointegration approach. They suggested a "locally linear" cointegration method, which basically captured the cointegration relationship only under $1°C$ where the bridge exhibited a distinct regime from others. The residual produced was largely stationary, but the damage information was unfortunately overwhelmed as well. This may be explained by the fact that using the cointegration relation under cold temperature to project

onto warm and even hot temperature regimes cannot accurately reflect the changes of cointegration in regimes. Inspired by this paper, part of the work in this thesis will attempt to model cointegration differently in different regimes, and use temperature as a instrumental variable to guide the regime shifts, which ultimately lead to an accurate damage alarm.

Focusing on the problems with the nonlinear cointegration method framed in [139], Zolna et al. proposed a modified nonlinear cointegration approach and also a statistical test method for the significance of heteroscedastic residuals [140]. A nonlinear cointegration would normally have the form such as $y_t = f(X_t) + \epsilon_t$, where $X_t$ can be either univariate or a multivariate vector. They find that the nonlinear function $f(\sim)$ can cause input-dependent or heteroscedastic noise in the residual term $\epsilon_t$. By employing a first-order Taylor expansion on $f(X_t)$, they derived the approximated form of the variance of the residual, which was correlated with $f(X_t)$. Therefore, based on the derivations, they proposed a modified residual term which has the following form: $(f(X_t) - y_t)/\sqrt{1 + [f(X_t)]^2}$, which may effectively cancel out some of the variance changes caused by the nonlinear manipulation on $X_t$. The next step was to impose a statistical test, named the Breusch-Pagan test, on the residual term, if the test was passed then there was no heteroscedasticity, if the test failed, then there existed heteroscedasticity. The proposed method was tested on three case studies: the first one was the synthetic dataset used in [139], the second being a simulation case mimicking the behaviour of the Z24 Bridge, which displays a piecewise linear relationship. This method managed to eliminate the heteroscedastic noise associated with the two datasets, and create accurate indication of damage. The third case study employed was from an operational wind turbine: the active power of the wind turbine was found to be nonlinearly related to the rotor speed, or bi-linearly to be more precise. The conventional cointegration method produced a residual series whose variance was greater when the turbine was at a transitional rotor speed. Using their proposed method, the residual series had significantly reduced its variances. However, this method did involve some assumptions that may limit its generalisation to broader applications. The Taylor expansion on $f(\sim)$ implied that this nonlinear function was a parametric function, which normally led to another problematic issue with parametric regressions, that was how to determine the form of the parametric model, whether it was quadratic or cubic, or even higher orders. They recommended to use a local regression algorithm, which fitted a linear regression model to each point using its neighbouring 12 points. This method may be good at nonlinear trend catching, but it may also be prone to outliers. This may

partly explain the variance increase in the last case study, where the rotor speed was at transitional phase and the outliers were significantly more than other phases.

To investigate how the selection of lags may affect the nonstationarity test, Dao et al. have reviewed some of the existing practices in the literature and proposed their own resolution to this issue in [141]. As reviewed in Section 4.3, the ADF test is a widely-used method for testing the existence of unit roots. One can observe from equation (4.14), the selection of the lag number $m$ can have a significant influence on the test itself, if $m$ is perfectly chosen, the residual term $\epsilon_t$ becomes a Gaussian white noise. The paper reviewed some of the model selection algorithms, which largely fall in two categories: information criteria based methods like the Akaike information criteria or the Schwarz-Bayesian criteria; and also likelihood ratio based methods, which finds the optimal lag by monotonically decreasing the lag number and comparing the likelihood ratios between two consecutive lag specifications. Based on these reviews, they proposed a exhaustive searching method to find the optimal lag number, which involved 4 main steps: 1. fix a range for possible lag number ranges; 2. form a cointegration for each of these possible lags and obtain their respective residuals; 3. Calculate the ADF statistics for each of these lag specification; 4. Find the optimal lag which corresponds to the most negative test statistics. Furthermore, they also used the ADF statistics as status indicators for damage detection purposes, such that once the system status deviated from its norm, the cointegrated residual was expected to become nonstationary, the ADF statistics would also change accordingly. The ideas were validated using several case studies, including Lamb wave data and vibroacoustic data. Some of the results had proved positive outcomes, yet some were not completely convincing at the moment. In summary, Dao et al. have pointed out a subtle yet crucial issue for the implementation of cointegration, and has developed a feasible approach for optimal lag selection in engineering context. One may also notice that apart from the lags, the ADF statistics are also dependent on the selection of sample data, which may render the proposed method restricted to an off-line approach. If the data are received in real time, even though there were occurrence of damage in the data, the power of ADF statistics may not be low enough to alarm damage in time.

There is other literature published attempting to use cointegration as a data normalisation tool. Liu et al. [142] combined the cointegration approach with a statistical control chart called the multivariate exponentially weighted moving average control chart, such that an adaptive confidence interval may be built with it. They also

proposed that by repeatedly dropping out one sensor data and re-evaluating cointegration, one can potentially find the "damaged"sensor. In [143], Michalak et al. found cointegration useful when dealing with cyclo-stationary time series, which was commonly observed in damage detection of gearboxes. A cyclo-stationary signal, as the name suggests, was periodically stationary, its mean and covariance repeated itself in every $T$ time steps. Therefore, they firstly decomposed the original signal into $T$ sub-signals by extracting every point at each sub-cycle. The sub-signals were then used to build cointegration relationship, embedded damage information may be effectively detected from the residual series. Very interestingly, the cyclo-stationary signals described in this paper had many common features with the seasonal time series observed in the economical and financial literature; the method proposed was a fundamental form of the seasonal cointegration model, for example in [144]. It is really intriguing to see interactions between these two remotely-related research areas. Dao et al. has introduced a complete framework for the on-line condition monitoring of wind turbines using the cointegration method [145]. The method was consistent with the previous literature reviewed here, cointegration was used as an efficient on-line algorithm to detect damage in streaming SCADA data. Cointegration has also been applied in damage detection of a real aeronautical structure [146]. As the strain of the structure was measured through a fibre Bragg grating (FBG) sensor network, which was very sensitive to temperature variations, cointegration was used to remove the undesired stress variations caused by temperature. In the automatic defect detection process of composites, ultrasonic guided waves were normally acquired from sensors; a major challenge for processing such signals is the underlying cumulative trend. Fuentes et al. have employed the cointegration method to remove such long term trend, which was hugely beneficial for rapid damage detection [147]. Comanducci et al. have presented a paper reviewing and comparing several of the state-of-the-art vibration-based damage detection methods using multivariate statistical algorithms [148]. The methods they have reviewed included dynamic regression models, linear and local principal component analysis, the combination of dynamic multiple linear regressions and local principal component analysis, which was proposed by them and finally, the cointegration method. All these algorithms were evaluated and compared based on real monitoring vibration data collected from an arch bridge in Portugal. Some artificial damage was simulated, they also tweaked the original dataset to create some nonlinearity in it. According to the performance measures defined in the paper, all these algorithms were effective in removing environmental and operational variations in the data. An

interesting finding in the paper was that, comparing to the other methods, cointegration required much less training data, which may be advantageous especially in the beginning period of the monitoring process. A more recent review paper is presented by Worden et al. [149], they reviewed some of the latest developments in algorithms based on nonstationary time series analysis. Statistical control chart methods, cointegration and Bayesian mixture of experts models were reviewed with examples; they were proved to be efficient in removing benign environmental changes and detecting anomalies. They also brought forward two open issues in cointegration analysis, which were heteroscedasticity and nonlinearity, and this thesis will attempt to address these two issues.

## 4.6 Conclusions

This chapter has reviewed the basic theories of cointegration. The link between cointegration - an econometric method - and SHM is illustrated with examples; cointegration is naturally suitable for dealing with the environmental and operational variations often found in SHM data. The different kinds of nonstationarity, trend-stationary and unit root series, are examined. The statistical tests for the existence of a unit root is also reviewed with derivations; the most commonly adopted method is the ADF test, which is a fundamental element of cointegration analysis. The Engle-Granger method and the Johansen procedures are two theoretical frameworks for testing and estimating cointegration relationships, the derivations of these two methods are also given in detail. Finally, a comprehensive literature review of the cointegration method in SHM is presented in the last section.

# Chapter 5

# Gaussian Processes for Nonlinear Cointegration

As reviewed in the last chapter, the cointegration approach finds possible linear combination of nonstationary time series which makes the residual series stationary; thus cointegration is normally deemed as a linear modelling method. A natural question will arise, when the underlying relationship is in fact nonlinear, will the conventional cointegration modelling framework still suffice?

## 5.1 Nonlinear Cointegration

Although there has been a great deal of work aiming to tackle the problem within econometrics, it is fair to say that there is currently no general theory of nonlinear cointegration. It is probably helpful to briefly look into the econometric literature at this point, where a wealth of theories and methods have been developed. The book [150] covers much of the historical work carried out within the community of econometrics. However in general, there are three important questions to answer [151]:

1. What properties have changed or have not changed after performing nonlinear transformation on integrated series? For example in [152], Granger and Hallman finds that integrated series are generally not cointegrated with the nonlinear transformation of themselves; however, if the same transformation is applied to a pair of

cointegrated series, the transformed series may be still cointegrated. Another paper has also looked at the same question, but they focus on fractionally integrated series [153]. One of the interesting findings from the paper is that every integer power transformation of a nonstationary $I(d)$ series will result in a deterministic trend in mean and variance.

2. How to estimate the nonlinear transformation function? There are two campaigns on this question: parametric and nonparametric. Parametric transformations can be classified into several classes: integrable functions, asymptotic homogeneous functions, exponential functions and super exponential functions. As the parameter estimation is heavily dependent on the form of nonlinear transformations, thus the literature has been focused on deriving the asymptotic distribution of these nonlinear estimators; for example in [154], Park et al. developed convergence and asymptotic theory for integrable and homogeneous functions, and in [155], Chang et al explored the model that accommodates linear time trend and stationary regressors. As for nonparametric transformations, Karlsen et al developed a Markov chain method to approximate the asymptotic theory of a kernel regression estimator [156]; As the joint dependence of variables in nonparametric regression is a major issue that can induce bias in estimation, Wang and Phillips proposed a local time density argument to relax the condition [157]; based on this argument, Chen et al proposed a nonparametric $M$-estimator, and they also developed its corresponding consistency and asymptotic distribution.

3. How to test for the existence of a nonlinear cointegration relationship? Breitung proposed a rank test for nonlinear cointegration, which is based on the difference between the sequences of ranks; if the difference tends to converge then there exists cointegration, and no cointegration if otherwise [158]. In [159], Choi and Saikkonen developed a testing method for nonlinear cointegration of $I(1)$ variables, which is to divide the model residual into subsamples, and apply a unit root test on these subsamples. They proved that as the sample size approached infinity, the limiting distribution of the test statistics are independent from the form of the nonlinear transformations.

In the context of SHM, however, the need for a nonlinear theory made itself clear quite quickly after the introduction of the method. Many engineering systems have nonlinear relationships between the measured features of interest, the Z24 Bridge data discussed in this thesis is a classic example. There have been a few attempts to exploit the adoption of nonlinear cointegration in SHM, [139][90][140] tried to

approach the problem through methods like evolutionary optimisation and statistical tests. These methods, as reviewed in Section 4.5, all exhibit some pitfalls. This thesis will further pursue investigation of nonlinear cointegration, via machine learning methods, as in this chapter, and time series methods in later chapters.

A potentially straightforward approach to nonlinear cointegration, as discussed in [150] (and partially adopted in [139]), is to simply extend the second step of the Engle-Granger framework reviewed in Section 4.4.1, to a nonlinear regression, e.g.

$$y_t = f(x_t) + \epsilon_t \tag{5.1}$$

with $f(\sim)$, some regression function estimated in a parametric or nonparametric manner; $x_t$ can also easily be extended to multivariate context. Neural networks were suggested for the representation in [150], but any appropriate machine learning algorithm could be used in principle and this idea is where a proportion of the recent nonlinear cointegration literature has concentrated its attention. One recent paper uses least-squares support vector machines to good effect [160], and incorporated a Bayesian approach. Motivated by a desire to increase the Bayesian element in the nonlinear regression, the current chapter will adopt Gaussian Process (GP) Regression in order to learn the required relationship in equation (5.1) from data. This brings the immediate advantage of providing natural confidence intervals for the regression model. To illustrate the use of the GP regression cointegration model, this chapter will re-examine the data from the simulation case study from [139] and [140], the proposed method will also be examined with a new synthetic dataset and the well-known Z24 Bridge SHM benchmark exercise. Before proceeding to a discussion of the GP regression approach and then to the case study, the next section will provide some background theory on Gaussian process.

## 5.2 Gaussian Process Regression

Gaussian process regression is a Bayesian machine learning approach that can deal with nonlinear regression problems in such a way that confidence intervals for predictions are produced in a natural way. Generally speaking, a GP can be considered to be a distribution over functions, any finite samples from which are jointly Gaussian distributed [161]. Just as a Gaussian distribution can be fully specified by its mean and variance, analogously, a GP can be fully defined by its mean function $m(x)$

and covariance function $k(x, x')$. This means that for any given inputs, the corresponding outputs are normally distributed, which gives possibilities for predicting unknown observations. Next, the essential technical details of GP regression will be given in a Bayesian inference manner.

First, define some notations: assume observation data is $D = \{\mathbf{X}, \mathbf{y}\}$, where $\mathbf{X} = \{\mathbf{x}_1, \mathbf{x}_2, ..., \mathbf{x}_N\}$ is an $N \times d$ input variable matrix, $d$ is the dimension of $\mathbf{x}_i$, and $N$ is the number of observations, $\mathbf{y}$ is the output vector. Also, denote the random functions induced by input variables as $\mathbf{f} = \{f(\mathbf{x}_1), f(\mathbf{x}_2), ..., f(\mathbf{x}_N)\}$. Note that unlike traditional parametric regression method, $\mathbf{f}$ here is defined as a set of random variables indexed by continuous variables, instead of a fixed-form function. As such, the aim of Bayesian regression here is to determine the posterior distribution of $\mathbf{f}$ and to make predictions based on posteriors.

**Prior**

As a GP is a distribution over functions, therefore it is legitimate to assign a GP prior to $\mathbf{f}$, which takes the form:

$$\mathbf{f} \sim \mathcal{GP}(\mathbf{0}, K) \tag{5.2}$$

the mean function of GP is taken to be $\mathbf{0}$ here for notational convenience, although it is not necessary to do so. If one wishes, the mean function can incorporate one's domain knowledge, a deterministic trend for example [162][161]. The covariance matrix $K$ is an $N \times N$ matrix composed of the kernel functions or covariance functions, such that $[K]_{i,j} = k(\mathbf{x}_i, \mathbf{x}_j)$, where $\mathbf{x}_i$ and $\mathbf{x}_j$ are two vectors of the input variables. The *isotropic squared-exponential (SE)* kernel will be used in this context as a running example, which has the following form:

$$k(\mathbf{x}_i, \mathbf{x}_j) = \sigma_f^2 \exp(-\frac{1}{2}(\mathbf{x}_i - \mathbf{x}_j)^T l^{-2}(\mathbf{x}_i - \mathbf{x}_j)) + \sigma_n^2 \mathbf{I} \tag{5.3}$$

where $\sigma_f$, $l$ and $\sigma_n$ are the undetermined *hyperparameters* of GP. The covariance function is really the heart of GP, as it dictates various properties of the GP, and more details on the selection and estimation will be covered shortly. As any finite samples from a GP are jointly Gaussian distributed, thus $\mathbf{f}(\mathbf{X})$, with a finite length, follows a multivariate Gaussian distribution:

$$p(\mathbf{f}(\mathbf{X})) = p(\mathbf{f}|\mathbf{X}) = \mathcal{N}(\mathbf{0}, K(\mathbf{X}, \mathbf{X}')) \tag{5.4}$$

### Likelihood

The observation data can be viewed as realisations of the underlying Gaussian process; for input $\mathbf{X}$, $\mathbf{f}(\mathbf{X})$ are their corresponding realisations. Knowing that $\mathbf{y}$ is the noisy version of $\mathbf{f}(\mathbf{X})$, with an *iid* additive Gaussian noise $\mathcal{N}(0, \sigma_n^2\mathbf{I})$. The likelihood of $\mathbf{y}$ given $\mathbf{X}$ and $\mathbf{f}$ is:

$$p(\mathbf{y}|\mathbf{X}, \mathbf{f}) = \mathcal{N}(\mathbf{f}(\mathbf{X}), \sigma_n^2\mathbf{I}) \tag{5.5}$$

### Posterior

The posterior can now be readily computed according to the Bayes' rule [161]:

$$p(\mathbf{f}|\mathbf{y}, \mathbf{X}) = \frac{p(\mathbf{y}|\mathbf{X}, \mathbf{f})p(\mathbf{f}|\mathbf{X})}{p(\mathbf{y}|\mathbf{X})} = \frac{p(\mathbf{y}|\mathbf{X}, \mathbf{f})p(\mathbf{f}|\mathbf{X})}{\int p(\mathbf{y}|\mathbf{X}, \mathbf{f})p(\mathbf{f}|\mathbf{X})df} \tag{5.6}$$

the numerator is the product of the prior and likelihood, the denominator is the likelihood with $\mathbf{f}$ marginalised out. One can substitute (5.4) and (5.5) into the above equation, after a few manipulations, the posterior distribution reads:

$$p(\mathbf{f}|\mathbf{y}, \mathbf{X}) = \mathcal{N}(K(K + \sigma_n^2\mathbf{I}^{-1})\mathbf{y}, K - K(K + \sigma_n^2\mathbf{I})^{-1}K) \tag{5.7}$$

This gives the distribution of the underlying function evaluated at the given set of inputs $\mathbf{X}$ where noisy realisations $\mathbf{y}$ are observed. Furthermore, the bottom part of (5.6), called the *marginal likelihood* or *model evidence*, plays an important role in estimating the model hyperparameters, it has the following form:

$$p(\mathbf{y}|\mathbf{X}) = \mathcal{N}(\mathbf{0}, K + \sigma_n^2\mathbf{I}) \tag{5.8}$$

which is normally easier to calculate after logarithm transformations:

$$\log p(\mathbf{y}|\mathbf{X}) = -\frac{1}{2}\log|K + \sigma_n^2\mathbf{I}| - \frac{1}{2}\mathbf{y}^T(K + \sigma_n^2\mathbf{I})^{-1}\mathbf{y} - \frac{N}{2}\log 2\pi \tag{5.9}$$

### Prediction

Now all the essential elements for GP are on the table, one can perform predictions for any input data points. Denote a test input vector as $\mathbf{x}^*$, and its corresponding test output as $f^*$. The prior $\mathbf{f}$ can now be extended to the test set, as the GP prior is placed on the whole function, not just a few specific points. Therefore, the observation output and the test output are also jointly Gaussian distributed, which

can be written as:

$$\begin{bmatrix} \mathbf{y} \\ f^* \end{bmatrix} = \mathcal{N}\left(\mathbf{0}, \begin{bmatrix} K(\mathbf{X},\mathbf{X}) + \sigma_n^2\mathbf{I} & K(\mathbf{X},\mathbf{x}^*) \\ K(\mathbf{x}^*,\mathbf{X}) & K(\mathbf{x}^*,\mathbf{x}^*) \end{bmatrix}\right) \tag{5.10}$$

where $K(\mathbf{x}^*, \mathbf{X})$ denotes a covariance matrix evaluated at every pair of all the observation and test points, and similarly applies to $K(\mathbf{x}^*, \mathbf{x}^*), K(\mathbf{X}, \mathbf{x}^*)$. Using the standard results of the Gaussian conditioning property on equation (5.10), one can arrive at the crucial posterior predictive distribution for GP regression:

$$p(f^*|\mathbf{y}) = \mathcal{N}(m(\mathbf{x}^*), cov(\mathbf{x}^*)) \tag{5.11}$$

where

$$\begin{aligned} m(\mathbf{x}^*) &= K(\mathbf{x}^*,\mathbf{X})[K(\mathbf{X},\mathbf{X}) + \sigma_n^2\mathbf{I}]^{-1}\mathbf{y} \\ cov(\mathbf{x}^*) &= K(\mathbf{x}^*,\mathbf{x}^*) - [K(\mathbf{X},\mathbf{X}) + \sigma_n^2\mathbf{I}]^{-1}K(\mathbf{X},\mathbf{x}^*) \end{aligned} \tag{5.12}$$

Note that the computation process requires the inverse of $K(\mathbf{X}, \mathbf{X}) + \sigma_n^2\mathbf{I}$, which has $\mathcal{O}(N^3)$ computation complexity; this may be prohibitive for the application of GPs to large data sets, although one can resort to sparse versions of the GPs, see an overview of sparse GPs in [163].

**Learning**

To learn the hyperparameters embedded in the covariance function, one maximise the marginal likelihood (5.8) or the log marginal likelihood (5.9) with respect to the hyperparameters, which in this case, can be formed in a vector $\theta = (\sigma_n^2, \sigma_f^2, l)$. Taking the partial derivative of $\log p(\mathbf{y}|\mathbf{X})$ with respect to $\theta_j$, one has:

$$\frac{\partial}{\partial\theta_j}\log p(\mathbf{y}|\mathbf{X},\theta) = -\frac{1}{2}Tr[(K_\theta)^{-1} + \frac{\partial(K_\theta)}{\partial\theta_j}] + \frac{1}{2}\mathbf{y}^T(K + \sigma_n^2\mathbf{I})^{-1}\frac{\partial(K_\theta)}{\partial\theta_j}(K + \sigma_n^2\mathbf{I})^{-1}\mathbf{y} \tag{5.13}$$

where $K_\theta = (K + \sigma_n^2\mathbf{I})$. Generally speaking, the marginal likelihood function of the GP tends to be a non-convex function, meaning that it may have multiple local maxima, which normally leads to a numerical optimisation algorithm, gradient ascent for example. One method to mitigate this problem is to start from different initialisation points. But to fully integrate the uncertainty of hyperparameters in the GP, one can perform a full Bayesian inference on the hyperparameters. A prior can be assigned to the hyperparameters, which is $p(\theta)$, therefore the posterior of $\theta$ is $p(\theta|\mathbf{y}) \propto p(\theta)p(\mathbf{y}|\theta)$, where $p(\mathbf{y}|\theta)$ is given in (5.8). If one wishes to do prediction

now, the new predictive distribution will then take the following form:

$$p(\mathbf{f}^*|\mathbf{y}) = \int p(\mathbf{f}^*|\mathbf{y}, \theta)p(\theta|\mathbf{y})d\theta \tag{5.14}$$

Although this integral is likely to be non-analytical, one would normally resort to an approximation method like MCMC sampling method or variational inference [161].

**Model Selection**

The SE kernel function is used to demonstrate how the GP works, but the choices for kernel function is far more than the SE kernel, the Matérn class kernels, the neural network kernels, the rational quadratic kernels, to name a few. One can even create new kernels from existing kernels by summation or multiplication, as long as they are symmetric positive semi-definite functions. The selection of a kernel is normally empirical, dependent on the prior knowledge of the time series to be modelled, whether it is stationary or nonstationary, does it contain a deterministic trend, or are there any underlying periodic patterns, etc. Recent work on automatic pattern discovery with kernel functions has been promising to address this issue, interested readers are encouraged to refer to an intriguing work by Wilson and Adams [164], where they constructed a kernel that is the Fourier transform of a Gaussian mixture, named a *spectral mixture* kernel, which has good performance in pattern discovery and extrapolation.

**Summary**

To summarise, this section has reviewed most of the key elements for performing a GP regression, detailing all the procedures involving training and learning a GP model. The GP regression is a nice and elegant framework, where one has great flexibility to create and modify model forms according to their demands. The GP also deep connections with many classical models, Bayesian linear regression models for instance, GPs can also be regarded as an infinite number of basis functions [161].

## 5.3 GP Regression as A Nonlinear Cointegration Function

Gaussian process regression is used in this thesis to estimate the nonlinear cointegrating function $f(\sim)$ as in (5.1). To estimate and test the nonlinear cointegration relationship, a sequence of steps should be followed.

1. Select suitable monitored variables for the model and calculate the order of the variables, which should be integrated to the same order. The ADF test is implemented on the variables to determine the integration order.

2. Separate the data sets into two parts: a training and test data set. Training data are used to train the GP regression model; the test data set is employed for the aim of monitoring potential system variation. The training data should not contain any data corresponding to damage, but should as far as possible span the range of EOVs anticipated.

3. Use the training data to train the GP regression model, then apply the ADF test again to testify whether the model residual series is integrated to a lower order than the original variables. Once this goal is achieved, one can say that the nonlinear cointegrating relationship is established successfully, the common trends are purged; therefore, the model residual series may be a potentially good indicator of damage-induced variations.

4. As the nonlinear cointegrating regression may have multiple model forms, the last step is to investigate all possible model forms, evaluate and select the best form as the final result. In order to measure the "goodness"of a model, one can use model fitness metrics, or information criteria, or test statistics to quantify the performance of different models.

## 5.4 Case Studies

In this section, the proposed method will be examined with two case studies, one synthetic case study originated in [139], the second one is a well-known benchmark study in SHM - the Z24 Bridge.

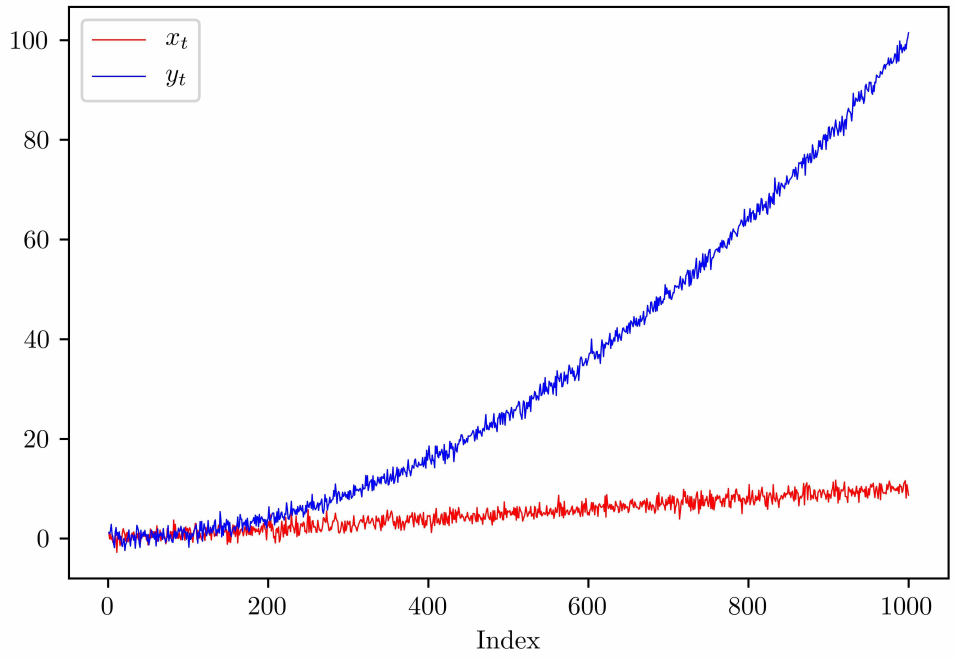


Figure 5.1: Simulated samples of $x_t$ and $y_t$ from equation (5.15).

### 5.4.1 Case Study I: Linear Trend-Stationary Series Versus Quadratic Trend-Stationary Series

It is not uncommon to see situations where damage-sensitive features are in fact nonlinearly related to some kind of external disturbances, therefore it becomes invalid for conventional linear cointegration to accurately model this relationship. To mimic such behaviour, Cross and Worden simulated two trend-stationary time series in [139], one with linear trend and the other with quadratic trend. To be explicit, assume $x_t$ and $y_t$ are two system variables observed, they are both affected by the same kind of external variations. But $x_t$ is linearly related to the variations of temperature while $y_t$ is quadratically related:

$$\begin{aligned} x_t &= \alpha T + \epsilon_t \\ y_t &= \beta T^2 + \varepsilon_t \end{aligned} \tag{5.15}$$

where $\alpha$ and $\beta$ are two constants, $\epsilon_t$ and $\varepsilon_t$ are two *iid* stationary measurement noises, $T$ represents external disturbances, temperature in this case. 1000 data points are simulated, $\alpha$ and $\beta$ are made equal to 1 for convenience, $\epsilon_t$ and $\varepsilon_t$ are

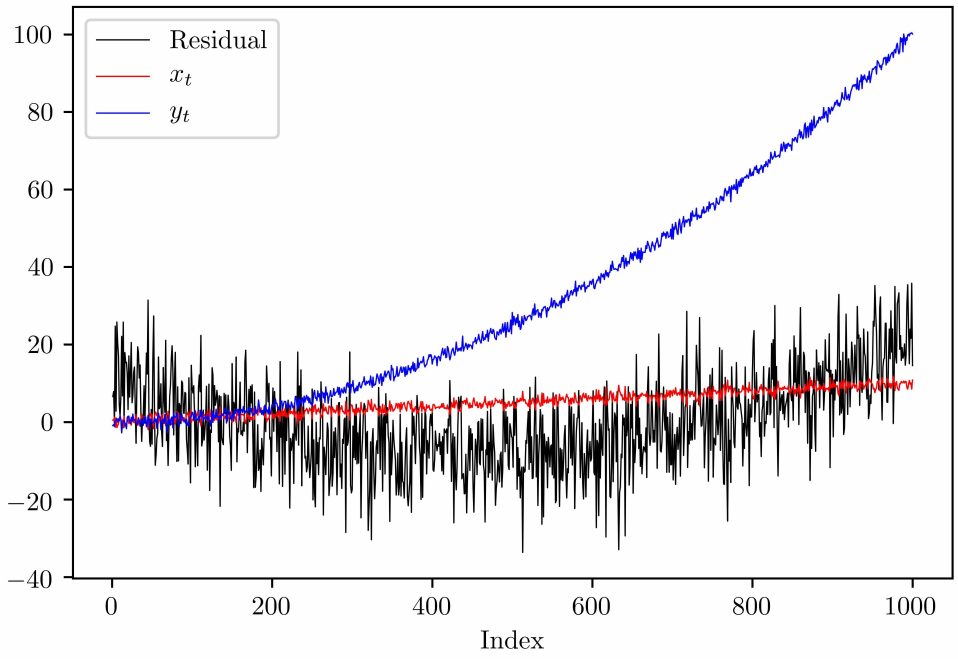


Figure 5.2: Residual series (black) of the linear cointegration model between $x_t$ and $y_t$.

| | ADF t-statistic | Critical Values | | | Results |
|---|---|---|---|---|---|
| | | 1% | 5% | 10% | |
| $x_t$ | -0.7227 | -3.437 | -2.865 | -2.568 | Nonstationary |
| $y_t$ | 10.2604 | -3.437 | -2.865 | -2.568 | Nonstationary |
| $\Delta x_t$ | -11.5427 | -3.437 | -2.865 | -2.568 | Stationary |
| $\Delta y_t$ | -4.6829 | -3.437 | -2.865 | -2.568 | Stationary |

Table 5.1: ADF test results for $x_t$, $y_t$, $\Delta x_t$ and $\Delta y_t$

simulated as two independent $\mathcal{N}(0,1)$ noise processes, and $T$ is a monotonically increasing series from 0 to 10. Simulated samples of $x_t$ and $y_t$ are shown in Figure 5.1.

If one follows the conventional cointegration method - the Engle-Granger method as reviewed in Section 4.4.1 - a linear regression model can be formed between $y_t$ and $x_t$, the model residual series is plotted as a black line in Figure 5.2. It is obvious to see that the residual is not stationary in the mean; [139] attempted to address this issue by forming a quadratic regression: $y_t = \theta x_t^2 + \psi_t$, but this method introduces unwanted heteroscedastic noise in the residual as a side effect of the quadratic transformation. Later, Zolna et al. modified the residual estimator by

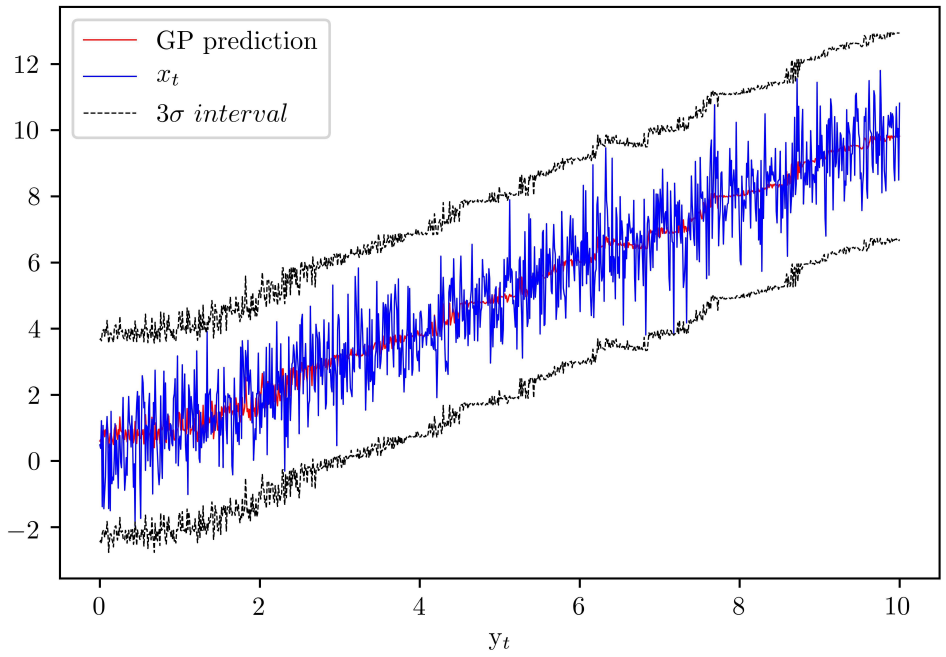


Figure 5.3: True values of $x_t$ are plotted in blue, GP regression predictions are shown in red, the black lines are the three standard deviation confidence interval of GP prediction.

dividing a correction term, which can suppress the changing variance in the residual [140]. However, there has not yet any discussion on how to choose a proper nonlinear transformation method, possible candidates including logarithm, exponential, polynomial, or Box-Cox transformation, and additionally, it is very difficult to tell whether a model has been overfitting or underfitting.

Now, following the procedures summarised in Section 5.3, one first employs the ADF test on $x_t$ and $y_t$, to see whether they are nonstationary or not; if nonstationary how many orders of integration are they. The results are summarised in Table 5.1, it suggests that $x_t$ and $y_t$ are nonstationary series, but they both turn stationary after differencing, or in other words they are both $I(1)$ series. Next, one forms a GP regression model. A different regression model from [139] will be used here, which is $x_t = \mathcal{GP}(y_t)$, the other possible model is going to be compared later. The aim here is to see whether the GP can produce a stationary residual series, therefore, there are no partitioning of training and testing dataset, ie. the whole dataset is used to train the GP regression model, and the squared-exponential kernel function (5.3) is selected.

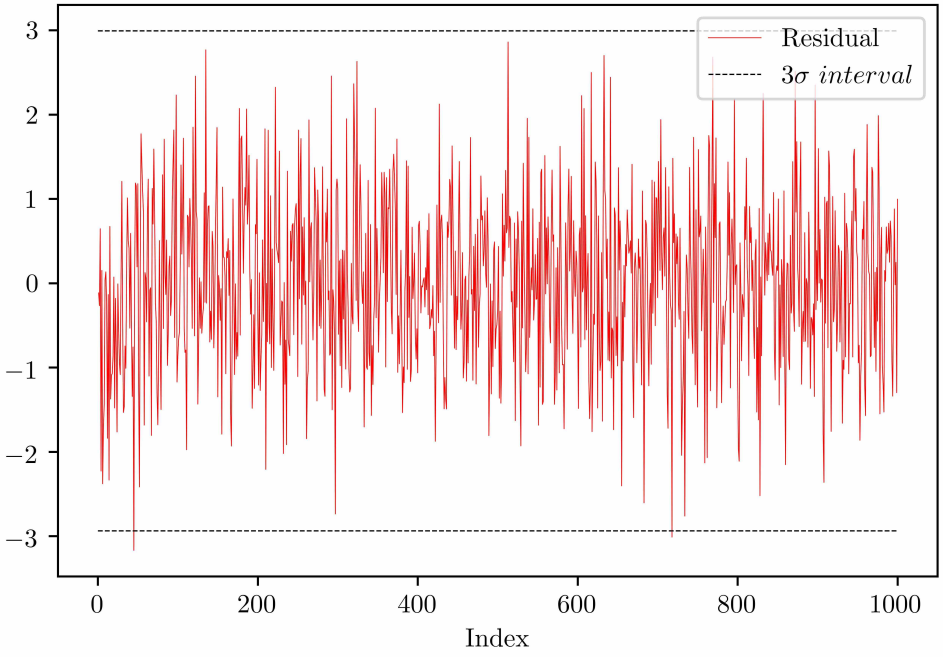


Figure 5.4: The residual series from the GP regression model, the black lines overlaid are the three standard deviation confidence intervals.

The GP regression prediction is shown in Figure 5.3; one can see that the upward trend of $x_t$ is very well captured by the GP, although the underlying trend is a straight line, the GP misinterprets very little portion of the noise as the signal, which causes the unsmooth prediction. But given that this is just a one-regressor model, and the regressor $y_t$ is nonlinearly related to the regression target $x_t$, the model seems to be quite accurate. Moreover, the confidence intervals the GP has produced are bounding quite tightly around $x_t$; to visualise the difference between them, one can refer to the residual series plot, as shown in Figure 5.4. From visual inspection, the residual series seems steady in both mean and variance, and the heteroscedastic phenomenon observed in [139] is effectively eliminated.

To confirm whether there exists a nonlinear cointegration between $x_t$ and $y_t$, one needs to perform the ADF test on the residual series, the test results are presented in Table 5.2, the t-statistic is safely below the critical value, suggesting that the residual series is indeed stationary, which further indicates that $x_t$ and $y_t$ are nonlinearly cointegrated. One can also visualise the nonlinear relationship, as shown in Figure 5.5; the horizontal axis is $y_t$ and the vertical axis is $x_t$, the blue dots are true data and the red asterisks are from GP prediction. This Figure can provide an intuitive

| | ADF t-statistic | Critical Values | | | Results |
|---|---|---|---|---|---|
| | | 1% | 5% | 10% | |
| Residual | -28.7488 | -3.437 | -2.865 | -2.568 | Stationary |

Table 5.2: ADF test results for the GP model residual.

| Model Form | Residual t-statistic | Critical Values | | | MSE | MAE |
|---|---|---|---|---|---|---|
| | | 1% | 5% | 10% | | |
| $y_t = \mathcal{GP}(x_t) + \epsilon_t$ | -28.7488 | -3.437 | -2.865 | -2.568 | 0.9634 | 0.7858 |
| $x_t = \mathcal{GP}(y_t) + \epsilon_t$ | -4.4544 | -3.437 | -2.865 | -2.568 | 101.0864 | 7.1755 |

Table 5.3: GP regression model comparison results.

view of how the GP is fitting the nonlinearity in the data, which helps explain why conventional cointegration fails.

The last step is to compare all the possible model forms and select the one having the best performance. As the model only has two variables, there are only two possible model forms; the other one is $y_t = \mathcal{GP}(x_t)$, so the same procedures are repeated for this model. For comparison, the mean squared error (MSE) and the mean absolute error (MAE) of the predictions, also the ADF t-statistics are used as metrics here; the results are summarised in Table 5.3. Both models have rejected the test, suggesting that the residual is stationary, but the first model has much smaller t-statistic, which means that it produces much a more "nonstationary"residual series; In terms of the MAE, the first model has slightly better mean fitting performance; for the MSE, the first model outperforms the second completely, it has much better variance explainability.

In summary, this case study is a demonstration of how the proposed procedures should be implemented. The synthetic dataset also comes from previous studies in the field, the proposed method can effectively eliminate the heteroscedastic variance in the residual, and produce a stationary residual purged of underlying trends. It is also important to note that, these two series $x_t$ and $y_t$ are in fact trend-stationary series, as examined in Section 4.2.2. A common practice in the time series literature is to first remove the deterministic trend and then proceed to standard stationary time series modelling procedures. However, in this study, the underlying trend in $x_t$ and $y_t$ are assumed unknown *a priori*, they are treated as stochastic trends as a result. This also confirms that GP regression is a robust estimation method, that can deal with all kinds of nonlinearity.

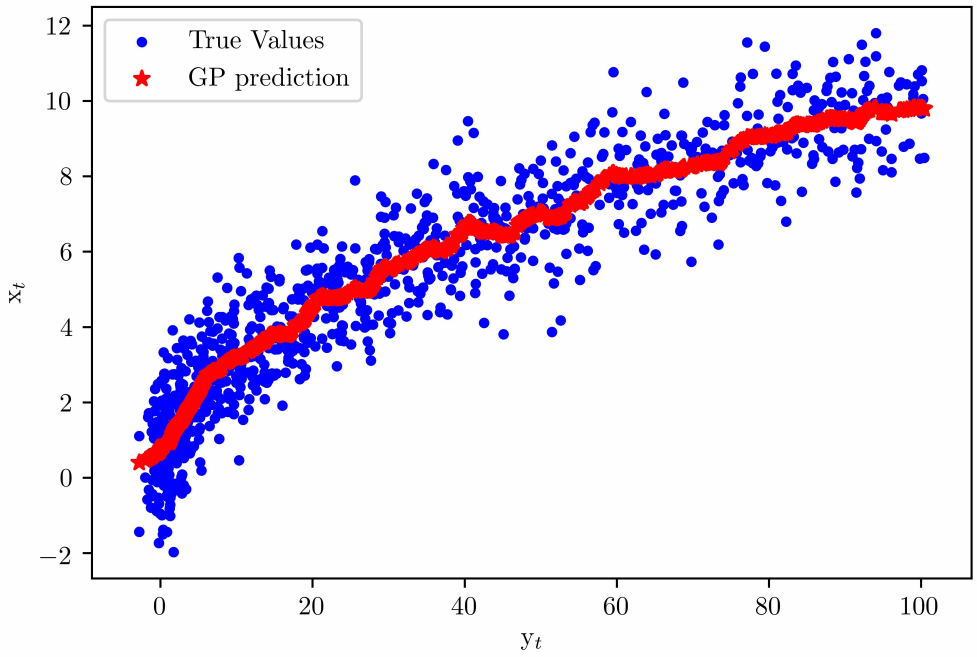


Figure 5.5: The nonlinear relationship between $x_t$ and $y_t$, the blue dots are true values, and the red asterisks are GP predictions.

### 5.4.2 Case Study II: the Benchmark Z24 Bridge

#### Introduction

As reviewed in Chapter 3, the Z24 Bridge benchmark shows a nonlinear behaviour to the change in the temperature. Figure 5.6 shows the first four natural frequencies with respect to observation numbers, the black dashed line shows the time when the first of the damage scenarios was implemented. However, due to the influence of environmental conditions, the natural frequencies show no significant sign of structural degradation. Furthermore, after nine months of monitoring of the normally functioning bridge, six kinds of damage scenarios were artificially employed on different parts of the bridge. All damage scenarios, with the corresponding date and data points are listed in Table 5.4. For more details about the monitoring systems and the progressive damage tests, the interested reader can refer to [66].

On further observation of Figure 5.6, it is obvious that the natural frequencies were affected by some external driver to a great extent, and this turned out to be temper-

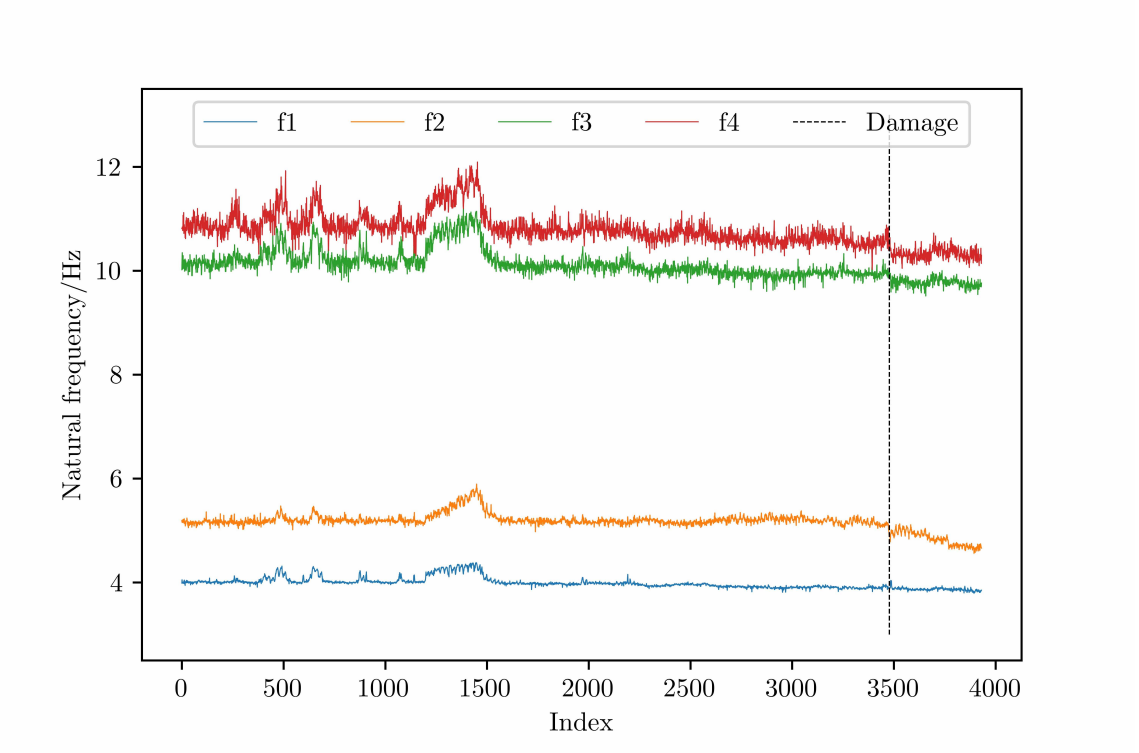


Figure 5.6: The first four natural frequency time series identified from the Z24 Bridge, the vertical dashed line indicates where first damage is introduced.

| Date | Damage Scenario | Day Index | Data Points |
|---|---|---|---|
| 10/08/98 | Settlement of Pier, 20 mm | 272 | 4918∼4941 |
| 12/08/98 | Settlement of Pier, 40 mm | 274 | 4966∼4989 |
| 17/08/98 | Settlement of Pier, 80 mm | 279 | 5084∼5107 |
| 18/08/98 | Settlement of Pier, 95 mm | 280 | 5108∼5131 |
| 19/08/98 | Tilt of Foundation | 281 | 5132∼5155 |
| 20/08/98 | 3rd Reference Point | 281 | 5156∼5179 |

Table 5.4: Progressive damage test scenarios and test dates [165].

| | $f_1$ | $f_2$ | $f_3$ | $f_4$ |
|---|---|---|---|---|
| $f_1$ | | Nonlinear | Linear | Linear |
| $f_2$ | Nonlinear | | Nonlinear | Nonlinear |
| $f_3$ | Linear | Nonlinear | | Linear |
| $f_4$ | Linear | Nonlinear | Linear | |

Table 5.5: Relationships between the first four natural frequencies

| | ADF t-statistic | 5% critical value | Stationarity |
|---|---|---|---|
| $f_1$ | -0.317481 | -1.940880 | N |
| $\Delta f_1$ | -14.37213 | -1.940880 | Y |
| $f_2$ | -0.741687 | -1.940880 | N |
| $\Delta f_2$ | -17.09163 | -1.940880 | Y |
| $f_3$ | -0.418102 | -1.940880 | N |
| $\Delta f_3$ | -28.57986 | -1.940880 | Y |
| $f_4$ | -0.423898 | -1.940880 | N |
| $\Delta f_4$ | -26.46857 | -1.940880 | Y |

Table 5.6: ADF test of the first four modal frequency time series and their difference series.

ature. See data points from 1800 to 2200 for example, the corresponding test dates were 28/01/1998 to 15/02/1998, when air temperature was mostly below zero during this period. There emerged a large peak of the natural frequencies approximately at data numbers 1800-2200; this may be explained by the nonlinear behaviour of the natural frequencies caused by stiffening of the asphalt. It seems that the effect of temperature may result in nonlinear relations between natural frequencies. Figure 5.7 plots the relationships between each of the extracted frequencies. With visual inspection, it can be seen that the second frequency is not linearly related with the other frequencies, while $f_1$, $f_3$ and $f_4$ appear to be mutually linearly related [90]. The results of the mutual relationships between frequencies are summarised in Table 5.5.

### GP Regression as Nonlinear Cointegration

Following the procedures in Section 5.3, the orders of integration for the time series of the four natural frequencies are determined using the ADF test; the results are given in Table 5.6, and show that these four natural frequency series are nonstationary at the 95% confidence level and integrated of order one, i.e. they are $I(1)$ series.

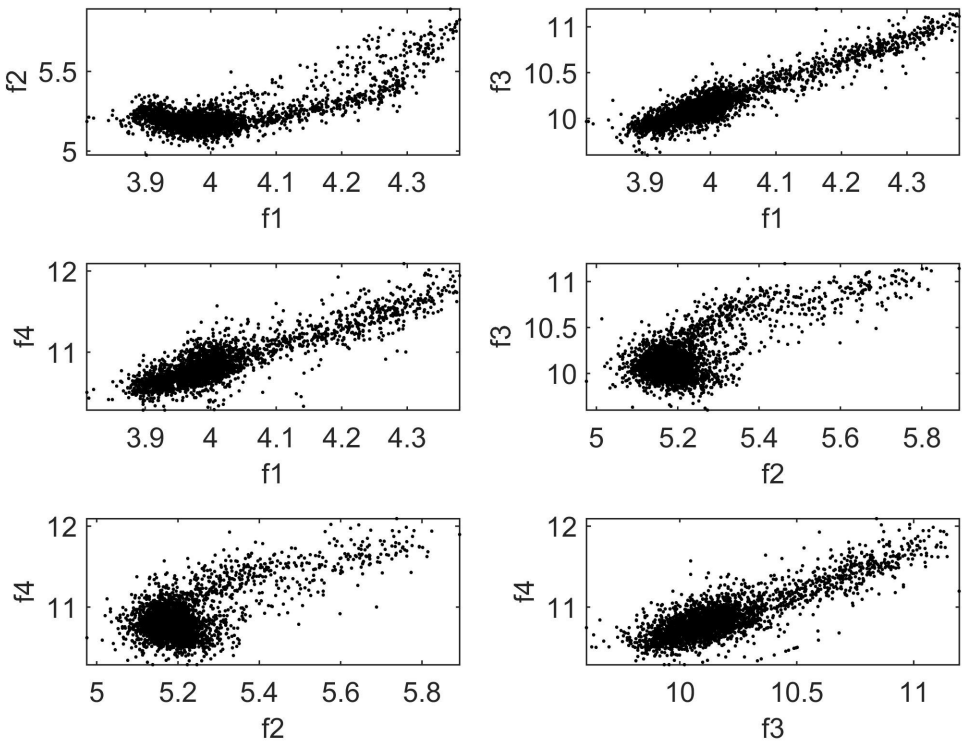


Figure 5.7: Mutual relationships of the first four natural frequencies.

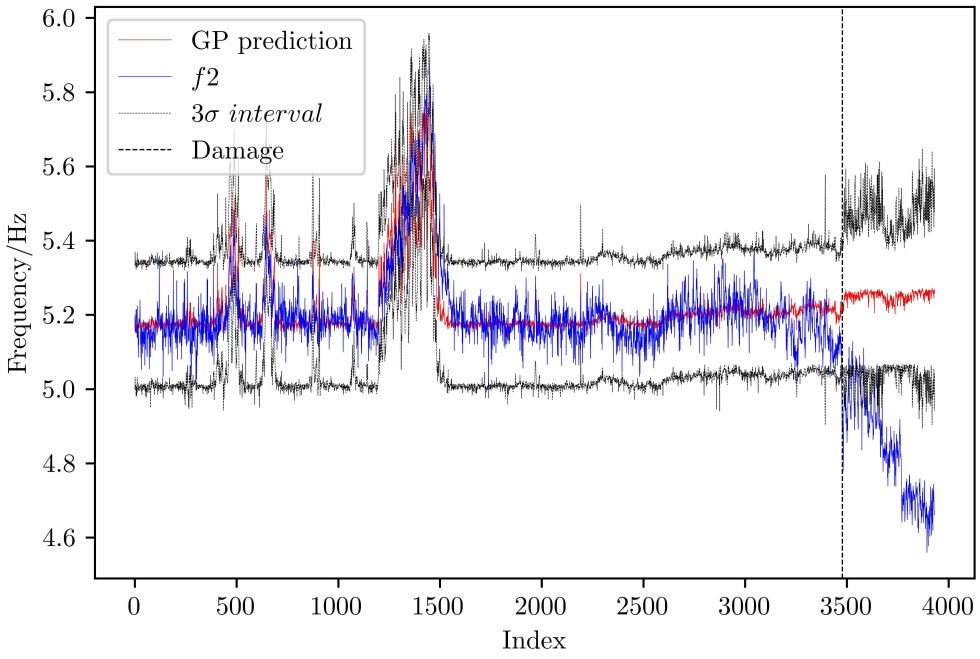


Figure 5.8: Gaussian process regression model $f_2 = \mathcal{GP}(f_1, f_3, f_4)$ predictions are in red, the real values of $f_2$. are plotted in blue, and the black horizontal lines are three standard deviation confidence intervals, the dashed vertical line indicates damage occurrence.

It might be difficult to find the specific physical meaning of a regression model between natural frequencies; however, from the view of cointegration, once the cointegration relationship of variables is built, the equilibrium relationship may indicate that the system is functioning under normal conditions, hence the model error may be sensitive to system variation induced by damage; if the model error tends to be stationary, the underlying common trends of the original data are successfully removed. To train a GP regression model properly, the training dataset has to cover as many variations of the data as possible, as the monitoring data contains at least three seasons before damage is introduced. Thus, one of every two points from point 1 up to 3000 are used to train the GP model, the rest of the data set is used for testing. As the system has 4 variables, therefore theoretically it has 28 possible model forms. $f_2 = \mathcal{GP}(f_1, f_3, f_4)$ is chosen to be the running example for now, and the rest of the model forms will be compared later in the section.

The trained GP model is used to predict on the whole dataset, and the prediction performance is shown in Figure 5.8, where for most of $f_2$, the GP has well captured its

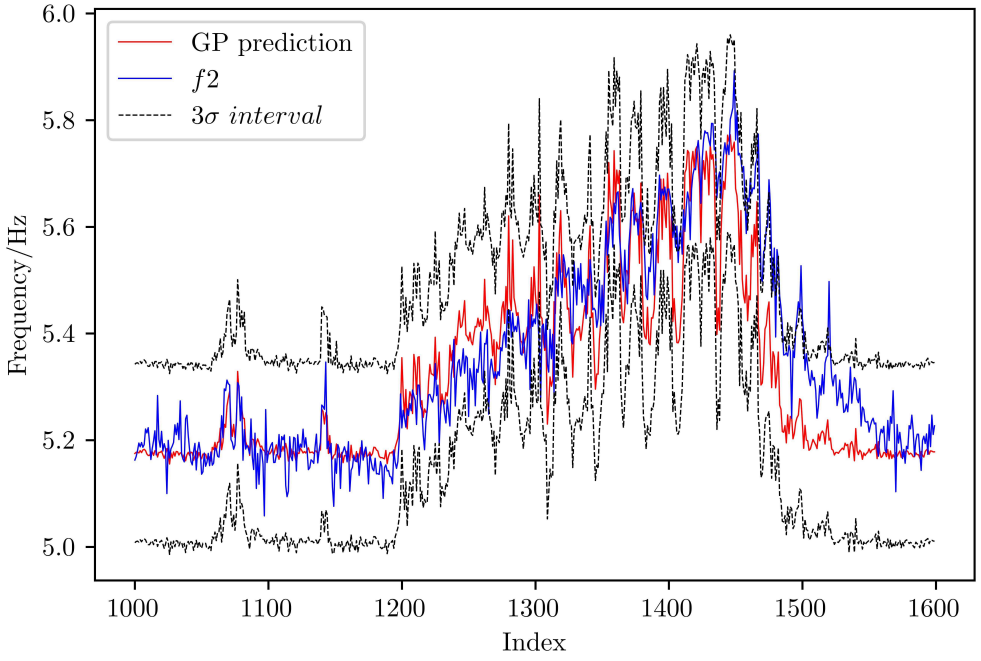


Figure 5.9: Zoomed-in view of data points from 1000 to 2000 in Figure 5.8.

fluctuations, it not only predicts the mean of $f_2$ when the temperature is not too cold (points 1 to 500 for example), and warm (point 2500 to 3000 for example), but also successfully follows the spikes where temperature is below zero (points 1200 to 1500 for example). Most importantly, as soon as the damage is introduced, the prediction of the GP starts to diverge from the measurements, and the measurements also immediately exceed the lower confidence interval. Figure 5.9 provides a zoomed-in view for the data points between 1000 to 2000, one can see that the small spikes in the beginning are very accurately predicted by the GP, and the GP is also showing a good fit when the mean suddenly starts to peak starting from point 1200, the variations of $f_2$ are also safely bounded by the GP's confidence intervals. However, when the frequency starts to descend from peak to normal, the predictions of the GP seem to be underestimated, and some of the blue lines even exceed the upper confidence interval. The most likely cause of this is perhaps the slope of the ascending and descending part is very different, the declination from point 1400 to 1500 is much steeper than the rising from point 1200 to 1400.

Although this model is a three-regressor model, which means that visualisation of the regression is not possible for three dimensions below, one can single out each

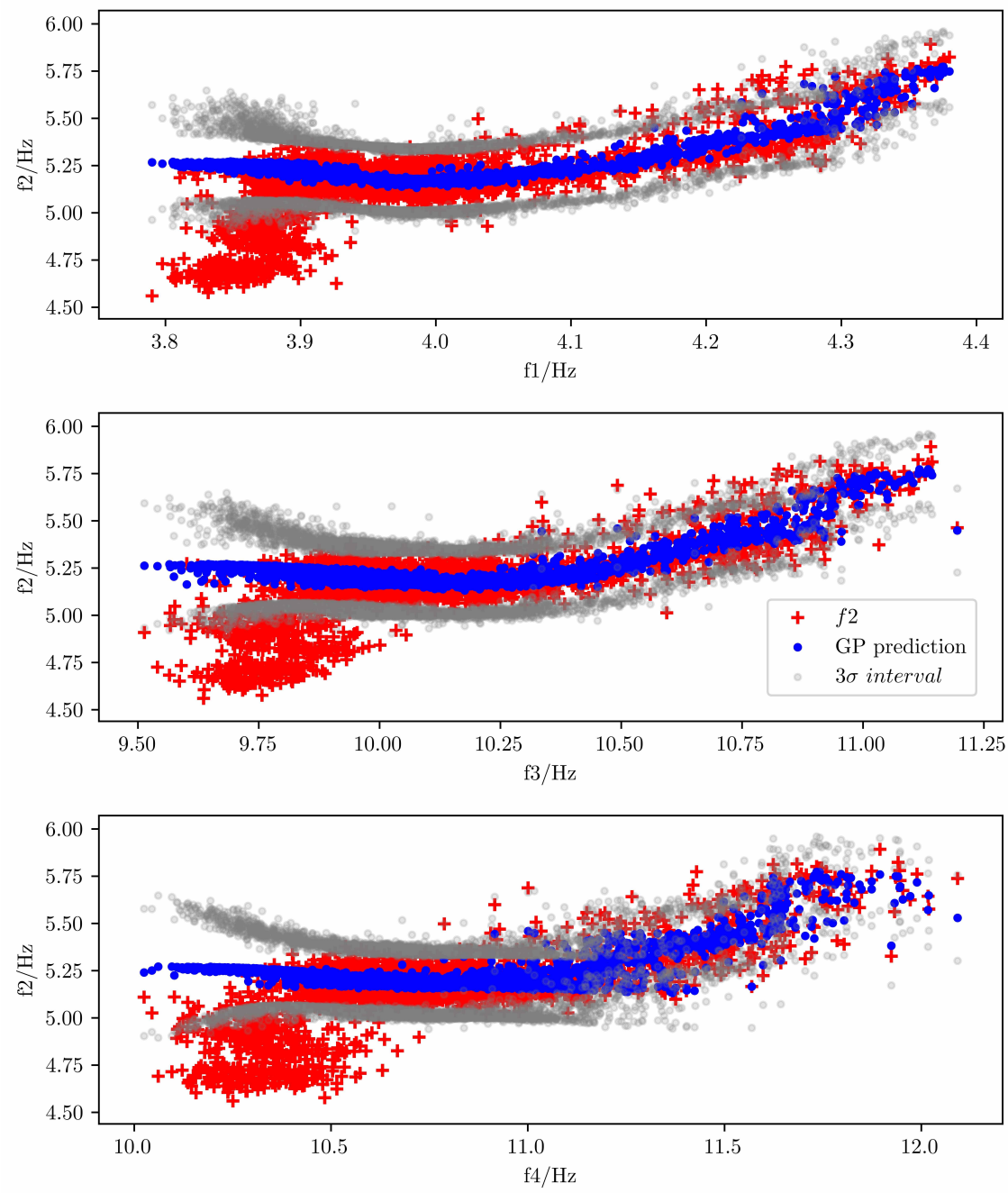


Figure 5.10: The predicted $f_2$ of GP model paired with its corresponding inputs, red crosses are true values of $f_2$, blue dots are GP's predictions, and the grey circles show GP's confidence intervals.

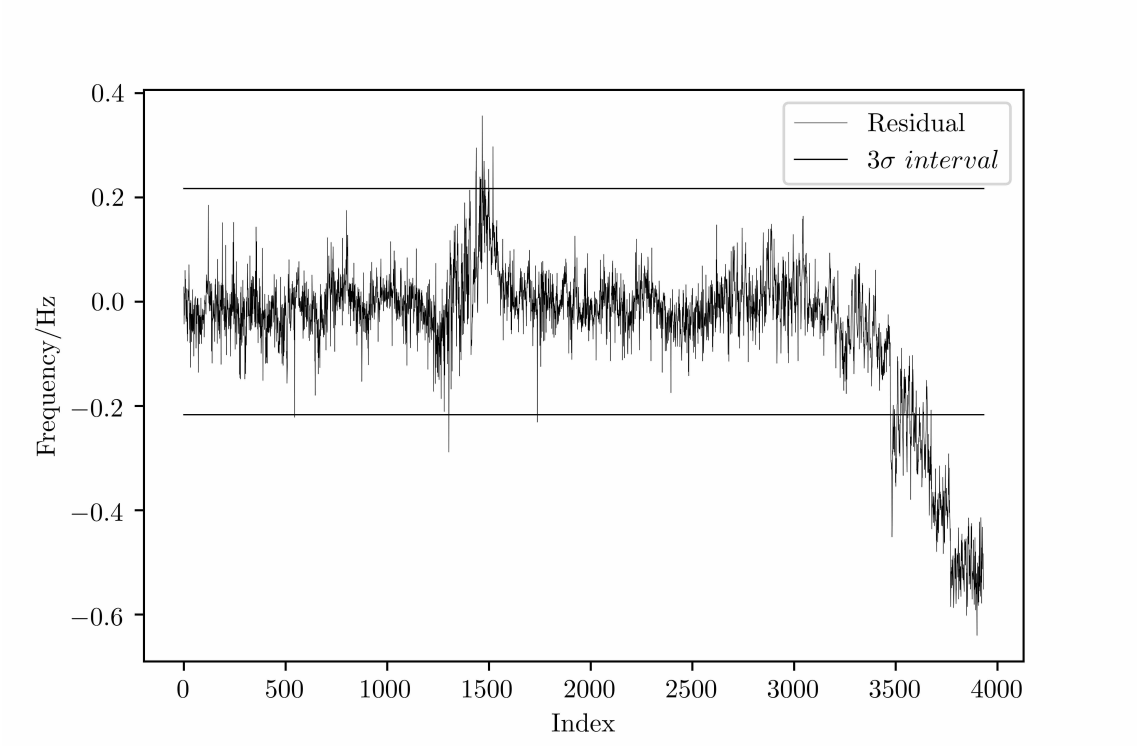


Figure 5.11: The residual series of the GP regression model $f_2 = \mathcal{GP}(f_1, f_3, f_4)$, with three standard deviation confidence interval overlaid.

pair of inputs and outputs, and observe how each input variable is behaving inside the GP regression, as shown in Figure 5.10. In these three figures, the red crosses in the lower left corners are actually corresponding to the data where damage was introduced, as they are clearly moving towards a different direction, which results in their successful detection by GP. What is more interesting is the red crosses in the top right corners, where are in fact under freezing conditions. Comparing to other regions, samples in the freezing zones tend to have larger variance, but as is known that normal GP regression assumes a *iid* noise condition, which makes the GP model underestimate the local variance, it helps to explain the prediction error spotted in Figure 5.9.

Furthermore, one can examine the difference between predictions and measurements, e.g. the residual plot in Figure 5.11. The result is quite consistent with the observations above; most of the changes induced by environmental variations have been effectively removed, except the region where temperature transits from peak to normal (points around 1500), causing the residual in this region to exceed the upper confidence bound. Most crucially, the damage detection in the residual series is

imminent, and even after the first damage instance, one can see that the residual is progressively moving downwards, indicating that system status has changed several times. After computing the ADF statistic of the training residual series, the t-statistic obtained is -4.7354, which is significantly below the critical value -1.940880 (as shown in Table 5.6), therefore the training residual series is a stationary one, and the nonlinear cointegration relationship can be said to be successfully established.

### Model Selection

In the current case study, there are four system variables, meaning that there are possibly 28 kinds of GP regression forms, as listed in Table 5.7. Therefore, in order to find the optimum model form, the last step is to evaluate the performance of all these models. The performance metrics used in this context is the *mean squared error (MSE), mean absolute error (MAE)* and the ADF statistics. The first two are used to measure the model fitting in the variance and mean respectively, whereas the last one is utilised as a measure of stationarity; that is the lower the statistic, the more stationary the series is.

Repeating all the procedures conducted above on all the rest of the models, and computing the above-listed metrics on the data points from 0 to 3000, the performances of all the models are illustrated in Figure 5.12. The horizontal axis represents the model indexes listed in Table 5.7, the left vertical axis is for the ADF statistic, and the right axis is for the MSEs and the MAEs. Overall, models with indexes from 7 to 13 outperform others especially in terms of ADF statistics, indicating that they have produced the most stationary residuals; besides, they also have quite low MSE and MAE scores. One can simply pick Model No.12, $f_2 = \mathcal{GP}(f_3, f_4)$,for it has the smallest ADF statistic. But Model No.13, $f_2 = \mathcal{GP}(f_1, f_3, f_4)$, has slightly lower MSE and MAE scores, although it does have a marginally larger ADF statistic than No.12, and more importantly, it contains all the available system variables. As a result, model No.13 is chosen to be the best GP regression model for this Z24 Bridge case study.

| Model Index | Regression Model Form | Model Index | Regression Model Form |
|---|---|---|---|
| 0 | $f_1 = \mathcal{GP}(f_4)$ | 14 | $f_3 = \mathcal{GP}(f_1)$ |
| 1 | $f_1 = \mathcal{GP}(f_3)$ | 15 | $f_3 = \mathcal{GP}(f_4)$ |
| 2 | $f_1 = \mathcal{GP}(f_2)$ | 15 | $f_3 = \mathcal{GP}(f_2)$ |
| 3 | $f_1 = \mathcal{GP}(f_4, f_3)$ | 17 | $f_3 = \mathcal{GP}(f_1, f_4)$ |
| 4 | $f_1 = \mathcal{GP}(f_4, f_2)$ | 18 | $f_3 = \mathcal{GP}(f_1, f_2)$ |
| 5 | $f_1 = \mathcal{GP}(f_3, f_2)$ | 19 | $f_3 = \mathcal{GP}(f_2, f_4)$ |
| 6 | $f_1 = \mathcal{GP}(f_4, f_3, f_2)$ | 20 | $f_3 = \mathcal{GP}(f_1, f_2, f_4)$ |
| 7 | $f_2 = \mathcal{GP}(f_1)$ | 21 | $f_4 = \mathcal{GP}(f_1)$ |
| 8 | $f_2 = \mathcal{GP}(f_4)$ | 22 | $f_4 = \mathcal{GP}(f_3)$ |
| 9 | $f_2 = \mathcal{GP}(f_3)$ | 23 | $f_4 = \mathcal{GP}(f_2)$ |
| 10 | $f_2 = \mathcal{GP}(f_1, f_4)$ | 24 | $f_4 = \mathcal{GP}(f_1, f_3)$ |
| 11 | $f_2 = \mathcal{GP}(f_1, f_3)$ | 25 | $f_4 = \mathcal{GP}(f_1, f_2)$ |
| 12 | $f_2 = \mathcal{GP}(f_3, f_4)$ | 26 | $f_4 = \mathcal{GP}(f_2, f_3)$ |
| 13 | $f_2 = \mathcal{GP}(f_1, f_3, f_4)$ | 27 | $f_4 = \mathcal{GP}(f_1, f_2, f_3)$ |

Table 5.7: All the GP regression model forms and their corresponding model indexes.

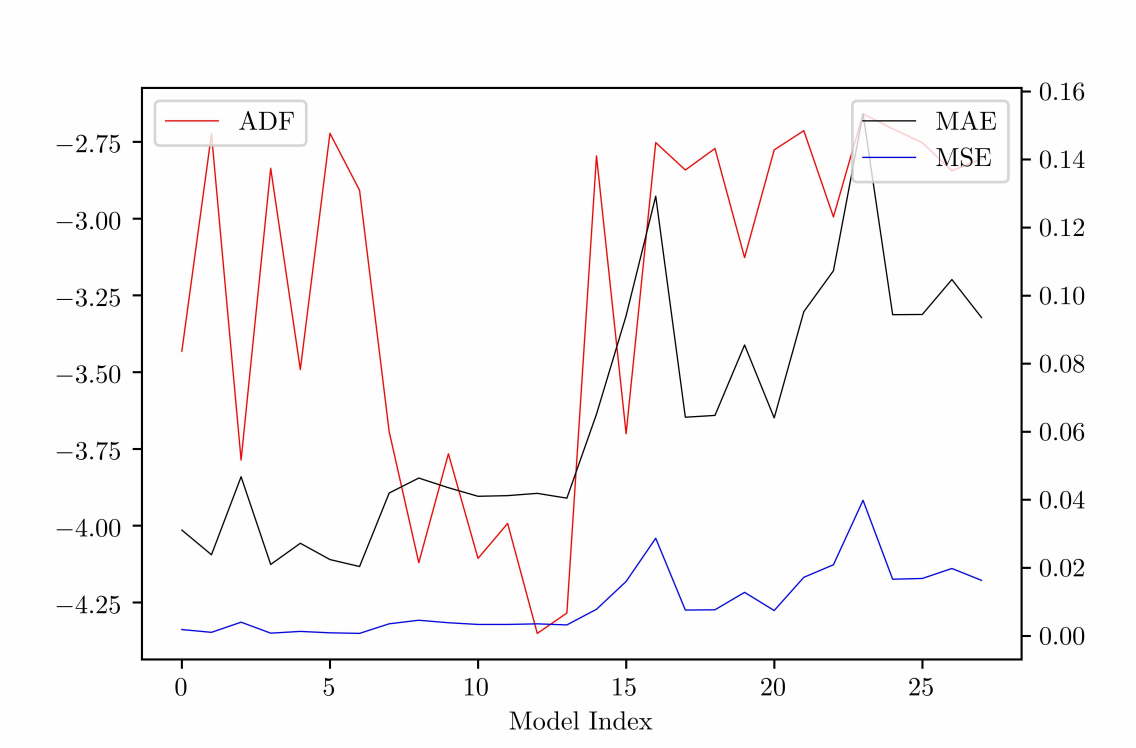


Figure 5.12: The MSE, MAE and ADF statistic of all possible models of the GP regression, the left axis is for the ADF statistic, the right axis is for the MSE and MAE, the horizontal axis is the model indexes listed in Table 5.7.

## 5.5 Conclusions

Cointegration has been used to model the long-run equilibrium relationships in economic series, it now can be utilised in SHM problems to find some linear combination of nonstationary variables sharing the same trend to construct a stationary residual, purged of common trends, which may serve as a damage indicator. As an extension of previous work, a nonlinear cointegration approach based on Gaussian process regression is proposed in this chapter, aiming to build nonlinear cointegrating relationships between variables. The idea is based on the framework of the Engle-Granger cointegration, except for using GP regression as the cointegrating function. The ADF test is implemented both before and after the cointegrating regression to determine the order of integration, and furthermore to examine whether a nonlinear cointegration relationship has been built. Two datasets are used to validate and examine the proposed method, the first dataset is a synthetic case study coming from the previous literature. Using the proposed method, one can successfully model the nonlinear relationships between variables, and build a stationary residual series purged of influences from the underlying trend. Real data from the Z24 Bridge is also used to validate this method, the results show that the model error series created from the model mostly stays stationary during normal operating conditions, which means that the trends induced by EOVs are effectively eliminated, yet the model series still maintain sensitive to structural damage.

One obvious advantage of implementing cointegration, comparing with other approaches like linear regression, is that it is clear that no direct measure of environmental or operational variations are necessary. This may provide great convenience for SHM, because the scale of structures of interest are growing massively, it is sometimes difficult to acquire measures of ambient variations accurately. And furthermore, GP is a very powerful framework, one can easily build things on GP models: one example would be to use a sparse GP to enable analysis on a large dataset [163], or one can discard the *iid* noise assumption, and adopt a input-dependent noise condition, then the heteroscedastic GP will come to the remedy [166][167]; or if the noise and also the mean are both input dependent, there is Bayesian CART-based Treed GP that can be exploited [91], where the input domain can be partitioned into different regimes. Throughout this chapter, the GP model was entirely built upon the Engle-Granger cointegration framework; one may also recall from the theory reviewed in Chapter 4, the Johansen procedure is sometimes a more appealing

framework for cointegration. The GP regression method can be adapted into a multiple output model [161], which potentially can be developed under the Johansen framework. The list goes on, if one wishes to encode their problem-specific problem in this method, and it will also be the direction of the author's future work.

# Chapter 6

# A Regime-Switching Cointegration Approach

## 6.1 Introduction

The last chapter focused on estimating a nonlinear cointegration model using Gaussian process regression, which treats the underlying nonlinear cointegration as a smooth function. This chapter however, will take a different direction to model the nonlinearity. Rather than modelling the original series as a whole, this chapter will pursue to separate the time series into segments, where conventional cointegration can be applied within each segment.

Regime switching is not an uncommon issue in the economic world; for instance, cointegrated stock indexes might change their inner dynamics from a "bull market" to a "bear market" because of external influences, e.g. monetary policy intervention, financial crisis or the latest unexpected event e.g. "Brexit". A large body of the econometric literature concerning this falls in the extension to threshold cointegration, first proposed by Balke and Fomby in 1997 [168]. In their framework, the adjustment term in the cointegrating regression is allowed to shift once some indication variable exceeds a threshold. Furthermore, there are several other variants built on the vector error correction (VEC) model, as expressed above in equation (4.18); in [169] and [170] for example, they allow a threshold effect on the lag terms and the intercept term respectively. Gregory and Hansen [171], however, take the

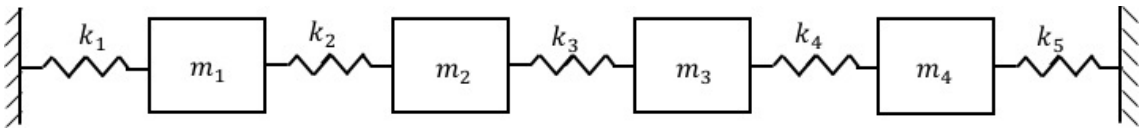


Figure 6.1: A four-DOF spring mass system.

opposite direction for allowing a cointegrating relationship to change, or in their terms, shift regime. More specifically, the cointegrating vector can change its value after a certain breakpoint, after which the system will stabilise itself at another long term equilibrium. The position of the breakpoint is unlikely to be determined in advance, thus they calculate the unit root statistic for each possible regime shift, and evaluate the smallest values across all possible breakpoints.

Inspired by Gregory and Hansen's work, a regime-switching cointegration method will be adopted to address the nonlinearity issue in this chapter. Different from their method however, instead of using the Engle-Granger framework, the more efficient Johansen procedure is implemented to estimate cointegrating vectors. The chapter is organised as follows: first a synthetic case study is presented to illustrate the concept of regime switching, and then the procedures of the proposed method are introduced; followed by a second case study, the Z24 Bridge data; this chapter will end with some discussions and conclusions.

## 6.2 A simulated spring-mass system

As discussed in the previous chapters, the conventional cointegration method may sometimes fall short because of the involvement of nonlinearity. To illustrate the issue more specifically, a simple system is simulated, and the proposed new method will be illustrated with it.

Consider a four degree of freedom (DOF) spring-mass system, where four lumped masses ($2kg$ each) are in a chain with both ends connected to ground, as shown in Figure 6.1. To mimic the effect of EOVs, temperature particularly in this case, a changing thermal field is applied to the system. 10000 real temperature measurements from the SHM campaign of the Tamar Bridge are used as the thermal field. The temperature data ranges approximately from -10°C to 20°C, which is fully displayed in the lower panel of Figure 6.2, representing readings from about one year [75]. To introduce artificial nonlinearity to the system, the springs in the system

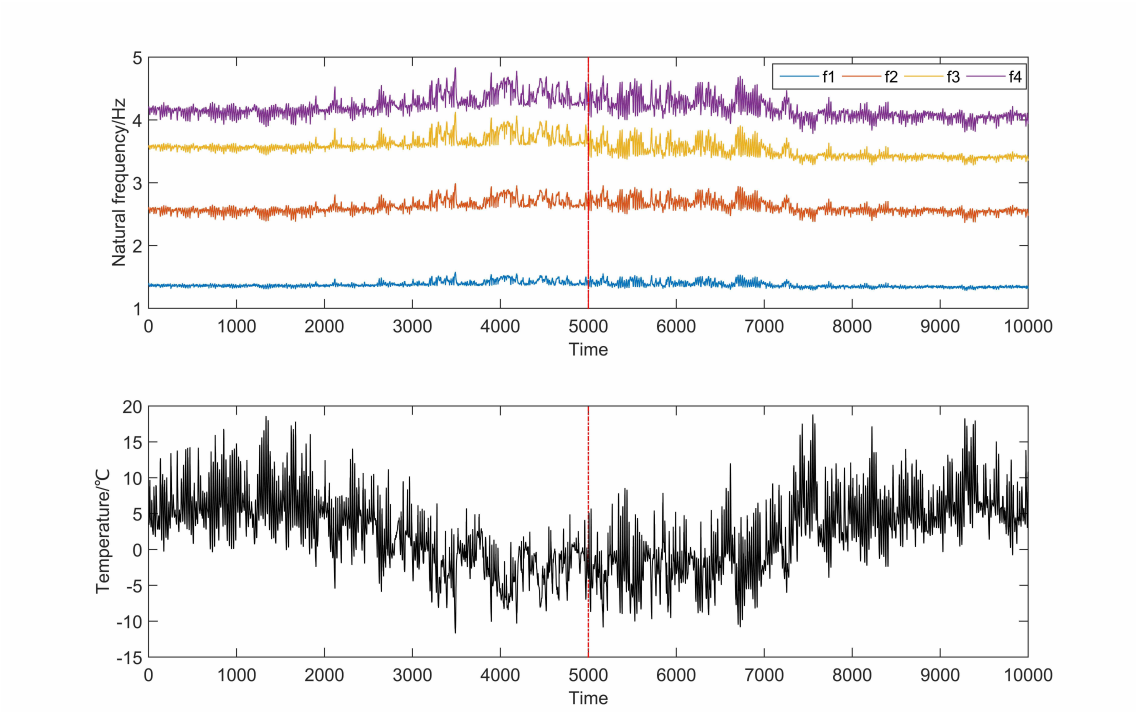


Figure 6.2: Upper panel: the four natural frequency series of the system in Figure 6.1 plotted as a function of time; Lower panel: temperature series plotted against time. Red dashed line indicates damage introduction.

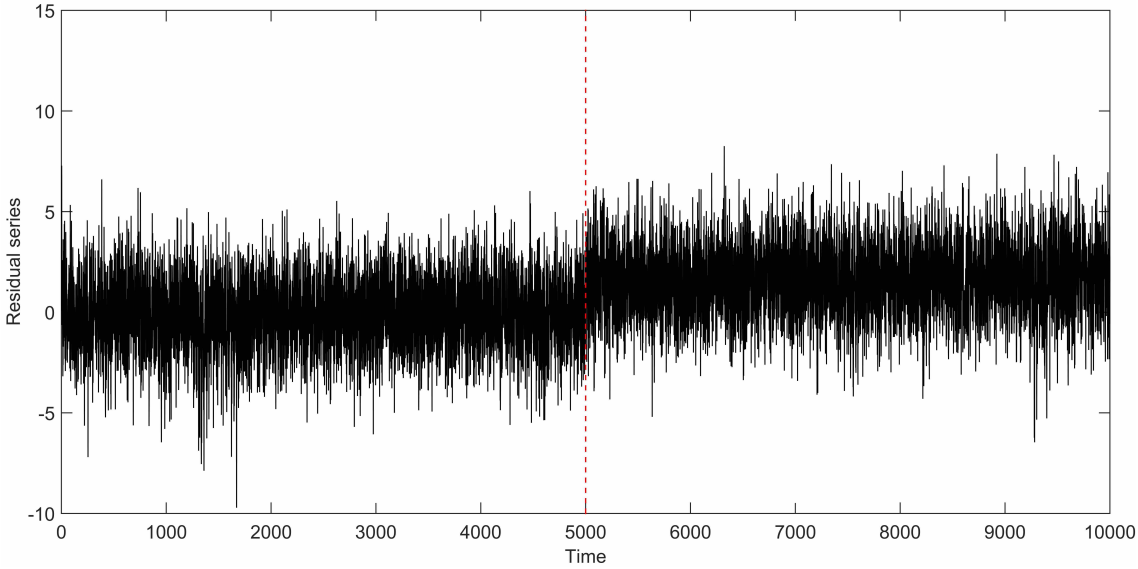


Figure 6.3: Residual series obtained using the conventional cointegration method, the red dashed line indicates where damage occurs.

are all set to have nonlinear influences from temperature, the third spring is set to have a slightly different effect from temperature. The explicit expressions of their stiffness versus temperature $T$ are given as follows:

$$k_1 = k_2 = k_4 = k_5 = \begin{cases} -0.15 \times T + 4, & \text{if } T < 0 \\ -0.05 \times T + 4, & \text{if } T \geq 0 \end{cases} \tag{6.1}$$

$$k_3 = \begin{cases} -0.15 \times T + 5, & \text{if } T < 0 \\ -0.25 \times T + 5, & \text{if } T \geq 0 \end{cases} \tag{6.2}$$

Because of the different behaviour of $k_3$, the nonlinear effect is introduced into the vibration modes in which the third spring is participating - the second and the fourth mode to be specific. Damage is simulated by letting the stiffness of the second spring $k_2$ decrease by 20%, at datapoint 5000 in the simulation. The four natural frequencies of the system are obtained at each time instant by solving the equations of motion. Additionally, a small amount of Gaussian white noise $N(0, 0.02)$ is added, to simulate measurement errors.

The upper panel of Figure 6.2 shows the identified four natural frequency series, plotted as a function of time. The dashed vertical line indicates where damage is introduced. It is clear from Figure 6.2 that the effect of temperature is significant. When the damage level is not high enough, damage information may be overwhelmingly masked by the changes caused by temperature. Following the conventional cointegration procedures proposed in [124], the data points ranging from point number 2000 to 4000 are used for establishing the cointegrating vector. From this data one can obtain the residual series as shown in Figure 6.3; here one can clearly see that the residual series is not very sensitive to the damage occurrence - the underlying cointegration relationship has not been accurately modelled and any conclusion drawn from this may therefore be misleading. Because of the nonlinear effect of the third spring, the mutual correlation between the four natural frequencies will shift from one regime to another, as soon as the temperature crosses the zero degree point. This regime switching may be evidently observed from Figure **??**, which shows that the mutual correlations among the four natural frequencies have a distinct bilinear relationship, the knee points in the images correspond to the zero temperature points.

## 6.3 A regime-switching cointegration method

The situation in the four-DOF system above is very similar to the phenomenon of regime switching, as it enters another regime as soon as the temperature drops below zero degrees. Thus in this section, a regime-switching cointegration model will be exploited to address this issue. The idea here is to split the original data into two halves, one of which consists of data points that are greater than 0, and the other half less than 0. As a result, in each of the subsample, the underlying relationship becomes linear again. Loosely speaking, the aim is to build a piecewise linear cointegration model, or more rigorously, a regime-switching cointegration model.

Firstly only a small amount of the data are needed for estimating the model, data points from point 2000 to 4000 are extracted for establishing the cointegrating vectors and breakpoints. The training series are rearranged according to the order of temperature, the rearranged series $\mathbf{f}_t = (f_{1t}, f_{2t}, f_{3t}, f_{4t}), t = 1, 2, ...N$, where $N$ is the sample size, is shown in the upper panel of Figure 6.4 , indexed by the temperature in the lower panel. Even though a breakpoint was simulated to occur at zero degrees (around point number 900 in Figure 6.4), there is no clear sign of a shifting regime in the figure.

The next step is to ascertain the position of the break point from the training data with the help of a unit root statistic - the ADF $t-$statistic. Assume the current breakpoint is at position $\tau$, then $\mathbf{f}_t(1:N)$ is split into two sets: $\mathbf{f}_{1\tau}(1:\tau)$, $\mathbf{f}_{2\tau}(\tau+1:N)$. One then uses the Johansen procedure presented earlier to estimate the cointegrating vector of each set, say $\boldsymbol{\beta}_{1\tau}$ and $\boldsymbol{\beta}_{2\tau}$, and to construct the residual series at this breakpoint, $e_\tau = (\boldsymbol{\beta}_{1\tau}\mathbf{f}_{1\tau}; \boldsymbol{\beta}_{2\tau}\mathbf{f}_{2\tau})$, where ";" is used to concatenate these two vector series; the subscript $\tau$ denotes the fact the residual series depends on the position of the breakpoint. From the residual series $e_\tau$, the ADF statistic can be calculated using (4). Note that not all positions are valid for $\tau$ because calculating the ADF statistic demands a small number of samples, therefore in practice, the data sets in the interval $([0.15N], [0.85N])$ are used to evaluate the possible breakpoint.

Following the procedures above, the ADF statistic of the four-DOF system is plotted in Figure 6.5, as a function of the training sample points. The blank space in the beginning and the end of the figure represents the fact that ADF statistics are only evaluated in the interval $([0.15N], [0.85N])$. The smallest value of the curve is at data point 976, corresponding to the temperature 0.4767°C, which is quite close to

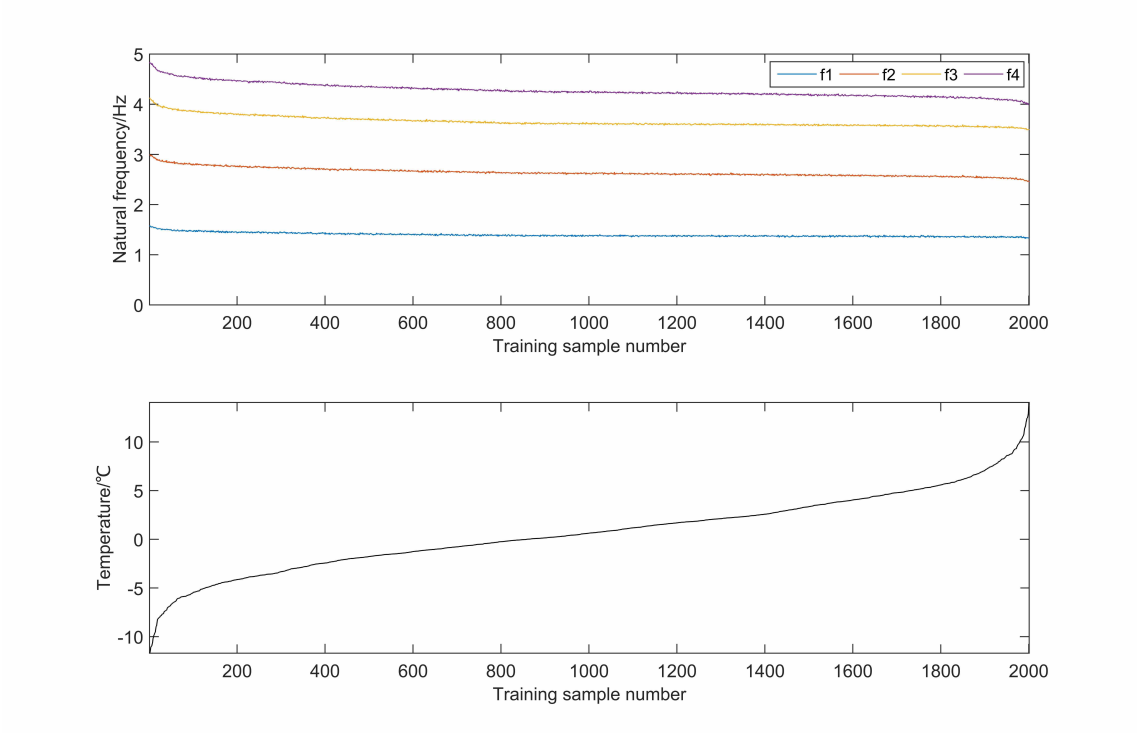


Figure 6.4: Upper panel: natural frequency series rearranged in the order of temperature; Lower panel: temperature series rearranged in the order of magnitude.

the simulation assumption. Furthermore, with the estimated best breakpoint and cointegrating vectors correspondingly, one can have the following regime-switching cointegration relationship which is indexed by the value of temperature:

$$\varepsilon_t = \begin{cases} 147.90 \times y_{1t} - 107.29 \times y_{2t} - 122.96 \times y_{3t} + 10.69 \times y_{4t} - 3.54, & \text{if } T \leq 0.4767 \\ -4.51 \times y_{1t} - 84.87 \times y_{2t} - 127.87 \times y_{3t} - 165.07 \times y_{4t} - 24.19, & \text{if } T > 0.4767 \end{cases} \tag{6.3}$$

Plotting the residual series from equation (6.3), as shown in Figure 6.6, it is clear that the series is stationary before damage introduction, any effect from temperature is effectively eliminated, and the nonlinear behaviour of the frequency response is precisely captured. After 5000 data points, the magnitude of the residual sees a sudden jump, which indicates strongly the occurrence of damage; the overlaid grey areas show where cointegration switches from one regime to the other. The result can be interpreted by the fact that the regime-switching cointegration is estimated with training data under normal condition, the healthy state of the system has been accurately modelled. Whenever damage occurs, the long term relationship of the variables no longer holds, thus the residual series turns nonstationary immediately.

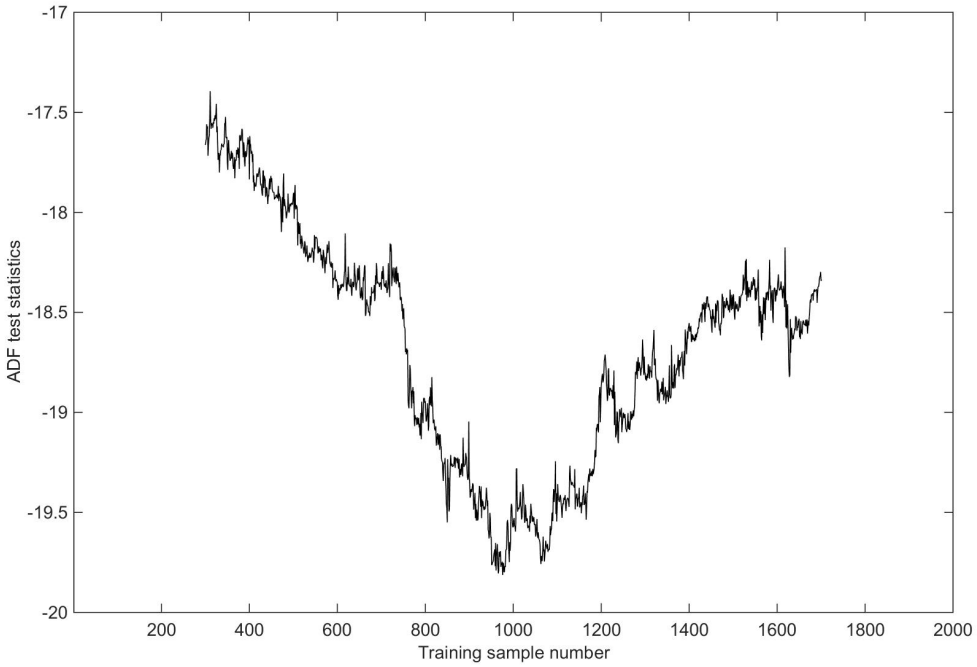


Figure 6.5: ADF statistics plot of the training sample points, the lowest point position determines the breakpoint position for the regime switch.

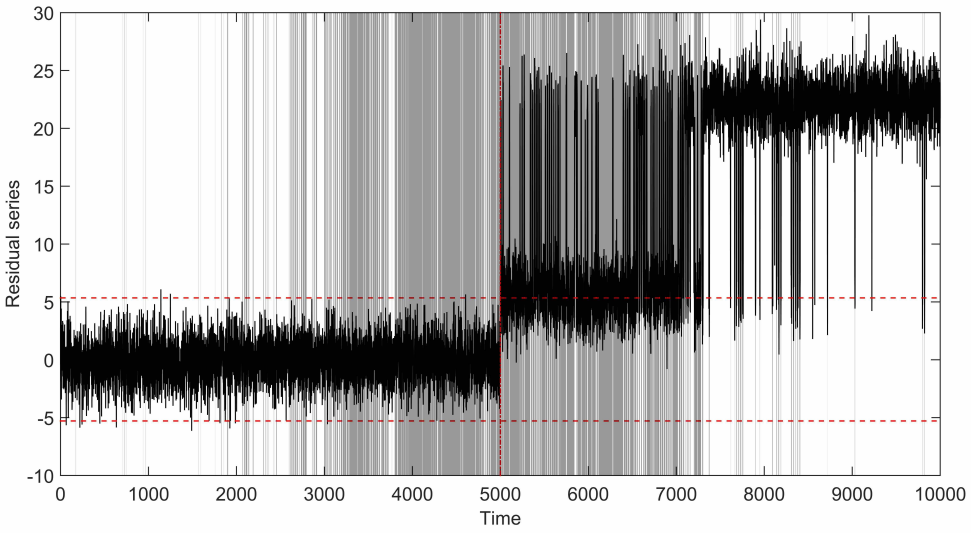


Figure 6.6: Residual series of the cointegration model, the vertical red dashed line indicates damage introduction, the two horizontal red lines represent the three standard error bars; the grey shaded areas show where cointegration switches regimes.

Despite the fact that the method suggests very good results, one may still argue that reordering the original series may break the underlying cointegrating relationship, therefore the estimation procedure might be ill-conditioned. This argument is partly true, that rearranging the order of series will surely break the underlying error correction mechanism, but the long term relationship stays the same, or in other words, the rearranged series have the same cointegrating vectors as the original series, because the cointegrating relationships are stacking pointwise in time. One should bear in mind that the final goal here is fundamentally different from the aim of the econometricians, the concern is more about the long term relationship between variables, the short term adjustments are less of interest for the moment. Therefore, it is legitimate to use temperature as a reference series to rearrange the original series, and estimate the cointegrating vectors of the yielded series.

Next, the proposed method will be briefly summarised and then a real engineering example will be used to examine the effectiveness of this method.

## 6.4 A brief summary of the proposed method

The procedure of the method is summarised as follows:

1. Rearrange the monitored series in the order of environmental or operational variable.

2. Insert a breakpoint at a position ranging from $([0.15N], [0.85N])$, where $N$ is the sample size.

3. At each possible breakpoint, split the series into two halves, use the Johansen procedure to estimate the cointegrating vectors for each half.

4. With the estimated cointegrating vectors, calculate the residual series of both halves and then merge them into one series, and determine the ADF $t-$statistic of the merged residual series.

5. Repeat procedures from step 2 to 4 at each point from $[0.15N]$ to $[0.85N]$, and construct a plot of all ADF statistics with respect to the breakpoint positions. Pick the minimum value of the curve; the corresponding position represents the optimal breakpoint.

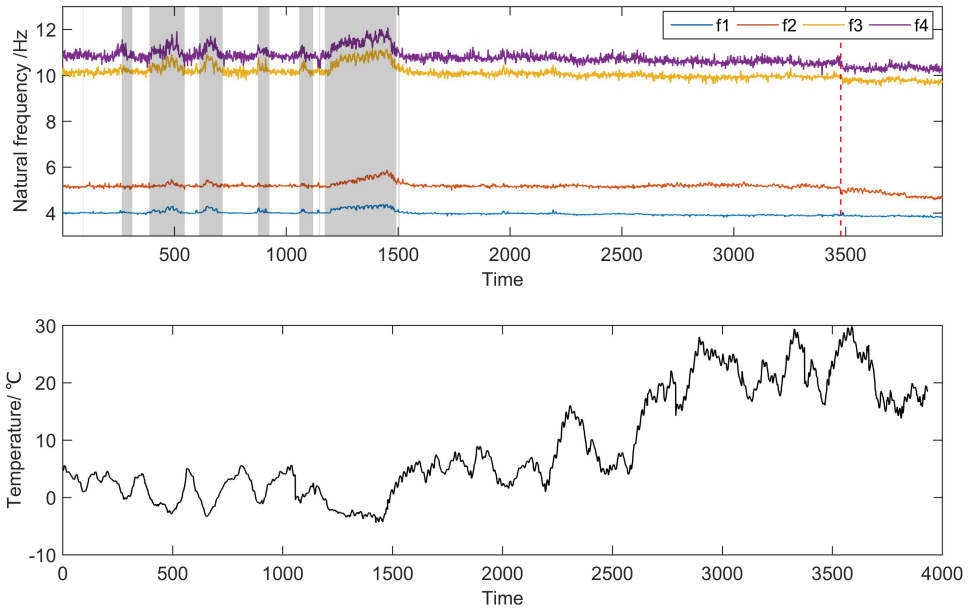


Figure 6.7: Upper panel: the first four natural frequency series of the Z24 Bridge, the red dashed line indicates damage introduction; Lower panel: the air temperature measurement during this time period.

6. With the optimal results from 5, using the environmental or operational variable as an index variable, construct a switching cointegration relationship and a stationary residual series, which should be purged of EOVs and still have the power to detect damage.

This regime switching cointegration method is suitable for dealing with nonstationary SHM data corrupted by EOVs, where system response may have two distinct behaviours with respect to EOVs. For example, bridges may have very different dynamic responses in hot and cold weather because of change of stiffness or boundary conditions. The current approach however, assumes that the measurements of the EOVs are accessible and only one kind of EOV is driving the nonlinear behaviour of the structure. Likewise, any engineering system with similar behaviour may be suitable for the proposed method, systems that accommodate more regimes can be possibly addressed by inserting more breakpoints in the proposed model.

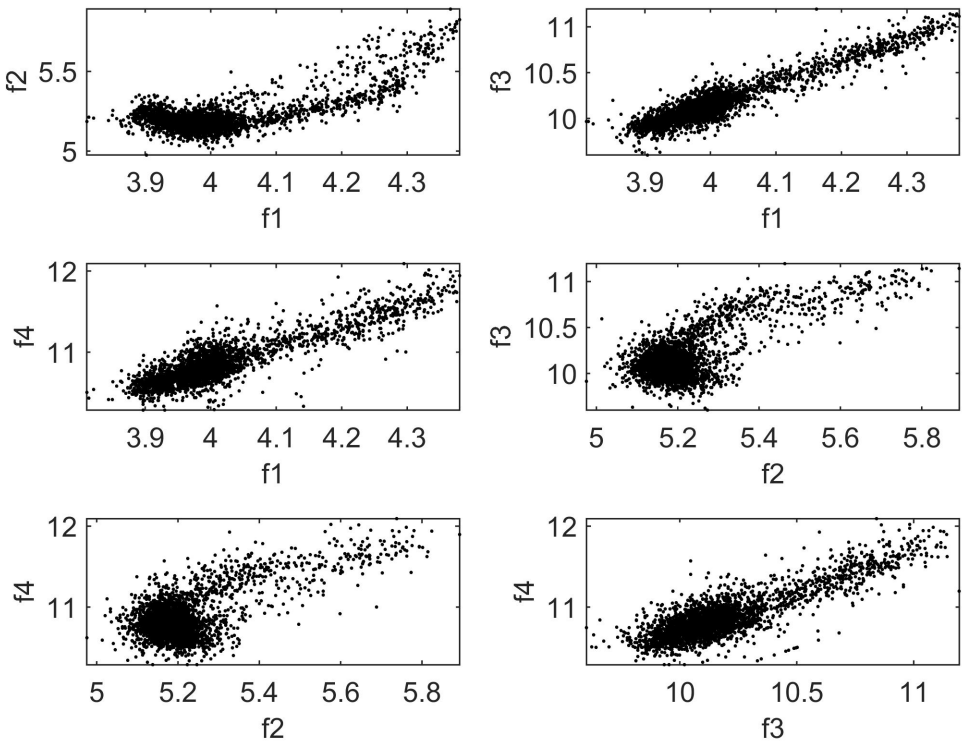


Figure 6.8: Mutual relationships of the first four natural frequencies.

## 6.5 An application to the SHM of the Z24 Bridge

The Z24 Bridge is now a benchmark study in the SHM community. The monitoring campaign spanned one year before the bridge was dismantled, before dismantling, several damage scenarios were implemented [66]. The monitoring campaign also recorded various environmental parameters including temperature, wind speed and humidity. In order to obtain the dynamic properties of the bridge, the natural frequencies were identified from acceleration measurements. The upper panel of Figure 6.7 illustrates the first four natural frequency series, $f_1$ to $f_4$, plotted with respect to time history; the vertical dashed line indicates the position where the first damage scenario was implemented. The temperature readings for this time period are plotted in the lower panel. Note that there are some missing data in the original dataset, thus the points corresponding to time instants when data missing occurs are all removed as a data pre-processing procedure.

On further examining the mutual relationship between the four natural frequen-

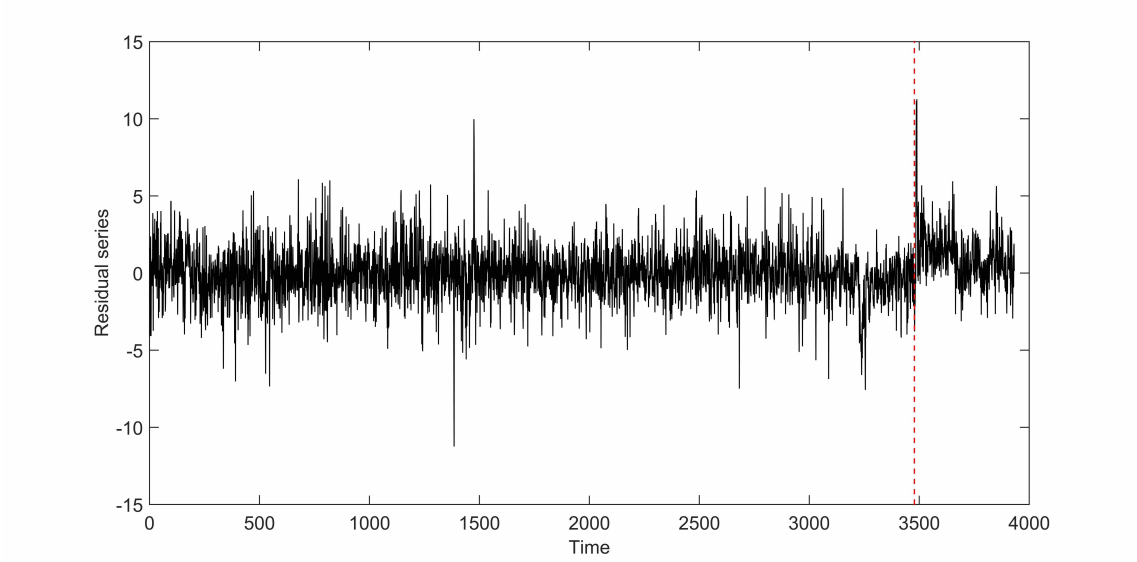


Figure 6.9: Residual series obtained using the conventional cointegration method, the red dashed line indicates where damage occurs.

cies, as shown in Figure 5.7 in Chapter 5, the second natural frequency $f_2$ has a clear bilinear relationship with the other three. As discussed above, it is a quite similar situation to the four-DOF system, the conventional cointegration method may therefore fail to model this phenomena. Following the cointegration approach proposed in [124], one out of every two from the first 3000 data points are used to estimate the cointegration model, and a residual series is obtained, as demonstrated in Figure 6.9. Even though the residual becomes largely stationary, the underlying cointegrating relationships are not accurately modelled, therefore the damage information has been smoothed out as well.

The aim is to build a damage indicator based on the healthy state of the bridge, so only the data before the dashed line are used for estimation; the same training data set from above (one out of every two from the first 3000 data points) are used for training purpose. Following the procedures in the last section, firstly the training series are rearranged in the order of the corresponding temperature series, as exhibited in Figure 6.10. Then the ADF statistics of all possible breakpoints are plotted in Figure 6.11, the lowest point of the curve is selected as the best breakpoint, the estimate is 0.98°C, and the estimated switching cointegration has

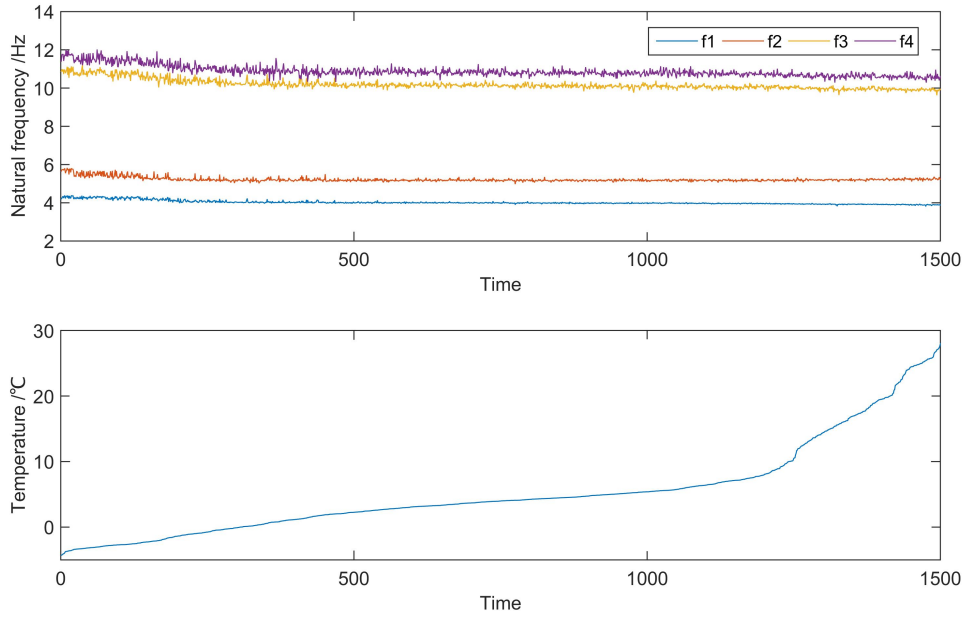


Figure 6.10: Upper panel: natural frequency series rearranged in the order of temperature; Lower panel: temperature series rearranged in the order of magnitude.

the following form:

$$\varepsilon_t = \begin{cases} 28.54 \times f1 + 6.53 \times f2 - 5.56 \times f3 - 9.62 \times f4 + 13.07, & \text{if } T \leq 0.98 \\ 23.02 \times f1 - 21.86 \times f2 - 1.00 \times f3 - 12.01 \times f4 + 161.15, & \text{if } T > 0.98 \end{cases} \tag{6.4}$$

Substituting the original series into (6.4), creates the residual series, which is plotted in Figure 6.12. The effect of EOVs has been mostly eliminated, the residual series before the dashed line is stationary. Three-sigma error bars are overlaid in the figure; one can see that the undamaged residual series lies predominantly within the confidence intervals; immediately after the damage introduction, the level of the residual has shifted drastically. To illustrate when the system enters another regime, the cold regime (when temperature drops below 0.98°C) is overlaid with shaded areas, the same shaded areas are duplicated on Figure 6.7. One can see during winter time that the bridge may switch frequently between two regimes; this may help to explain why conventional linear cointegration fails to model the relationships between the natural frequencies.

However, note that in Figure 6.12, there are several blips before the dashed line, nonetheless they will not affect the global stationarity. Several reasons may account

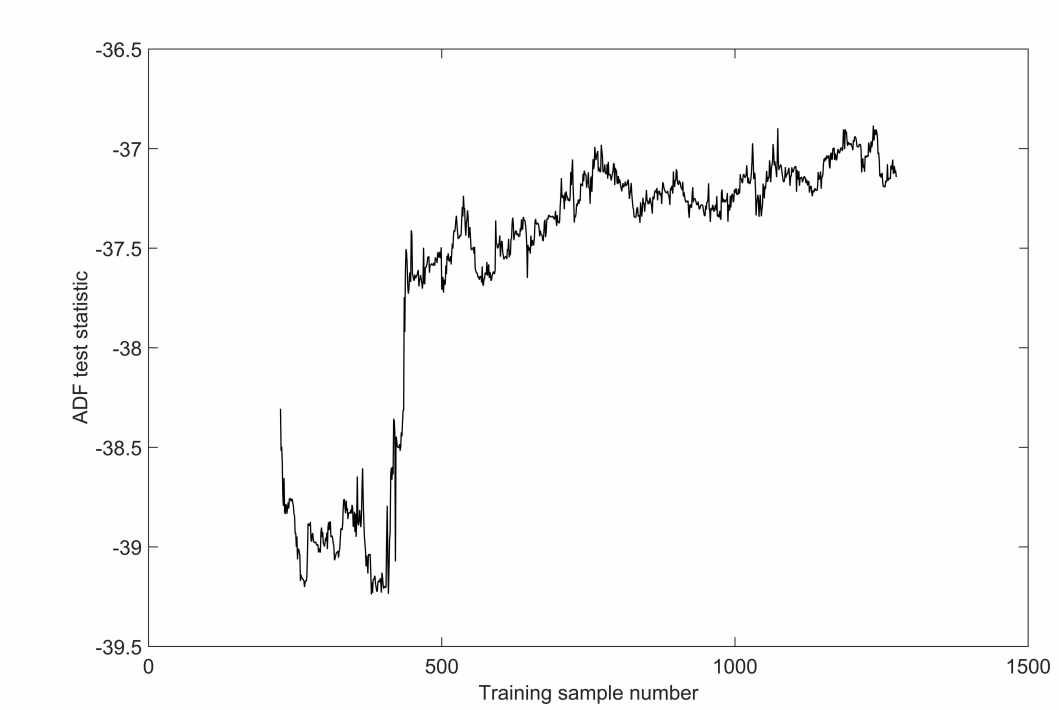


Figure 6.11: ADF statistics plot of the training sample points, the lowest point position determines the breakpoint position.

for these blips. Firstly, as the Johansen procedure is a maximum likelihood method, the cointegrating vectors are all point estimates, thus it is naturally prone to outliers. This may be further improved by putting the cointegration approach in a Bayesian framework, so as to give the posterior distribution of all the parameters. Another possible reason is the effect of the missing values referred to earlier; it may be that this has biased the estimation. Because of sensor faults, a small proportion of the original data are invalid, all the time instants when missing data occurs have been removed, which might bias the estimation of the breakpoint position, causing a small number of data points to enter the wrong regime.

Moreover, despite the fact that most parts of the residual series manifest safely within the error bars, there is a potentially upward trend between data points 3000 to 3500, before damage happens. There may be two main reasons to explain this trend: firstly, this trend might be a local behaviour of the stationary residual series, the local mean value may deviate from global mean sometimes, but it will eventually revert back to the global mean. One may observe that near data point 3500, the residual series has already started to drop back. Another possible explanation for this trend is that the training data used above are from cold seasons, while data

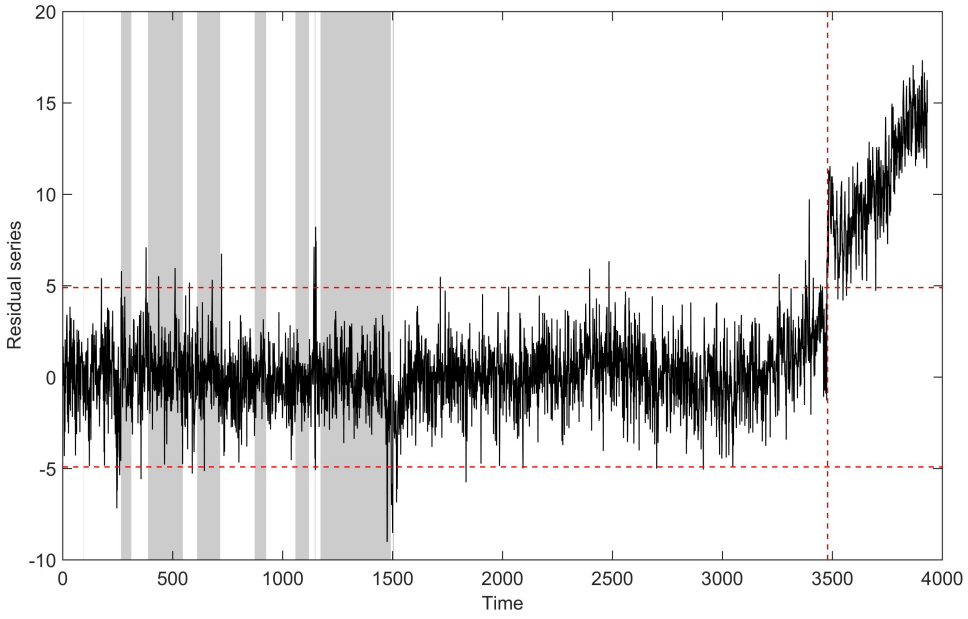


Figure 6.12: Residual series of the cointegration model, the red vertical dashed line indicates damage introduction, the two horizontal red lines represent the three standard error bars; the grey shaded areas show where cointegration switches regimes.

point 3000 to 3500 correspond to hot seasons, thus there might be another regime in the hot season. Unfortunately, due to the limited length of data (10 months), the behaviour of the regime-switching cointegration method cannot be evaluated in hotter months.

### Three-regime cointegration results

It is straightforward to apply the proposed method to a three-regime case, it is attempted here as at least one of the relationships shown in Figure 6.8 could be described as being more complex than bilinear (particularly that between $f1$ and $f2$). In the procedures of the last section, one should insert two breakpoints instead of one breakpoint in step 2; and then make the first breakpoint fixed and evaluate the second breakpoint at every possible position; subsequently, move the first breakpoint to the next position, and evaluate the second breakpoint again at every possible position; repeat the previous steps until every possible breakpoint position is evaluated. This is essentially an exhaustive search; it is feasible in the situation considered here as the size of the training set is not too large. In general problems,

it would be necessary to use a more sophisticated optimisation/search routine.

Data points 1 to 3000 shown in Figure 6.7 are used as training samples to estimate the two breakpoints, results are presented in Figure 6.13, where the vertical and horizontal axes represent the positions of the first and the second breakpoints, the colour indicates the magnitude of the ADF statistic evaluated at the corresponding breakpoints. The darkest point is selected as the optimal breakpoint position. According to Figure 6.13, two breakpoints are selected at 2.36°C and 3.95°C, and the estimated regime-switching cointegration has the following form:

$$\varepsilon_t = \begin{cases} -4.80 \times f1 + 1.14 \times f2 + 11.31 \times f3 - 9.27 \times f4 - 1.12, & \text{if } T \leq 2.36 \\ 27.76 \times f1 + 13.35 \times f2 + 8.26 \times f3 + 7.82 \times f4 - 348.94, & \text{if } 2.36 < T < 3.95 \\ -20.41 \times f1 + 14.40 \times f2 + 19.28 \times f3 - 5.64 \times f4 - 127.03, & \text{if } T \geq 3.95 \end{cases} \tag{6.5}$$

Substituting the original series into (6.5), one can obtain a residual series, as shown in Figure 6.14. The blue and grey areas show the first and second regimes respectively, and the left areas are the third regime. As expected, the three-regime-switching cointegration produces a stationary residual series which is still sensitive to damage. Interestingly, the residual shown in Figure 6.14 appears more stationary during the undamaged period than the results from one switching point. The two breakpoints estimated in this model coincide well with the switching response surface model estimated in [92], where a Bayesian treed linear model is fitted. Comparing to the previous chapter where Gaussian process regression is used to build the nonlinear cointegration relationship using an Engle-Granger approach, this chapter implements a cointegration method using the more powerful framework of the Johansen procedure. A more stationary residual is obtained in this chapter; a more interpretable model is presented, and the model itself is even easier to implement in practice.

## 6.6 Discussions and conclusions

The contents of this chapter are mainly about an exploratory approach aiming to enhance the conventional cointegration method in the context of structural health monitoring. Conventional cointegration methods can be used to remove the common trends in SHM data induced by environmental and operational effects; however, in

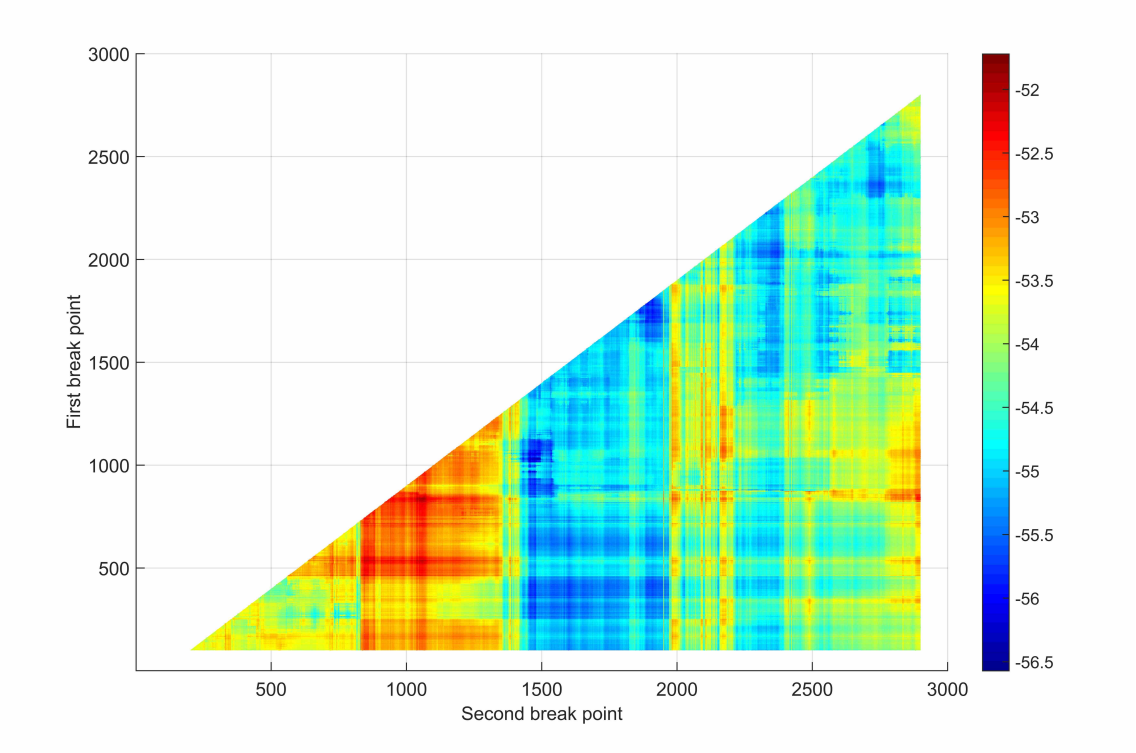


Figure 6.13: ADF statistic plot of the training sample points, the vertical axis represents the positions of the first breakpoint, the horizontal axis represents the positions of the second breakpoints; the colours in the plot indicate the value of the ADF statistic evaluated at the corresponding breakpoints.

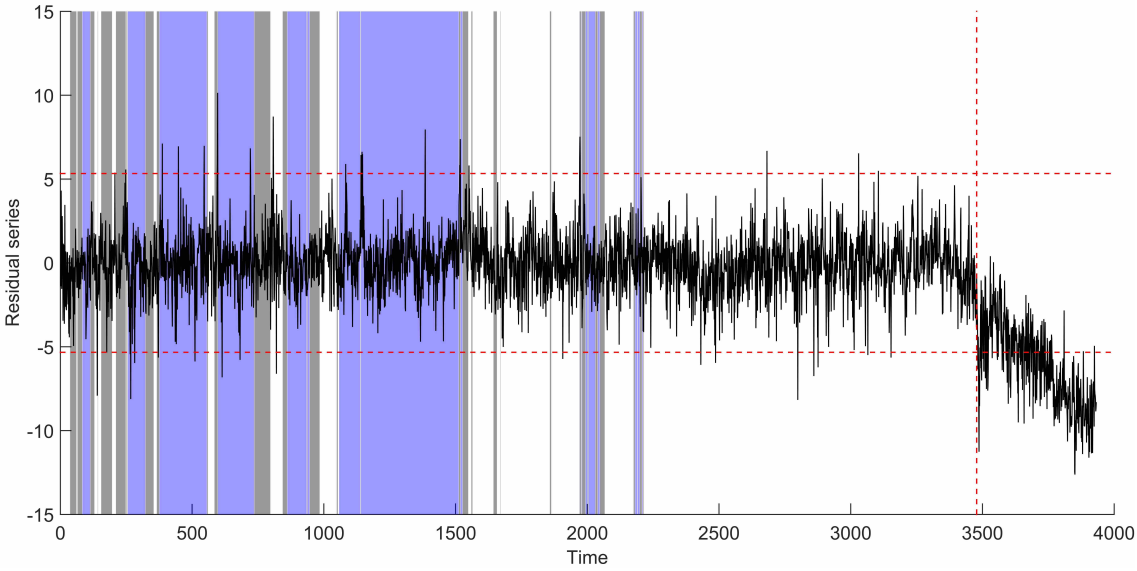


Figure 6.14: Residual series of the regime-switching cointegration model, the red vertical dashed line indicates damage introduction, the two horizontal red lines indicate the three standard error bars; the grey and blue shaded areas show where cointegration switches regimes.

some circumstances, nonlinearity in the system may undermine the cointegrating relationship; as such, a regime-switching cointegration method has been introduced in this chapter to address both nonlinearity and nonstationarity in SHM data. System responses may become nonstationary because of the effect of environmental variation, while sometimes the effect can simultaneously induce a nonlinear relationship between features. The proposed method allows the cointegrating relationship to switch according to the variation of environmental variables, the switching point is called a breakpoint. The position of the breakpoint is not likely to be known beforehand, thus all possible positions are evaluated by inserting a breakpoint at a time and assessing the global nonstationarity property of the residual series, the procedure is repeated throughout all possible breakpoint positions, and the test statistics are compared to find the most probable breakpoint position. The proposed method is employed here in two case studies, a simulated four-DOF system and the benchmark study of the Z24 Bridge; they both give very promising results, showing that all the benign environmental effects have been successfully removed. Once damage occurs, the underlying cointegration relationship no longer holds, therefore the residual series shows a very significant indication of damage, as the residual series become nonstationary again. However, it is important to note that there are still some restrictions of the current approach, which will be future directions for the authors:

- The Johansen procedure implemented is a maximum likelihood method, which gives a crisp estimate of the cointegrating vector. It is known that the maximum likelihood approach can be greatly affected by outliers and dependent on the selection of training data. A possible solution to this issue might be using cross validation to ascertain the model, but the variation of noise level and data missing can be difficult to deal with. Another possible direction would be to put the Johansen procedure in a Bayesian framework, instead of giving point estimates of cointegrating vectors, one could ideally have the whole posterior distribution of them; however, the complexity of Johansen procedure will present a big challenge.

- In this chapter, environmental measurements of temperature have been used to direct the regime shift of the system. One of the main benefits from the previous cointegration framework is that the measurements of EOVs are unnecessary. However, conventional cointegration is linear in nature, and may not suffice to account for the nonlinear behaviour observed in this chapter. To

address this, the measurement of temperature is taken into account to build a nonlinear model which still maintains a simple form. In this situation, temperature is the main driving variable of the nonlinear relationship between the natural frequencies, and other EOVs including wind speed, humidity are unnecessary in the analysis.

Strictly speaking, the method presented here should be considered a hybrid regression/cointegration approach. In using measurements of the temperature in order to construct the cointegration regimes, the approach represents a step forward, followed by a small step back; however, there are overall advantages. It is important to note that, if a linear switching behaviour is present, any global model  polynomial or otherwise  is likely to be *input-dependent*, and may not generalise well away from the training data. On a related issue, global models may need more parameters to explain piecewise-linear behaviour and will be less parsimonious.

An ideal enhancement here would be to allow the choice of a switching point without measurement of the environmental variable. One possible direction would fall in the domain of change point detection, a good reference can be found in [172], where a Bayesian online change point detection algorithm is developed, which might be helpful to identify a switching point purely based on data. Another interesting possibility is provided by the idea of inferential parametrisation [173]. As in [173] one could in principle, infer a proxy for the temperature measurement directly from the natural frequencies themselves. In fact, a preliminary study has shown that this can be accomplished for the Z24 data; however, there is an important issue to overcome before those results can be shown with confidence. The point is this; if the switching parameter (temperature) in this case is learned from data, it has to be learned from training data unaffected by damage. This means that there is no guarantee that, when damage occurs, the previously learned inferential parameter is still accurate. The Z24 data itself is not sufficient to validate the approach because the full range of environmental conditions were not available for any of the damage states of the bridge. The inferential parameterisation approach is a work in progress.

- Another possible enhancement of this method is to incorporate more regimes in the cointegration. In the current method, only two and three regimes are used, which captures well the nonlinear property of icing of the bridge. How-

ever in many other cases, there are possibly more than three regimes. The approach itself can be easily extended to the multiple regime context, however the difficulty is how to determine the number of regimes. More specific hypothesis test methods can be developed accordingly.

- Away from the example presented here, it is possible, or indeed likely, that a structure may be influenced by multiple EOVs at the same time. However, not every EOV may induce nonlinear (regime-switching) behaviour in the features of interest. Observing the phenomena of stiffening of the asphalt in the Z24 case, this chapter assumes that temperature is the main EOV driving the regime-switching behaviour of that particular structure. This assumption, however, may be violated in more of an operational environment, if, for example, the bridge had been opened to traffic. A challenging scenario in this context would be if multiple EOVs with multiple regimes induced a nonlinear relationship between features of interest. In such a case, an entire embedded submanifold of switching points might be present within the space of EOVs. A possible solution to this issue may be to put the model in the framework of decision tree learning [174], where a high-dimensional input space can be partitioned into finite discrete domains, each domain representing a class of features determining the regime in which the structure is behaving. Again, research is in progress on this matter.

# Chapter 7

# The TBATS Model for Heteroscedastic Cointegration

With the rapid advancement of sensing technology, the availability and accessibility of all kinds of data from structures has been greatly improved. As the duration of recorded data grows, seasonal effects become inevitably important, especially for long-term monitoring. Meteorological variations and human activities might couple with the behaviour of the structures, making the modelling of underlying states of the structure extremely difficult. More specifically, the seasonal effects may produce input-dependent noise in the measurements of the structure, or heteroscedastic noise as in the statistical literature. As is well known, many statistical and machine learning estimation methods are based on ordinary least squares (OLS) or maximum likelihood; thus heteroscedastic noise may bias the estimation of the model, causing misleading judgements of the health state of the structure. Therefore, this study seeks to further strengthen the practice of the cointegration method; a well-established method from the time series literature, called the TBATS model, is explored to deal with seasonal effects in SHM data. After suppressing the heteroscedasticity in the series, cointegration analysis is performed to build a damage sensitive residual series.

This chapter begins with a motivating example, followed by brief theoretical introductions to the exponential smoothing method and the TBATS model. A synthetic case study will be presented in the fifth part to illustrate the proposed method. Another case study of the National Physical Laboratory (NPL) Bridge with the

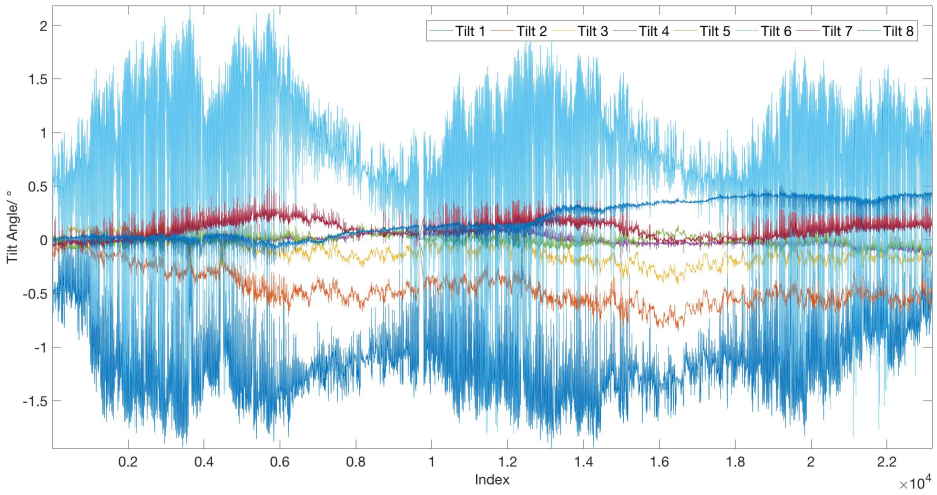


Figure 7.1: Data collected from all the 8 tilt sensors installed on the NPL Bridge.

proposed method is presented in the same section, the last part includes summary and some discussions.

## 7.1 A Motivating Example

Nowadays, many long-term SHM studies have continuously collected years, if not decades, worth of sensor data from structures. When time span and resolution of available data are sufficient, seasonality or periodicity is becoming crucial for data modelling.

Consider the National Physical Laboratory (NPL) Bridge for example; the NPL Bridge was monitored for an extensive time span, covering a wide range of seasonality induced by environmental variations. The monitoring campaign also introduced several kinds of damage scenarios to the bridge. However, observing time series of measured tilt data, as shown in Figure 7.1, no immediate damage information is available as it is overwhelmed by the environmental variations. These time series are clearly nonstationary, both in mean and variance, unfortunately, few methods are valid for such kinds of time series. Worden et al. [175] attempted to model the tilt sensor data using the linear cointegration method (theories of which will be reviewed shortly).

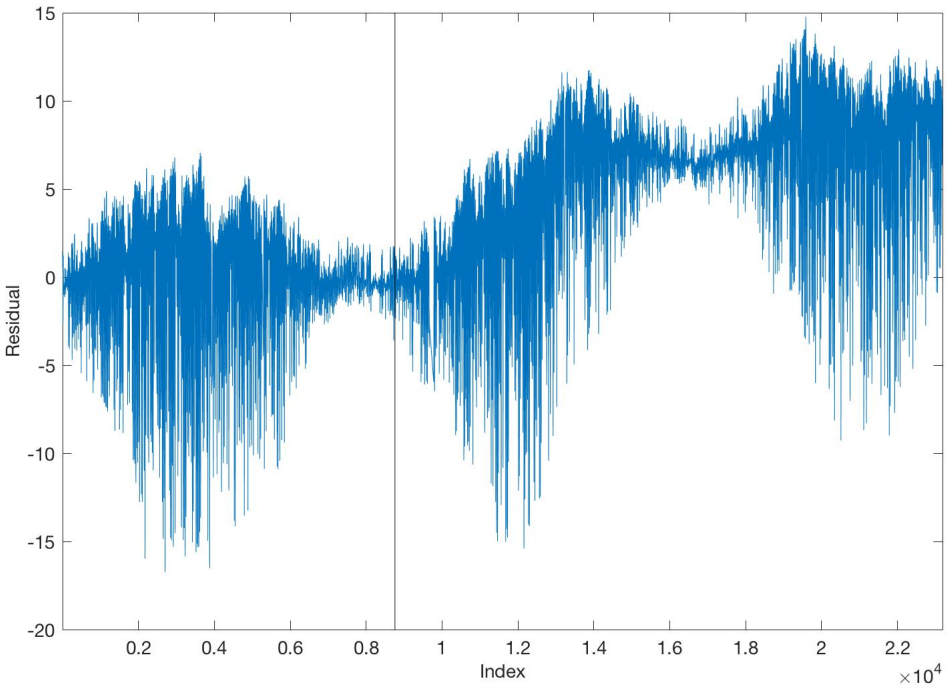


Figure 7.2: Cointegrated residual series from the 8 tilt sensor signals acquired from the NPL Bridge; the vertical black line indicates the end of the training data for cointegration.

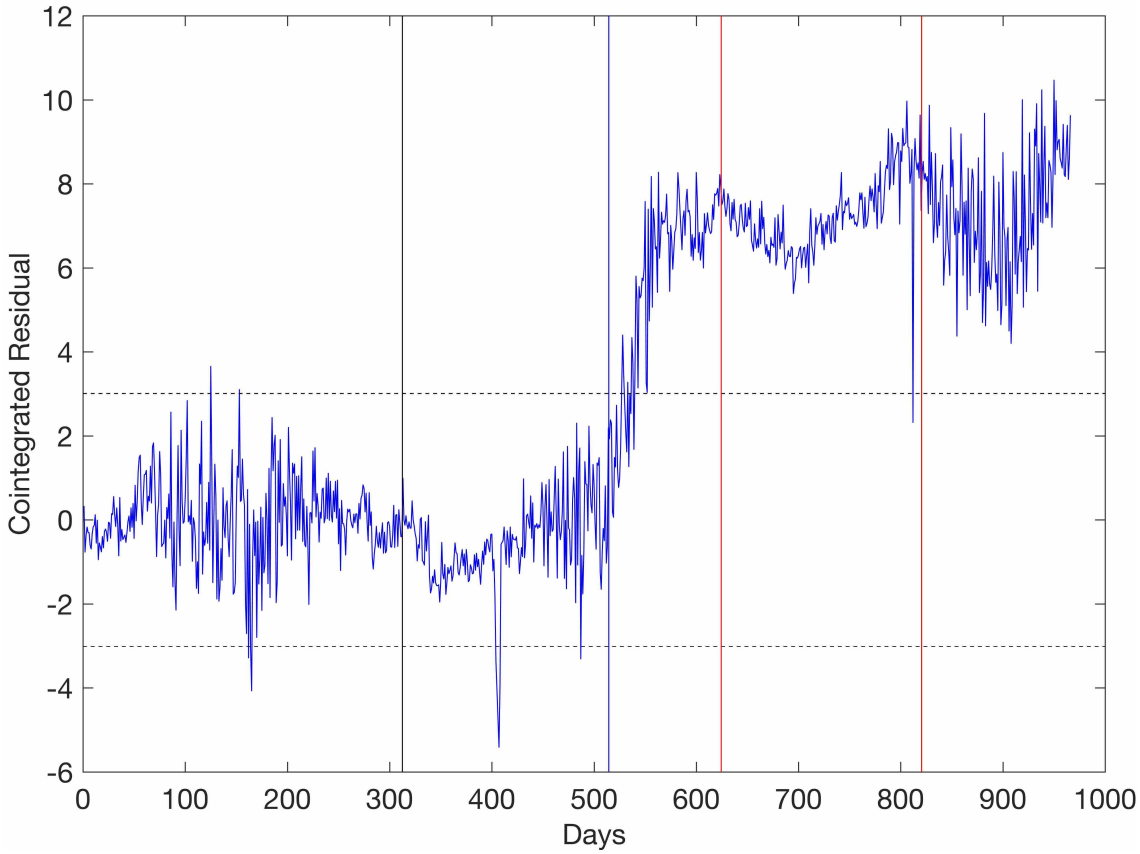


Figure 7.3: X-bar chart plot of the cointegrated residual.

Cointegration was applied to the eight tilt sensor time series, in order to form a stationary residual for damage detection purposes. As demonstrated in Figure 7.2, the vertical black line shows the end of the training samples for cointegration, which accounted for a full year of environmental variations. The residual series clearly possesses time-varying variance, the underlying seasonality has severely undermined the effectiveness of the algorithm. With the help of the Statistical Process Control (SPC) chart, the "X-bar chart"in this case [176], the situation can be somewhat alleviated. The measurements of the tilt sensor were hourly-based, every 24 measurements were averaged to obtain a daily representative sample, the resulting residual series is shown in Figure 7.3, the horizontal dashed lines indicate $\pm 3\sigma$ (standard deviation) control limits, the vertical blue line marks where the first damage scenario was implemented. Despite the nonstationarity in the residual variance, the algorithm clearly retains the power of damage detection, such that after the damage introduction, the mean of the residual gradually goes beyond the control limits.

In terms of seasonality/periodicity in the NPL Bridge data, the daily cycle is an

apparent one (usually synchronised with the daily cycle of temperature). Another important observation is that as time approaches the middle of a year, the amplitude of the daily cycle gets bigger as well, it will then shrink towards the end of a year. This might be caused by the fact that the tilt sensors may be sensitive to temperature variations, such that their associative measuring errors may be amplitude dependent as well. Many econometric studies have attempted to integrate seasonality into the original cointegration framework, most of them stem from [144], where seasonal unit root tests and seasonal cointegration are developed. However, this chapter will look in a different direction, which is to understand the different components in the original time series, and apply cointegration on the decomposed long-term trend components. This is partly inspired by [57], which finds that cointegration tends to manifest itself on longer time scales. Thus, it can be advantageous to decompose the original time series into long-term trend components, heteroscedastic seasonality components and noise, and then apply cointegration on the trend components, which contain information that is of most interest. In the subsequent sections, the decomposition framework adopted in this chapter, the TBATS model, will be reviewed in detail; the NPL Bridge will be re-examined with the proposed method in the later section.

## 7.2 Exponential Smoothing and The TBATS Model

### 7.2.1 Introduction

To decompose a time series, there are many possible solutions offered by various research communities: From the perspective of signal processing, Fourier-based transforms, the discrete wavelet transform (DWT), the empirical mode decomposition, etc. are some of the mainstream methods adopted. Consider the DWT for example, it passes a raw signal through a series of quadratic mirror filters, both high-pass and low-pass filters. The high-pass filter produces details and the low-pass produces approximations. The process is repeated on the detailed signal until the last level is reached, the detail at each level expresses how the signal manifests itself at that level (scale band). In the wavelet context, each level is expressed by a number of wavelets which can be fitted to the interval of interest [57]. While in the time series domain, time series data are normally considered to be combinations of different components which exhibit distinct behaviours, examples of such components are

trend components, seasonal components, and error components, and the forms of combination can be additive, multiplicative, or both.

Studying the characteristics of the motivating example above, this chapter chooses a time series decomposition method over a signal processing method for the following reasons. First, as the magnitude of the daily cycle in the NPL data is time-varying, filter-based methods will struggle to separate this out, whereas time-series-based methods can have greater flexibility in specifying the seasonal components. Secondly, the TBATS model is chosen to be used in this chapter, because it is good at dealing with multiple seasonality in time series models, and also able to model multiplicative seasonal components, whereas other conventional time series decomposition methods, the STL decomposition for instance [177], tend to incorporate just one time-invariant seasonal component. Finally, the TBATS model is built using state space models, which enable probabilistic predictions rather than point estimates.

Exponential smoothing methods have been amongst the most widely-used and successful time series methods for decomposition and forecasting, since they were established in the late 1950s. Generally, predictions with exponential smoothing are made with weighted averages of the past observations, with the weights exponentially decaying as the observations move away from the current time instant. Recent developments have established that exponential smoothing methods can be greatly enhanced within the framework of an innovations state space model [178]. They can not only generate the same point estimate, but also calculate the prediction intervals. The innovations state space model differs from its conventional analogue, the state space model, such that it only allows a single source of error (innovations) for both state and measurements equations, but it is more robust, and it has fewer undetermined parameters; a thorough investigation on this topic can be found in [179].

### 7.2.2 TBATS Model Forms

Complex seasonal patterns exist in real engineering applications, for example multiple seasonality, dual-calendar effects (the coupling effect of the solar calendar and the Chinese calendar for instance). To overcome this issue, De Livera et al. have introduced a novel approach based on an innovations state space model called the TBATS

model [180]. The acronym 'TBATS' represents their key features: **T**rigonometric seasonality, **B**ox-Cox transformation, **A**RMA errors, **T**rend and **S**easonal components. Consider a time series $\{y_t\}_{t=1}^{N}$, the TBATS model has the following form:

$$y_t^{(\omega)} = \begin{cases} \frac{y_t^{(\omega)}-1}{\omega}; & \omega \neq 0 \\ \log y_t; & \omega = 0 \end{cases} \tag{7.1}$$

$$y_t^{(\omega)} = l_{t-1} + \phi b_{t-1} + \sum_{i=1}^{T} s_{t-1}^{(i)} + d_t \tag{7.2}$$

$$l_t = l_{t-1} + \phi b_{t-1} + \alpha d_t \tag{7.3}$$

$$b_t = (1-\phi)b + \phi b_{t-1} + \beta d_t \tag{7.4}$$

$$s_t^{(i)} = \sum_{j=1}^{k_i} s_{j,t}^{(i)} \tag{7.5}$$

$$s_{j,t}^{(i)} = s_{j,t-1}^{(i)} \cos \lambda_j^{(i)} + s_{j,t-1}^{*(i)} \sin \lambda_j^{(i)} + \gamma_1^{(i)} d_t \tag{7.6}$$

$$s_{j,t}^{*(i)} = -s_{j,t-1} \sin \lambda_j^{(i)} + s_{j,t-1}^{*(i)} \cos \lambda_j^{(i)} + \gamma_2^{(i)} d_t \tag{7.7}$$

$$d_t = \sum_{i=1}^{p} \varphi_i d_{t-i} + \sum_{i=1}^{q} \theta_i \epsilon_{t-i} + \varepsilon_t \tag{7.8}$$

Equation (7.1) is the Box-Cox transformation of the series $y_t$, which is designated to eliminate skewness of the distribution of the data, such that the data becomes more normally distributed, making it easier to implement maximum likelihood in the estimation part. This can be particularly beneficial for SHM data, as this mostly tends to be non-normally distributed. Like many other transformation methods, the Box-Cox transformation may raise some concerns about its applicability. Given the fact that the aim of SHM is to detect the presence of outliers, would that be undermined by the Box-Cox transformation? The author argues that one need not worry too much, as the idea here is to create series for cointegration, and damage will manifest itself by breaking the cointegration relationship when damage occurs. This is fundamentally different from the conventional metric-based outlier detection methods.

Equation (7.2) is the main representation of the TBATS model, where $y_t^{(\omega)}$ is the transformed series of $y_t$, $l_{t-1}$ is the local level at time $t-1$, and $b_{t-1}$ is the short-run

trend at time $t-1$, $s_{t-1}^{(i)}$ is the seasonal components, $i$ is the index of the type of seasonality (as the model may allow multiple types of seasonal components), and $T$ is the total number of types of seasonality, $d_t$ is an ARMA process disturbance.

Equations (7.3) to (7.8) explain the corresponding components in detail. Equation (7.3) explains that the current level of the series is determined by the previous level and the short run adjustment $b_{t-1}$ times a damping parameter $\phi$; $\alpha$ dictates the smoothness of the level series. Equation (7.4) indicates the fact that the short-run trend consists of effects from the long-run trend $b$ and the left over short-run effect from the previous time step, the damping parameter $\phi$ is the same as the one in equation (7.3). In practice, the short-run adjustments can sometimes be omitted if one only wants the smooth trend series. Equations (7.5) to (7.7) are seasonal components based on a Fourier series with ARMA errors. Equation (7.8) is a stationary ARMA residual.

### 7.2.3 Innovations State Space Model Forms

To derive the model likelihood and subsequently estimate the model parameters, one can first rewrite the TBATS model into an innovations state space model form. For the sake of parsimony of this illustrations, only two seasonal patterns are considered here, and each seasonal component consists of only one harmonic (one frequency component); the error process is set to be an ARMA(1,1) process, i.e. $T = 2, k_1 = 1, k_2 = 1, p = 1, q = 1$. Therefore, equation (2) can be reorganised as:

$$y_t^{(\omega)} = l_{t-1} + \phi b_{t-1} + \sum_{i=1}^{2} s_{t-1}^{(i)} + \varphi_1 d_{t-1} + \theta_1 \epsilon_{t-1} + \varepsilon_t \tag{7.9}$$

The corresponding innovations state space model has the following form:

$$y_t^{(\omega)} = \mathbf{w}' \mathbf{x}_{t-1} + \varepsilon_t, \tag{7.10}$$

$$\mathbf{x}_t = \mathbf{F}\mathbf{x}_{t-1} + \mathbf{g}\varepsilon_t \tag{7.11}$$

where the state vector $\mathbf{x_t} = (l_t, b_t, \mathbf{s_t^1}, \mathbf{s_t^2}, d_t, d_{t-1}, \varepsilon_t, \varepsilon_{t-1})'$, where $\mathbf{s_t^1} = (s_{1,t}^{(1)}, s_{1,t}^{*(1)})$, $\mathbf{s_t^2} = (s_{1,t}^{(2)}, s_{1,t}^{*(2)})$; the emission vector $\mathbf{w}$ equals $(1, \phi, 1, 0, 1, 0, \varphi_1, \theta_1)'$, and $'$ is a

transpose operator; the transition matrix $\mathbf{F}$ has the following form:

$$\mathbf{F} = \begin{bmatrix} 1 & \phi & 0 & 0 & 0 & 0 & \alpha\varphi_1 & \alpha\theta_1 \\ 0 & \phi & 0 & 0 & 0 & 0 & \beta\varphi_1 & \beta\theta_1 \\ 0 & 0 & \cos\lambda_j^{(1)} & \sin\lambda_j^{(1)} & 0 & 0 & \gamma_1^{(1)}\varphi_1 & \gamma_1^{(1)}\theta_1 \\ 0 & 0 & -\sin\lambda_j^{(1)} & \cos\lambda_j^{(1)} & 0 & 0 & \gamma_2^{(1)}\varphi_1 & \gamma_2^{(1)}\theta_2 \\ 0 & 0 & 0 & 0 & \cos\lambda_j^{(2)} & \sin\lambda_j^{(2)} & \gamma_1^{(2)}\varphi_1 & \gamma_1^{(2)}\theta_1 \\ 0 & 0 & 0 & 0 & -\sin\lambda_j^{(2)} & \cos\lambda_j^{(2)} & \gamma_2^{(2)}\varphi_1 & \gamma_2^{(2)}\theta_2 \\ 0 & 0 & 0 & 0 & 0 & 0 & \varphi_1 & \theta_1 \\ 0 & 0 & 0 & 0 & 0 & 0 & 0 & 0 \end{bmatrix}$$

and $\mathbf{g} = (\alpha, \beta, \gamma_1^{(1)}, \gamma_2^{(1)}, \gamma_1^{(2)}, \gamma_2^{(2)}, 1, 1)'$. Since TBATS models can be converted into standard innovations state space model forms, they can be nicely fitted into the framework of the Kalman filter. However, the unknown parameters, including the initial conditions, are computationally heavy to estimate, the authors in [180] used a smart algorithm to significantly reduce the computational burden, which will be briefly introduced in the following section. It is also worth noting that the above specifications are just for the simplest form of the TBATS model, one can adapt the above matrices according to specific model settings, comprehensive notations and derivations can be found in [180].

### 7.2.4 Parameter Estimation

After the Box-Cox transformation, a maximum likelihood estimation method is then used to estimate all the parameters in the model. One can immediately see that the main obstacle here is the large number of parameters, which includes all the damping parameters, the smoothing parameters, the Box-Cox transformation parameter, the ARMA coefficients, and also the initial conditions of the innovations state space model. The trick that the paper [180] employed is to make use of the single error term $\varepsilon_t$, and concentrate the initial conditions out of the likelihood: substituting (7.10) into (7.11), one can have $\mathbf{x}_t = \mathbf{F}\mathbf{x}_{t-1} + \mathbf{g}(y_t^{(\omega)} - \mathbf{w}'\mathbf{x}_{t-1}) = (\mathbf{F} - \mathbf{g}\mathbf{w}')\mathbf{x}_{t-1} + \mathbf{g}y_t^{(\omega)}$; then, by substituting $\mathbf{x}_t$ back to $\mathbf{x}_0$ in equation (10), one can have,

$$\begin{aligned} \varepsilon_t &= y_t^{(\omega)} - \mathbf{w}'\mathbf{x}_{t-1} \\ &= y_t^{(\omega)} - \mathbf{w}' \sum_{j=1}^{t-1} (\mathbf{F} - \mathbf{g}\mathbf{w}')^{\mathbf{j-1}}\mathbf{g}y_{t-j}^{(\omega)} - \mathbf{w}'(\mathbf{F} - \mathbf{g}\mathbf{w}')\mathbf{x_0} \end{aligned}$$

From above, one can see that the initial condition $\mathbf{x_0}$ can be regarded as linearly related to the error term $\varepsilon_t$, therefore $\mathbf{x_0}$ can be estimated using an ordinary least squares method and substituted into the likelihood. This is one of the advantageous features of innovations state space models in comparison to the conventional state space model alternatives, it leads to savings on parameter estimation and perhaps, more accurate predictions. The representation and derivation of the likelihood is cumbersome and omitted here, readers can find the full details in [180].

### 7.2.5 Model Selection

For most applications, seasonal periods are known *a priori*. In the motivating example, a daily cycle seems an obvious choice, as the measured tilts are aligned with the daily temperature cycle. Additionally, the yearly cycle is also a common seasonal period, unfortunately in the NPL data, only one year worth of data can be used for training, making it hard to single out the yearly components from the training data. In cases where seasonal periods are unknown, one can apply a Fourier analysis on the series first to identify significant frequency components. In the scenario of multiple seasonality, one can use the Akaike Information Criteria (AIC) to evaluate every possible seasonal model, and choose the optimal model based on AIC values.

To determine the number of harmonics $k_i$ in the seasonal components in equation (7.5), appropriate de-trending algorithms need to be applied to the original series first; then one fits the linear regression $\sum_{i=1}^{T}\sum_{j=1}^{(k_i)} a_j^{(i)}\cos(\lambda_j^{(i)}t) + b_j^{(i)}\sin(\lambda_j^{(i)}t)$ to the de-trended series. Starting from one harmonic and gradually adding more, one applies an F-test to each number of harmonics, so as to find the most significant $k_i$ for the $i^{th}$ seasonal component. The above procedure is repeated for every seasonal component and one computes the corresponding AIC value, adding the number of harmonics until the minimum AIC is achieved.

To determine the orders $p$ and $q$ of the ARMA models, first a TBATS model without the ARMA error is fitted as a baseline model, the residual series of which will be fitted with an ARMA$(p, q)$ model; then a model is fitted again but with an ARMA$(p, q)$ error process. If the newly fitted model has a lower AIC value then the baseline model, then the orders $p$ and $q$ will be accepted.

### 7.2.6 Summary

TBATS can be viewed as a model decoupling the seasonality and trend components which are often modelled together in many seasonal models (SARIMA for example [181]). A few advantages that the TBATS model may offer are obvious: firstly, time varying parameters in the seasonal components (equations (7.5) to (7.7)) are suitable for describing changing variances in the data. Secondly, it allows for the accommodation of possible multiple seasonal effects, for example the nested effect of daily, weekly, monthly and annual periodicity, potentially suitable for analysis of operational data. Lastly, it allows any autocorrelation in the residuals to be taken into account.

However, the TBATS model can also cause trouble in a few ways: a large parameter space is set to be estimated, including the initial state of the parameter space. Furthermore, the Box-Cox transformation limits its application to only positive time series; but possible pre-processing of data can overcome this difficulty. Note that the Box-Cox transformation is an invertible transformation, one can easily recover the original series after transformation. It is also worthwhile to explore other forms of mathematical transformations, affine transformation for instance, might be a good choice. Finally, irregular calendar effects, for example the Chinese lunar calendar, might cause trouble, but this may also be addressed by introducing a dummy variable [180]. Therefore, complex seasonal variations observed in long-term monitoring data can be well modelled by the TBATS model, which can be hugely beneficial for further research.

## 7.3 Case Studies

Normally, cointegration analysis requires the noise term to be *i.i.d.* stationary Gaussian noise. In fact, *i.i.d.* stationary Gaussian noise assumption is ubiquitous in many time series methods, which often employ ordinary least squares or maximum likelihood estimation approaches. However, *i.i.d.* stationary Gaussian noise or homoscedastic noise is not always the case in real world applications, the existence of input dependent noise or heteroscedastic noise may therefore bias many estimation algorithms. In the context of SHM, the existence of multiple seasonality/periodicity is sometimes the source of heteroscedastic noise. Motivated by this, this section will

first separate the seasonal components from the original time series, in a attempt to suppress the associated heteroscedasticity. Cointegration is then applied to the de-seasonalised series. The proposed idea will be tested on two case studies here, a simulated cantilever beam and real monitoring data from a bridge.

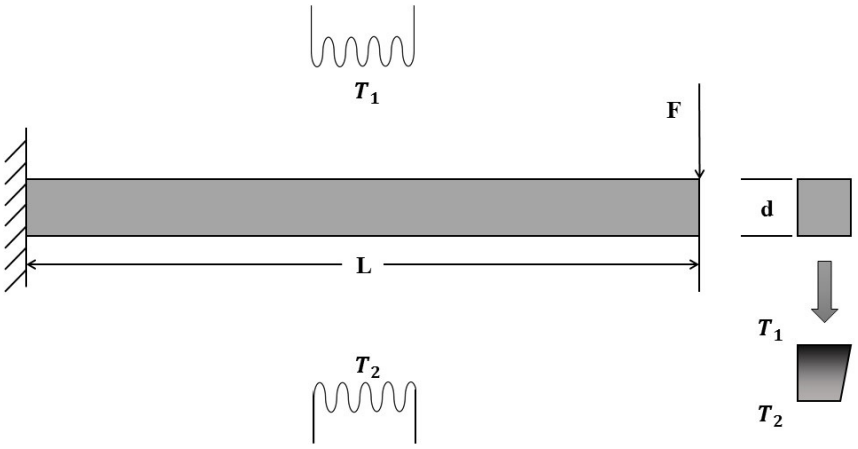


Figure 7.4: Schematic plot of a cantilever beam with a force applied on the end; the top and bottom of the beam are applied with different temperature fields, the cross-section plot shows the gradient distribution of temperature.

### 7.3.1 Case Study I: A Cantilever Beam

Consider a steel cantilever beam with a force applied to the free end, as shown in Figure 7.4. Different thermal fields are applied onto the top and bottom of the beam, so as to mimic the uneven distribution of the temperature profile of a structure operating in a real environment. In addition, to mimic the daily and seasonal patterns, and a linear trend of temperature in the real world, the temperature fields $T_1$ and $T_2$ are imposed to be:

$$T_1 = 10 \times \left\{\sin(12\pi t) + \sin(4\pi t) + 3t \times 10^{-3} - 2\right\} \tag{7.12}$$

$$T_2 = 8 \times \left\{\sin(12\pi t - 0.5\pi) + \sin(4\pi t) + 3t \times 10^{-3} - 2\right\} \tag{7.13}$$

As the beam is made from isotropic material, the temperature of the beam is monotonically decreasing from the top to the bottom, with a linear gradient, which is illustrated in the cross-sectional plot in Figure 7.4. 10000 sample points are simulated, as shown in Figure 7.5. Because temperature is assumed to change over time, the stress and deflection of the beam will also change accordingly. There are two reasons why the beam's deflection will change with temperature; firstly, the Young's modulus of steel is normally considered to be linearly correlated with temperature; secondly, the temperature gradient of the beam will also change with time, thus the thermal expansion of the beam will be varying with time. The angle of rotation of the beam is therefore composed of two parts, mechanical and thermal rotation, as expressed in the following equations:

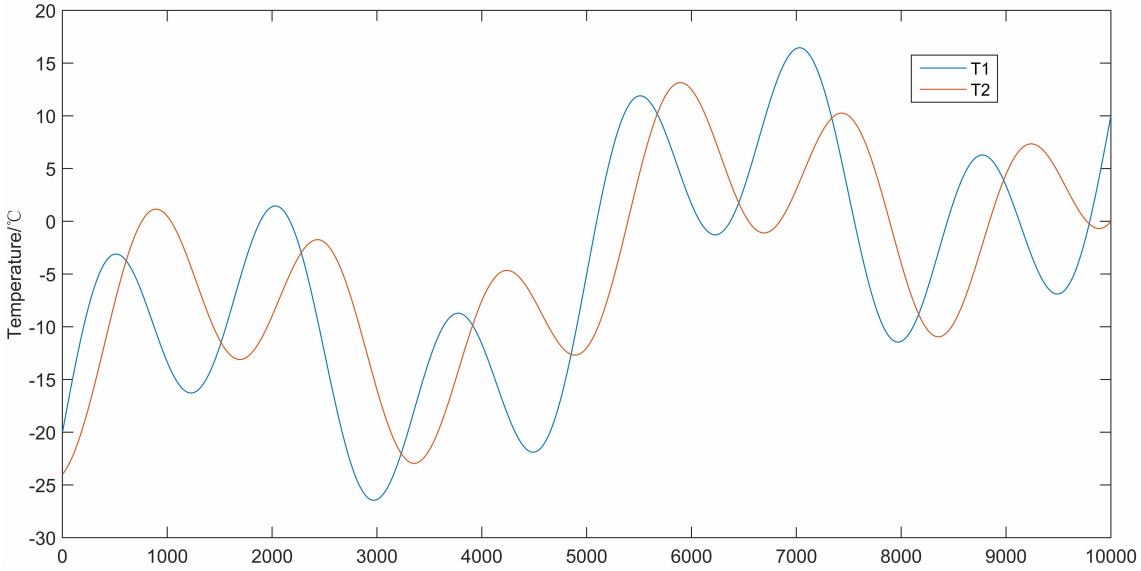


Figure 7.5: Temperature of the top of the cantilever beam $T_1$, and temperature of the bottom $T_2$.

$$Thermal : \theta_T = \frac{\alpha(T_1 - T_2)x}{d} \tag{7.14}$$

$$Mechanical : \theta_M = \frac{F(-Lx + \frac{1}{2}x^2)}{EI} \tag{7.15}$$

$$Overall : \theta = \theta_T + \theta_M \tag{7.16}$$

where $\alpha$ is the thermal expansion coefficient, and $x$ is the position of the beam from the fixed-point at the left end.

### Simulations

The thermal field in Figure 7.5 is applied to the cantilever beam, and the angles of rotation of four positions on the beam, $(0.25L, 0.5L, 0.75L, L)$, are evaluated. $4 \times 10000$ samples points are therefore obtained. It is not uncommon in engineering, that measurement noise can be input-dependent, or in econometric terms heteroscedastic noise. To simulate this situation, an amplitude-dependent Gaussian noise is added to the theoretical results, as expressed by the following:

$$\hat{\theta} = \theta + 0.1 \times \theta \times \epsilon_t \tag{7.17}$$

where $\hat{\theta}$ is the measured rotation, $\epsilon_t$ is Gaussian noise with $\epsilon_t \sim N(0, 1)$. The measurements with heteroscedastic noise corruption are plotted in Figure 7.6.

To simulate damage, the stiffness of the beam is reduced by 50% after data point 7500, as illustrated by a black vertical line in Figure 7.6. Although damage is introduced, only a slight shift in amplitude is visible; changes due to temperature variations are still dominant.

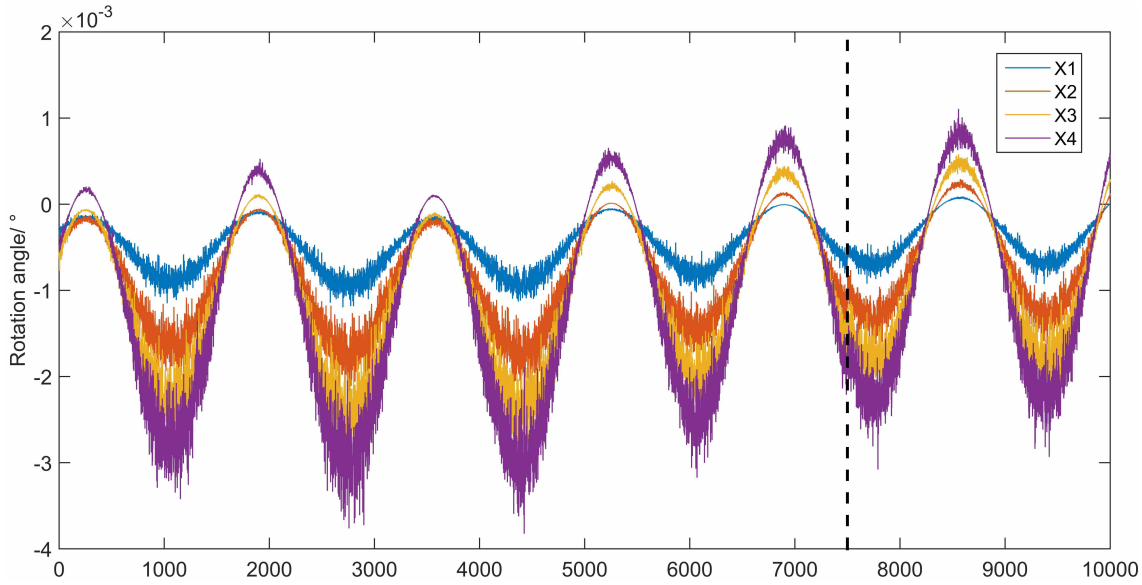


Figure 7.6: The angles of rotation measured at the four positions$(0.25L, 0.5L, 0.75L, L)$ of the beam, corrupted with heteroscedastic noise; the black vertical line indicates where damage is simulated.

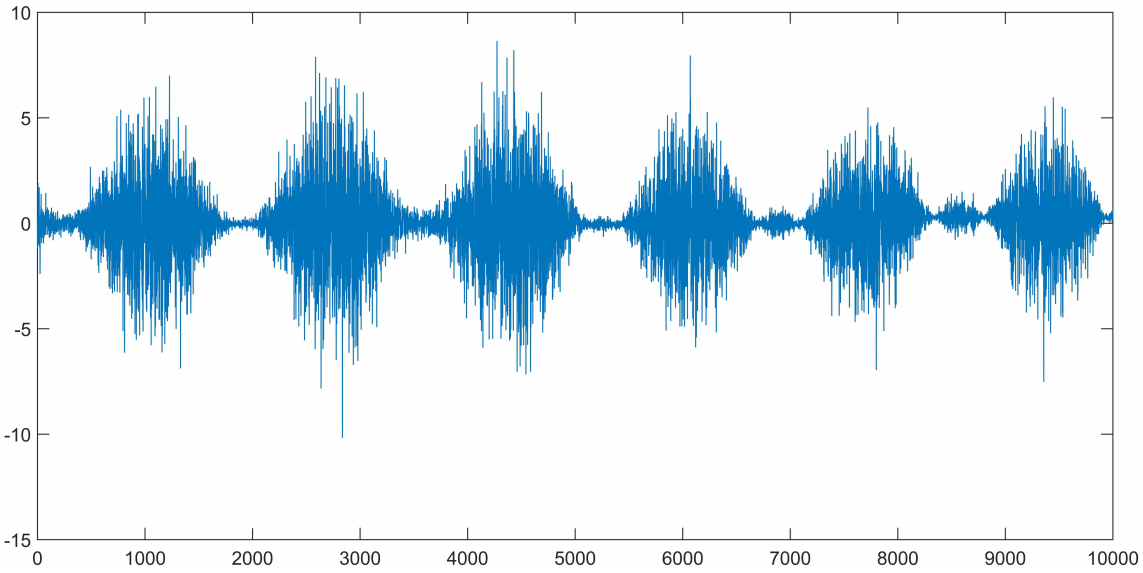


Figure 7.7: The residual series obtained using the conventional cointegration method.

### Results

If one uses the conventional cointegration method to cointegrate the four series with the training set ranging from point 1 to 5000, the cointegrated residual series is shown in Figure 7.7. As expected, the heteroscedastic noise sabotages the required condition of normally-distributed noise, which comes from the fact that the Johansen procedure is a maximum likelihood method.

The TBATS decomposition is therefore applied, in order to extract the daily and seasonal components first, and apply the cointegration method is applied. A representative result of the decomposition of $X_1$ is shown in Figure 7.8. One can see the seasonal and daily patterns have been accurately identified, and most of the noise is left in the level term. Damage information can also be clearly discerned in the level term.

Although damage information is clear in this case, it is likely that in other scenarios, the trend term itself is great enough to disguise the damage information. The de-seasonalised series are subsequently fed to cointegration, and the cointegrated residual series is now shown in Figure 7.9. With the three standard deviation confidence interval overlaid, the plot is much clearer than Figure 7.7, the residual stays mostly stationary in the mean, and the nonstationary level in the variance has also been somewhat suppressed; most importantly the damage information is evident

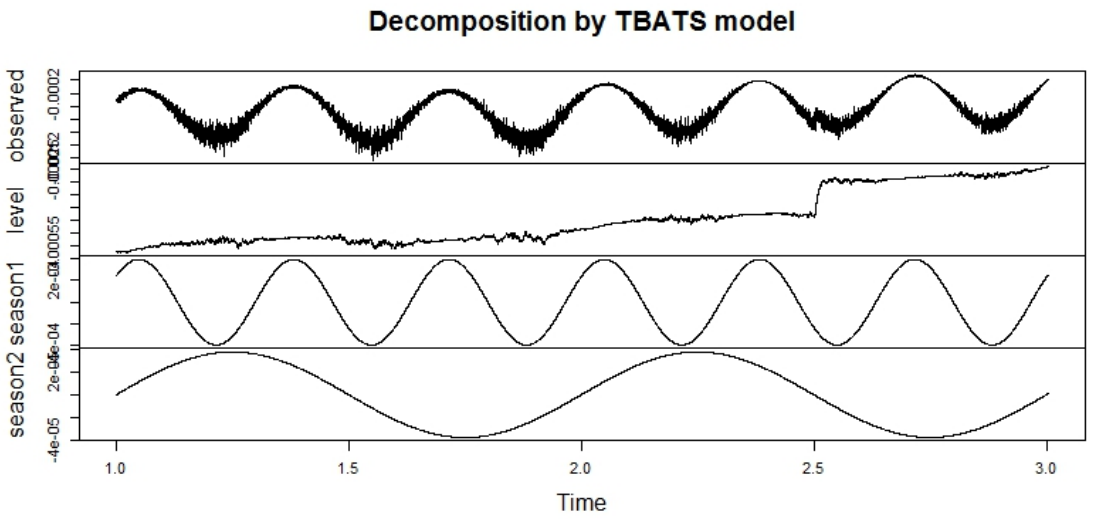


Figure 7.8: Decomposition results from the TBATS model.

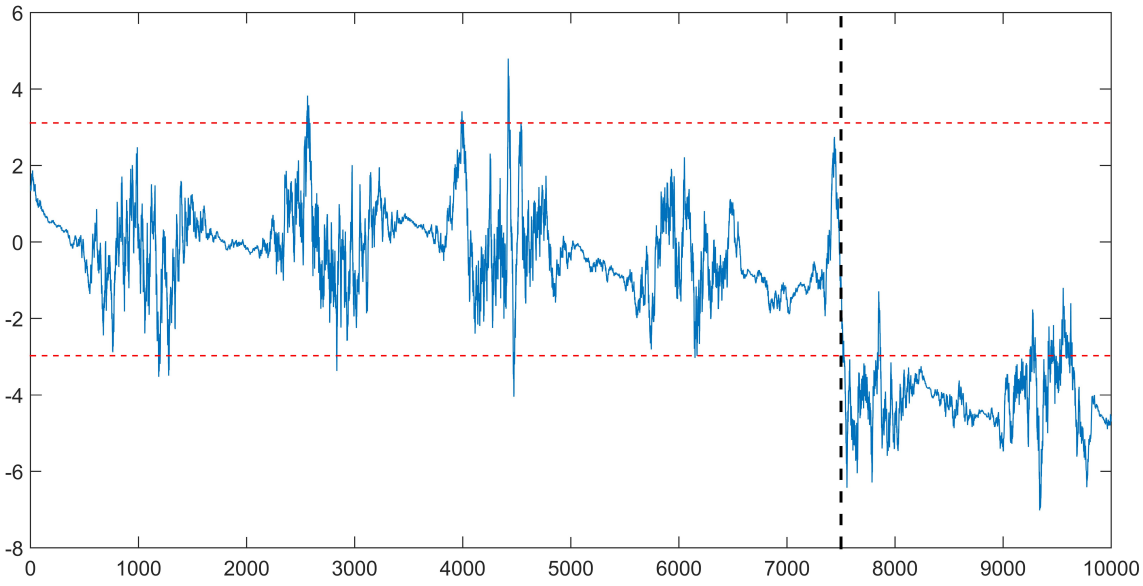


Figure 7.9: Cointegrated residual series of the de-seasonalised series; red horizontal lines indicate three standard deviation intervals; black vertical line marks the damage introduction point.

immediately after it is introduced.

### 7.3.2 Case Study II: The NPL Bridge

Having briefly reviewed the NPL Bridge in Section 7.2, this section will present more details of the SHM of the NPL Bridge, and revisit the heteroscedastic issue

concerned with the data, the subsequently attempt to address it with the proposed method.

### The SHM of the NPL Bridge

The NPL Bridge is 20 m long and 5 m high, weighing around 15 tonnes, as illustrated in Figure 7.10. After it was in service for nearly 50 years, the bridge was moved to a new location to conduct long-term monitoring experiments with a variety of different sensors, during the years 2009 to 2011. The monitoring covered an extensive time period consisting of at least two full seasonal variations. The monitoring campaign implemented several testing events, the respective time lines are summarised in Figure 7.11. The bridge was subjected to a series of static short-term and sustained loading tests, starting from March 2009. Loading was employed with water tanks of different weights, at the edge of the bridge deck, as illustrated in the left end of Figure 7.10. Apart from loading tests, a few damage scenarios were also realised on the bridge; on $18^{th}$ October 2010 for example, artificial damage was introduced by cutting the rebar on the top of the bridge deck, so as to represent the decrease of the cross section. A number of other test events were also implemented, readers can find details from [182].

As mentioned above, this bridge was heavily instrumented with many kinds of sensors, but only the tilt sensor data will be analysed in this study. The tilt sensors were installed by the ITMSOIL instrumental company in December 2008; Figure 7.10 shows the schematic of all the locations of the 8 tilt sensors. Tilt sensors are used to measure the local inclination of the structure, therefore they can potentially be used to indicate the onset of damage in the structure. The data was originally collected at a five-minute time interval except for a number of days of special tests. Consequently, before doing any analysis, the first thing is to make the data regularly sampled. As the data were carefully labelled with a time stamp, the data on the hour were used to form a new time series, a representative example of the tilt sensor 1 (TL1) data is shown in Figure 7.11, the time stamps for the important test events are summarised in Table 7.1.

Notice that in the original study of the monitoring campaign, thermal sensors were also installed on multiple positions of the bridge. However, after investigating the origins of measurement uncertainty, Barton and Esward [183] found that the temperature measurements at different locations of the bridge might have a lagged effect

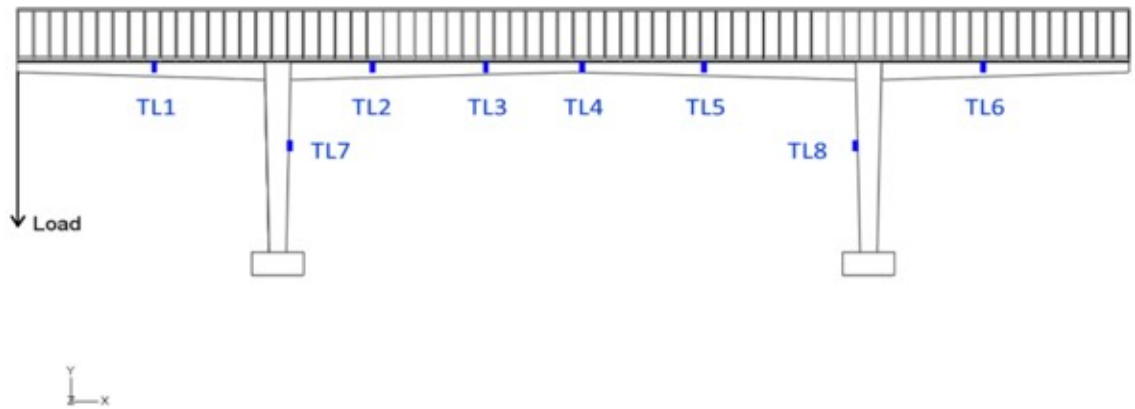


Figure 7.10: Layout of all tilt sensors on the bridge and the loading implementation position.

| Index | Time | Test Event |
|---|---|---|
| 1 | 2009.03.24 | Static loading |
| 2 | 2009.06.29 | Static loading |
| 3 | 2009.08.03 | Static loading |
| 4 | 2010.06.30 | Static/Dynamic loading |
| 5 | 2010.10.08 | Static loading |
| 6 | 2010.10.18 | Damage: removing rebars |
| 7 | 2010.11.01 | Repairing damage |

Table 7.1: Important test events and their corresponding time stamps.

due to the temperature gradients caused by heating from the sun. In this study, temperature data will not be used, as cointegration is able to remove environmental variations without the measurements of the environmental variables.

### Results and Discussion

It is not difficult to see from Figure 7.11 that the tilt sensor measurements are quite nonstationary, both in mean and variance. The changes in mean could be caused by environmental variations or destructive test implementation, and obviously any potential changes induced by damage are overwhelmingly masked by environmental variations. While the changes in the variance are a bit more complex, one can roughly observe that the volatility level in the winter time is significantly smaller than that in the summer time, and the volatility level has a repeated pattern resembling seasonal variations. As the measurements were taken in a time period of two years and eight months, two complete seasonal cycles can be visualised; the first

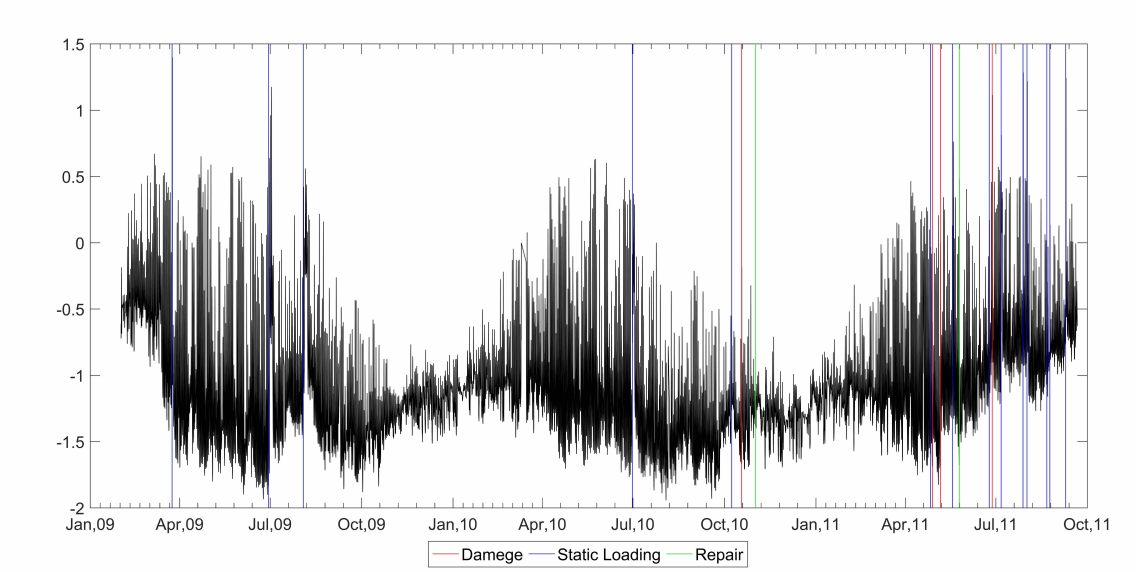


Figure 7.11: Time table of the respective destructive tests implemented on the NPL Bridge and hourly data of tilt sensor 1 (TL1) during February 2009 to September 2011.

ranges from February 2009 to February 2010, the second seasonal cycle starts in February 2010 and ends in February 2011. Barton and Esward found that the thermal expansion of this bridge was unexpectedly large and complex, it could produce almost the same strain level that was caused by a two-tonne loading [183].

As mentioned above, cointegration has been developed to deal with environmental and operational variations, and the Johansen procedure is normally used to estimate cointegration relationships. However, the Johansen procedure is a likelihood-based method, which would naturally require the residuals to be an *i.i.d.* process; marked seasonality in the data would therefore sabotage this condition and underestimate the variance level. In this chapter, the TBATS time series decomposition method will be employed first, in order to concentrate out the underlying complex seasonal components; subsequently, a normal cointegration analysis will be carried out to the de-seasonalised series.

A representative example of the TBATS decomposition of the sixth tilt sensor data is shown in Figure 7.12. The top plot is the original time series, the decomposed components are shown in the middle and bottom plots, and they are the level and seasonal series respectively. The level series can be thought to be the extracted trend of the original series, purged of observation noise and seasonality. One can see that the level series is much smoother than the original series, most of the

fluctuations have been removed, and the long-term trend is well preserved. The seasonal pattern is set to be 24 hours (daily cycle), as expressed in equations (7.5) to (7.7), which means that the seasonal series has a daily pattern whose magnitude changes over time. Comparing the shape of the envelope of the seasonal series with the original series, most of the time-varying daily cyclic components have been accurately singled out, potential damage information is manifested in the long-run component, the trend component, hence cointegration can be subsequently applied for damage detection.

After conducting TBATS decompositions to all the eight tilt sensor datasets, one can obtain eight de-seasonalised trend series and error series. The data ranging from February 2009 to February 2010 are used to form a training set, as this period covers a full seasonal variation. The Johansen procedure is then applied to the eight trend component series using the training data set, in order to estimate a cointegration relationship. A residual series is then formed using the whole data set, as shown in Figure 7.13. The shaded area in the figure indicates a 95% confidence interval. The region between the beginning of the series and the first black vertical line consists of the training set. Apart from a few occurrences of alarms, the series stayed mostly stationary, and the changes caused by environmental variations are largely eliminated. The blue vertical line at around June $30^{th}$ 2010 indicates when a major static test was conducted. One can see that after this date, the residual series has a major shift in the mean and also exceeded the lower confidence boundary, which can be regarded as a clear alarm signal. This can be explained by the fact that once the health state of the structure has changed, the underlying cointegration relationship may no longer hold, and consequently the cointegrated residual will no longer stay stationary.

From Figure 7.11, it is also known that after June $30^{th}$, the campaign implemented a few other events on this bridge. It is worth noticing that on May $6^{th}$ 2011, the campaign introduced a severe damage (removing the damaged concrete) to the bridge. Correspondingly on Figure 7.13, the mean level of the residual series undergoes a significant increase after this date, which is an indication that the bridge is experiencing a change of state. Although the mean of the residual seems to return to the mean of the training set, it certainly does not mean that the bridge is recovering to its healthy state. In order to further detect any damage after June $30^{th}$, one would possibly need to re-evaluate the latest cointegration relationship of the bridge, and form a new state of normal condition.

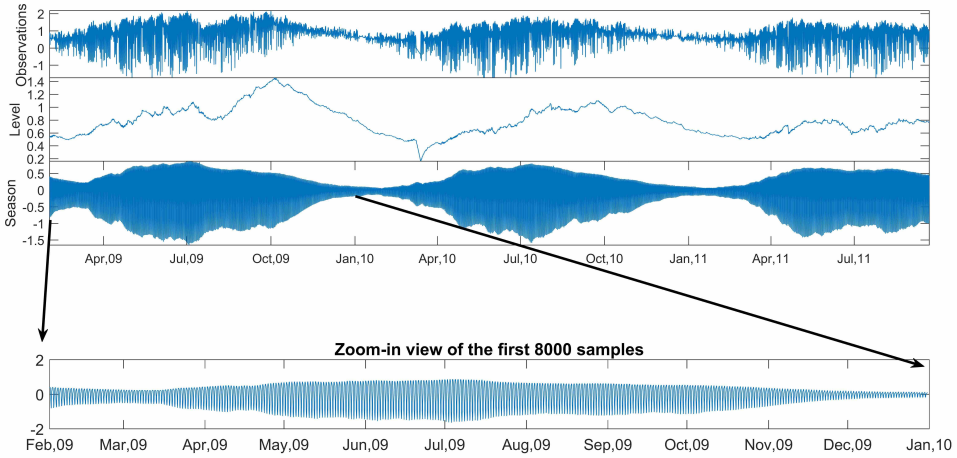


Figure 7.12: A single seasonal TBATS decomposition of the tilt sensor 6 (TL6) data.

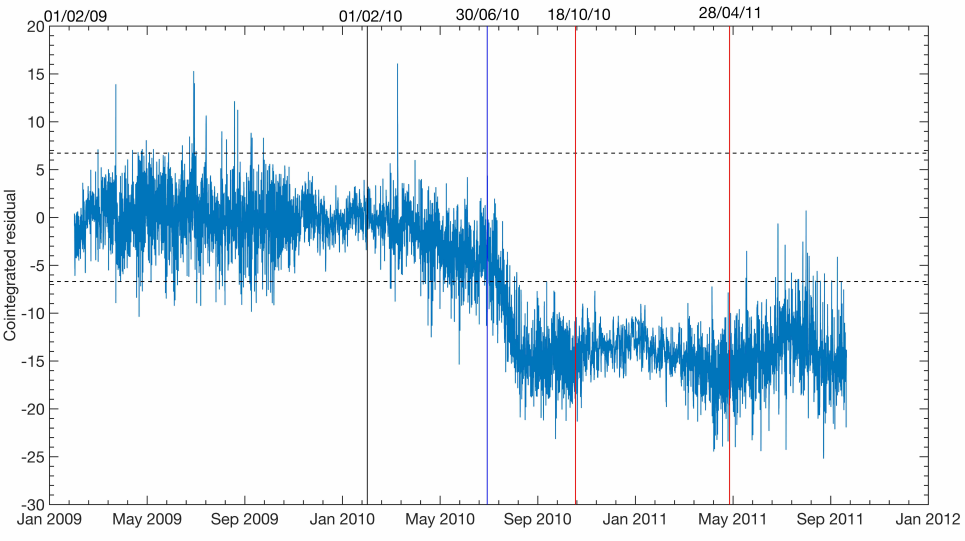


Figure 7.13: Cointegrated residual with confidence intervals marked with black horizontal lines; the black vertical line indicated the end of the training data; the blue line shows when a static and dynamic test was conducted; the red lines imply damage introduction.

### Comparison with the linear cointegration method

Comparing the results in Figure 7.13 with the cointegrated residual plotted in Figure 7.2, one can draw the following conclusions:

First of all, the heteroscedastic noise in the residual has been significantly suppressed, the residual series before the first blue line is quite stationary both in mean and variance, the environmental variations have been largely purged; this confirms the assumption that most of the heteroscedasticity is manifested in the seasonal components;

Secondly, Figure 7.13 has accurately captured the long-term trend component; any information about structural changes to the bridge is well reflected in the residual series. For example, on June $30^{th}$ 2010, the monitoring campaign conducted both static loading and dynamic loading on the bridge, the residual in the figure presents a sudden rise in the mean and exceeds the upper confidence interval soon after the time mark. In contrast, in Figure 7.2, the underlying trend is overwhelmed by the heteroscedastic noise. Interestingly, the residual series behaves quite differently even after it goes beyond the control limit; for example, points between the two red lines and the points after the second red line show distinct characteristics. However, one needs to notice that once the cointegration relationship has "broken", it is necessary to update with a new cointegration relationship, and a new cointegrated residual needs to be estimated as well.

The TBATS model above has successfully dealt with heteroscedastic noise, but if one also wishes to apply the X-bar chart, similar to the one used in [175], it is trivial to obtain the plot, shown in Figure 7.13. Comparing with Figure 7.11, one obvious improvement is that the time varying variance has been eliminated here, the residual during the undamaged condition maintains stationary. Although, near the first blue line, the residual gives early alarms, this is probably because that the TBATS model is an off-line method in nature, meaning that it has to decompose the series as a whole, which may smooth out sharp changes in the trend component.

Moreover, from a practical perspective, if one wishes to apply the proposed algorithm to a real world engineering practice, say the SHM of a bridge in operation, one would first need to acquire sufficient amount of sensor measurements of the bridge under healthy conditions; then, the proposed method can be used to build a baseline model and a baseline residual series; as new data come in, the TBATS decomposition

is applied on the whole dataset, including training data and newly-arrived data, followed by the cointegration analysis; finally, the baseline model can be updated on a regular basis, in order to improve computational efficiency.

## 7.4 Conclusions

In this chapter, an extension of previous studies of the cointegration method for SHM has been explored. The TBATS model from the time series community has been tested in order to project out the seasonality observed in SHM data. The TBATS model is a flexible and robust state space model with a single source of error, which has been widely adopted in the analysis of seasonal time series. As long-term SHM data is inevitably affected by daily, seasonal and annual environmental variations, and maybe in some cases the interactions of human activities, it will be beneficial if the seasonal component can be extracted before doing subsequent analysis. As cointegration has proved to be a powerful tool to deal with the issue of environmental and operational variations in SHM, the TBATS model can be seen as a pre-processing tool for cointegration analysis. Because by removing the seasonality, one may potentially suppress the heteroscedastic noise caused by seasonality, as the Johansen procedure for cointegration would normally require the noise to be an *i.i.d.* process, this might help to rectify any ill-conditioned procedures. In the fourth section of the chapter, two case studies are presented. A synthetic case simulates a cantilever beam under varying temperature conditions; heteroscedastic noise is added to the simulations. The TBATS model is first used to separate the two seasonal components, and then the cointegration approach is applied, damage information can then be visualised in the residual series. Another case study of the NPL bridge is presented with the proposed method. The result is encouraging, in that the TBATS model can elegantly extract the daily cycles from the original series, most of the heteroscedasticity is accounted for by the seasonal components. The long-term trend series is then applied with cointegration analysis, the residual series is mostly stationary in the training set, most of the environmental variations have been removed, the residual series remains sensitive to damage information.

# Chapter 8

# Conclusions and Future Work

## 8.1 Summaries

This thesis has aimed to address one of the fundamental challenges to the community of structural health monitoring, that is to understand and alleviate the confounding influence from the variations of environmental and operational conditions, which is often referred to as the data normalisation problem. The thesis is titled with "Nonlinear Cointegration Method", thus the main methodology studied is centred around cointegration, a systematic framework to tackle the data normalisation problem. Cross et al. [124] laid the groundwork for the application of cointegration in SHM; this thesis intends to further strengthen the applicability of cointegration. In the present work, cointegration methods have been exploited in directions of time series analysis and machine learning, robust methods that can deal with nonlinear and heteroscedastic data have been developed, and tested on both simulated and real-world datasets.

This chapter seeks to conclude the thesis by summarising all the results and conclusions of the previous chapters, and provide some discussions on some of the potential directions in which one may extend the work of this thesis.

**Nonlinear Cointegration with Gaussian Process Regression**

Chapter 4 gives a full account for the cointegration theories that are used in the thesis. The reason that cointegration works for SHM is actually straightforward, as cointegration is a econometric framework for modelling nonstationary time series, and cointegration is a property of nonstationary time series who share the same kind of stochastic trend. Analogously, environmental and operational variations simultaneously affect dynamic responses of structures, which can be deemed as the "common trend"in the SHM context. The implementation of cointegration is not difficult; the framework associated with this part is the Engle-Granger framework, which is in fact linear regression in its simplistic form. To confirm the existence of a cointegration relationship, one needs to impose statistical tests on the original variable and the cointegrated residual. In the context of SHM, once the cointegration relationship between variables is established, then the cointegrated residual series, which is theoretically stationary, becomes a natural choice for a damage indicator. When there is the onset of damage, the "old" cointegration relationship is consequently breached, which shall be reflected in the cointegrated residual series by presenting an imminent change of magnitude.

The novelty proposed in this part is concerned with a nonlinear cointegrating function expressed by a Gaussian process regression. As mentioned above, the Engle-Granger framework is ultimately linear, hence it is not sufficient in cases where EOVs have a nonlinear effect on the system responses. Chapter 5 proposed to use GP to approximate this nonlinear relationship. The GP was selected for a few reasons: (1) GP is a probabilistic modelling approach, which is especially favourable if one wishes to quantify the uncertainty in the model prediction; (2) the GP is also a Bayesian regression method, meaning that it can fully account for the uncertainty in the model forms and even hyperparameters, making it much less prone to overfitting, comparing with other machine learning regression methods; (3) the GP is also a very flexible and powerful framework; for example, different types of covariance function may have completely different properties, implying that the GP can model various types of datasets. Possible extensions with the GP framework will be discussed in the Future Work section shortly.

The proposed method was examined with two case studies. The first case study was a simulation experiment from [139], where a linear trend-stationary series and a quadratic-trend stationary series were simulated. The GP was capable of ap-

proximating the underlying relationship between the two series. A model selection scheme was also proposed in this section, which was to find the model form with the smallest ADF statistic, MSE and MAE of the residual series. The second case study was about the famous Z24 Bridge benchmark. As reviewed in Chapter 3, the dynamic properties of the Z24 Bridge exhibited a bilinear relationship because of the changes of temperature. The GP successfully modelled the underlying nonlinear cointegration, and the model residual series showed little effect from the external EOVs and maintained stationary until damage occurred. The assumption behind this case study was that the cointegration relationship transitioned smoothly from one regime to the other, the GP was utilised to capture this smooth transition function.

**Regime-Switching Cointegration**

The GP modelled the nonlinear cointegrating function as a smooth function; Chapter 6 took a different approach by proposing a regime-switching cointegration method. The idea was motivated by Gregory and Hansen's regime-shift model [171], where the cointegrating relationship shifted to another regime after the onset of a breakpoint. Therefore, this chapter explored the method to find the breakpoint for regime changes. In economic systems, regime shifts are normally caused by exogenous impact, similarly in SHM systems, the nonlinear system behaviour stems from the EOVs. Hence, this chapter adopted temperature as an exogenous variable to control the regime switching. To find the positions of regime switches (breakpoints), an exhaustive searching algorithm was proposed, the procedures of which are roughly listed in the following: (1) all the system variables need to be sorted with respect to the values of EOV variable; (2) insert a breakpoint at 15% point of the training data; (3) apply the Johansen procedures on both half of the series, and calculate the ADF statistic for the combined residual series; (4) repeat (2) and (3) for every possible breakpoint position; (5) evaluate the optimal breakpoint position with the smallest ADF statistic. One important remark here is that the cointegration estimation used in this chapter was the Johansen procedures, rather than the Engle-Granger framework from the last chapter, the reasons are two-fold: firstly, the Johansen procedure is a maximum likelihood estimation method, the estimated cointegrating vectors are ranked according to the magnitude of the eigenvalues, thus the cointegrating vector with the maximum eigenvalue can be chosen as a representative one. Secondly, because the cointegration relationship is expressed in a vector error correction form,

it is not necessary to perform model selection like in the Engle-Granger framework.

The proposed method was tested on two case studies. The first one was a multi-degree-of-freedom mass-spring system, which is a basic form of dynamic system. To mimic the nonlinear effect from EOV, the spring was simulated to be a bilinear function of temperature, which switched at 0°C. The breakpoint searching algorithm found the breaking temperature to be 0.4767°C, which was quite consistent with the simulation. A stationary residual series was produced, the residual series went over the three-standard-deviation confidence interval immediately after damage was introduced. The second case study was still the Z24 Bridge, the algorithm found a break point at 0.98°C, and also produced a damage-sensitive residual series. The chapter also went further to consider the three-regime-switching case. The augmented algorithm was relatively straightforward, which was simply a two-dimensional exhaustive search. The two breakpoints found were 2.36°C and 3.95°C, which interestingly was near to the findings in the TGP regression in [92].

**Heteroscedastic Cointegration**

Chapter 7 focused on a different type of challenge arising in SHM data, which is the time-varying noise, or heteroscedasticity. As it is known that many time series and machine learning methods are based on maximum likelihood estimation, assuming the observation noise is independently identically distributed; heteroscedasticity may sabotage this assumption, resulting in biased estimation results. The method proposed in this chapter was to first use a time series decomposition method, the TBATS model, and then apply cointegration on the decomposed trend components. The reason for decomposing a time series was mainly based on the observation that most of the heteroscedasticity came from the changes in the cyclic/seasonal components, the noise was associated with the magnitude of these cyclic components. Therefore, these time-varying cyclic components needed to be isolated first. The TBATS model, is a state space-based model which is capable of expressing time series as structural components, including trend, seasonal (cyclic) and disturbances. The seasonal component in particular is represented by a time-varying Fourier series, which fits the situation herein very well. Once the raw time series were properly decomposed, the heteroscedastic noise could be significantly suppressed, the standard linear cointegration analysing method could then be applied.

Two case studies were presented to validate the proposed method. The first one

was a cantilever beam, subjected to an uneven sinusoidal temperature field. Heteroscedastic noise was added to the simulated rotational angle signal. The TBATS decomposition could accurately find the sinusoidal components embedded in the observing signal. Cointegration was then applied on the trend components only, and the sensitivity to damage was successfully recovered. The second case study was a real engineering situation, which used the SHM data from the NPL Bridge. The data was dominated by the daily cycle caused by temperature variations, structural degradation information was completely masked. The TBATS model was applied to the raw tilt sensor data, in order to find the time-varying daily cyclic components. The decomposition was applied to every sensor signal, cointegration was then applied to the trend components from the TBATS model. The bad influences from the heteroscedastic noise was significantly reduced, and the damage detection became effective.

## 8.2 Directions for Future Work

#### Nonlinear Cointegration with Gaussian Process Regression

As briefly alluded to in the conclusions of Chapter 5, the GP regression can be extended to a series of variants. For instance, one can readily replace the normal GP regression with a treed GP (TGP) regression. The TGP algorithm partitions the input space using a Bayesian CART, within each independent region, a GP model is fitted. Recalling the Z24 Bridge case, the data in cold regime and warm regime indicate totally distinct statistical properties, hence, this regime-switching cointegration can be potentially modelled with the treed partition, then a number of GPs can be used to model the different mean and variance properties in each independent input space.

Also, note that the covariance function in GP almost controls all the characteristics of a GP. One can explore different types of covariance functions and how they might affect the fitting of the model. Particularly, the automatic relevance determination (ARD) covariance, with the form $k(x, x') = \sigma_0^2 exp[-\frac{1}{2}\sum_{d=1}^{D}(\frac{x_d - x'_d}{\lambda_d})]$, can be used to understand the importance of each input dimension by assigning and learning a different length scale hyperparameter to each individual input dimension. This can be potentially beneficial for variable selection, especially in cases where the number

of input variables is large.

The other direction for GP is about the scalability to big data applications. It is known that a normal GP requires $\mathcal{O}(N^3)$ computational cost and $\mathcal{O}(N^2)$ memory cost, which can be problematic if the number of observation $N$ is large (10000 is often deemed as a practical maximum $N$ for performing a normal GP). Many scalable GP methods have been developed to address this issue, the FITC method [163] and variational sparse GP [184] are two excellent frameworks that have made scalable GPs practical.

So far, it is all about GPs; however, there exists a diverse set of methods in the econometric literature for modelling nonlinear cointegration. Cointegration with smooth transition regression (STR) has been neglected in this thesis, one can use a parametric function form, for example a logistic function or exponential function, to approximate the regime switching [126].

### Regime-Switching Cointegration

The regime-switching method proposed in Chapter 6 used temperature as an exogenous variable that controlled the timing of regime switches. Naturally, it is tempting to develop an algorithm whose regime switches are determined endogenously, that is to take the EOV measurements out the cointegration model. One way to achieve this is to construct a Markov-switching cointegration model which has a latent state variable deciding what hidden state current observation is in, and the hidden states may evolve with time, following a Markov process. This framework may resemble the famous hidden Markov model (HMM), except that it is in the regression context.

One can also approach this problem by making the vector error correction (VEC) model switch in different regimes. But reflecting on the complex procedures of the Johansen procedures, one can foresee that this direction may not be trivial at all; one obvious obstacle is that the cointegrating rank may actually be different in different regimes, the number of parameters may hence dramatically increase, making the parameter estimation extremely cumbersome.

### Heteroscedastic Cointegration

The proposed method first decomposed a time series into different components, and then applied cointegration to the trend components. One obvious direction for dealing with heteroscedastic cointegration is to adapt the GP nonlinear cointegration method into heteroscedastic context. As Lázaro-Gredilla and Titsias have proposed in [166], a variational approximation of heteroscedastic GP can be used in the cointegration context, seeking to obtain a time-varying confidence interval, which can be hugely advantageous for reducing false positive alarms.

The other direction of work can be adapted from the seasonal cointegration literature [144]. Taking the NPL Bridge for instance, because the tilt sensor measurements were hourly recorded, the daily cycle of temperature has a huge influence on the estimation of cointegration. Like the seasonal cointegration model, one can estimate a cointegration model for every hour mark, therefore 24 cointegration models can be built for the NPL Bridge, associated anomaly detection algorithms wait to be investigated.

## 8.3 Concluding Remarks

At the time being, SHM has quickly drawn considerable interests from diverse groups of research disciplines and industry sectors. This has been fuelled by the fact that the costs of sensors, data storages and computing machines have been brought down significantly, while the computing power, data infrastructures and communication technologies have advanced dramatically in the same time period, and SHM sits right in the intersection of these global trends. SHM is at a critical stage, transitioning from laboratory to real world usage; commercial applications of SHM can already be seen in the market. SHM systems are often installed on critical structures including but not limited to bridges, aircraft, wind turbines, and nuclear plant, they have to be reliable and effective. Therefore, any algorithms developed have to be explainable, robust to uncertainties, and tailor-designed for each individual system, these will be the goals for the author to always remember and pursue in the future.

# Bibliography


[1] BSNA EN. Uk national annex to eurocode: Basis of structural design. *British Standards Institution, London*, 2005.

[2] BBC News. Seized pin caused forth road bridge fault, engineer tells holyrood inquirys, January 2016. URL `http://www.bbc.co.uk/news/uk-scotland-scotland-politics-35354846`. [Accessed 03-March-2018].

[3] Gethin W Roberts, Christopher J Brown, Xiaolin Meng, Oluropo Ogundipe, Christopher Atkins, and Barry Colford. Deflection and frequency monitoring of the forth road bridge, scotland, by gps. *Proceedings of the ICE-Bridge Engineering*, 165(2):105–123, 2012.

[4] Gethin Wyn Roberts, CJ Brown, and X Tang. Correlated gnss and temperature measurements at 10-minute intervals on the severn suspension bridge. *Applied Geomatics*, 9(2):115–124, 2017.

[5] Guido Morgenthal, Sebastian Rau, Jakob Taraben, and Tajammal Abbas. Determination of stay-cable forces using highly mobile vibration measurement devices. *Journal of Bridge Engineering*, 23(2):04017136, 2017.

[6] Charles R Farrar and Keith Worden. *Structural Health Monitoring: A Machine Learning Perspective*. John Wiley & Sons, 2012.

[7] Anders Rytter. *Vibrational based inspection of civil engineering structures*. PhD thesis, Dept. of Building Technology and Structural Engineering, Aalborg University, 1993.

[8] Lei Clifton, David A Clifton, Peter J Watkinson, and Lionel Tarassenko. Iden-

tification of patient deterioration in vital-sign data using one-class support vector machines. In *Computer Science and Information Systems (FedCSIS), 2011 Federated Conference on*, pages 125–131. IEEE, 2011.

[9] V Jyothsna, VV Rama Prasad, and K Munivara Prasad. A review of anomaly based intrusion detection systems. *International Journal of Computer Applications*, 28(7):26–35, 2011.

[10] Christopher P Diehl and John B Hampshire. Real-time object classification and novelty detection for collaborative video surveillance. In *Neural Networks, 2002. IJCNN'02. Proceedings of the 2002 International Joint Conference on*, volume 3, pages 2620–2625. IEEE, 2002.

[11] Cecilia Surace and Keith Worden. Novelty detection in a changing environment: a negative selection approach. *Mechanical Systems and Signal Processing*, 24(4):1114–1128, 2010.

[12] Marco AF Pimentel, David A Clifton, Lei Clifton, and Lionel Tarassenko. A review of novelty detection. *Signal Processing*, 99:215–249, 2014.

[13] Andrew KS Jardine, Daming Lin, and Dragan Banjevic. A review on machinery diagnostics and prognostics implementing condition-based maintenance. *Mechanical systems and signal processing*, 20(7):1483–1510, 2006.

[14] ZK Peng and FL Chu. Application of the wavelet transform in machine condition monitoring and fault diagnostics: a review with bibliography. *Mechanical systems and signal processing*, 18(2):199–221, 2004.

[15] Robert Bond Randall. *Vibration-based condition monitoring: industrial, aerospace and automotive applications*. John Wiley & Sons, 2011.

[16] Christian U Grosse and Masayasu Ohtsu. *Acoustic emission testing*. Springer Science & Business Media, 2008.

[17] Y Gotoh, H Hirano, M Nakano, K Fujiwara, and N Takahashi. Electromagnetic nondestructive testing of rust region in steel. *IEEE transactions on magnetics*, 41(10):3616–3618, 2005.

[18] Sergey Kharkovsky and Reza Zoughi. Microwave and millimeter wave nondestructive testing and evaluation-overview and recent advances. *IEEE Instrumentation & Measurement Magazine*, 10(2):26–38, 2007.

[19] Bruce W Drinkwater and Paul D Wilcox. Ultrasonic arrays for non-destructive evaluation: A review. *Ndt & E International*, 39(7):525–541, 2006.

[20] Jay Lee, Fangji Wu, Wenyu Zhao, Masoud Ghaffari, Linxia Liao, and David Siegel. Prognostics and health management design for rotary machinery systemsreviews, methodology and applications. *Mechanical systems and signal processing*, 42(1-2):314–334, 2014.

[21] Ajay Raghavan. Guided-wave structural health monitoring. 2007.

[22] PW Wilcox, MJS Lowe, RP Dalton, and P Cawley. The rapid monitoring of structures using interdigital lamb wave transducers. *Smart Materials and Structures*, 9(3):304, 2000.

[23] Charles H Keilers-Jr and Fu-Kuo Chang. Identifying delamination in composite beams using built-in piezoelectrics: part iexperiments and analysis. *Journal of Intelligent Material Systems and Structures*, 6(5):649–663, 1995.

[24] DC Carter and Karen Margaret Holford. Strategic considerations for the ae monitoring of bridges: a discussion and case study. *Insight-Non-Destructive Testing and Condition Monitoring*, 40(2):112–116, 1998.

[25] Karen Margaret Holford and Robert John Lark. Acoustic emission testing bridges. 2005.

[26] Archana Nair and CS Cai. Acoustic emission monitoring of bridges: Review and case studies. *Engineering structures*, 32(6):1704–1714, 2010.

[27] K Bremer, M Wollweber, F Weigand, M Rahlves, M Kuhne, R Helbig, and B Roth. Fibre optic sensors for the structural health monitoring of building structures. *Procedia Technology*, 26:524–529, 2016.

[28] XW Ye, YH Su, and JP Han. Structural health monitoring of civil infrastructure using optical fiber sensing technology: A comprehensive review. *The Scientific World Journal*, 2014, 2014.

[29] P Moyo, JMW Brownjohn, R Suresh, and SC Tjin. Development of fiber bragg grating sensors for monitoring civil infrastructure. *Engineering structures*, 27 (12):1828–1834, 2005.

[30] Jie Huang, Tao Wang, Lei Hua, Jun Fan, Hai Xiao, and Ming Luo. A coaxial

cable fabry-perot interferometer for sensing applications. *Sensors*, 13(11): 15252–15260, 2013.

[31] Irwan Rawal Husdi, Kentaro Nakamura, and Sadayuki Ueha. Sensing characteristics of plastic optical fibres measured by optical time-domain reflectometry. *Measurement Science and Technology*, 15(8):1553, 2004.

[32] Farhad Ansari. Practical implementation of optical fiber sensors in civil structural health monitoring. *Journal of intelligent material systems and structures*, 18(8):879–889, 2007.

[33] Branko Glisic and Daniele Inaudi. *Fibre optic methods for structural health monitoring*. John Wiley & Sons, 2008.

[34] Kenneth J Loh, Junhee Kim, Jerome P Lynch, Nadine Wong Shi Kam, and Nicholas A Kotov. Multifunctional layer-by-layer carbon nanotube–polyelectrolyte thin films for strain and corrosion sensing. *Smart Materials and Structures*, 16(2):429, 2007.

[35] Jerome P Lynch and Kenneth J Loh. A summary review of wireless sensors and sensor networks for structural health monitoring. *Shock and Vibration Digest*, 38(2):91–130, 2006.

[36] Glenn M Light, Hegeon Kwun, Sang Kim, and Robert L Spinks. Magnetostrictive sensor for active health monitoring in structures. In *Smart Nondestructive Evaluation for Health Monitoring of Structural and Biological Systems*, volume 4702, pages 282–289. International Society for Optics and Photonics, 2002.

[37] Justin G Chen, Neal Wadhwa, Young-Jin Cha, Frédo Durand, William T Freeman, and Oral Buyukozturk. Modal identification of simple structures with high-speed video using motion magnification. *Journal of Sound and Vibration*, 345:58–71, 2015.

[38] Keith Worden, Charles R Farrar, Graeme Manson, and Gyuhae Park. The fundamental axioms of structural health monitoring. In *Proceedings of the Royal Society of London A: Mathematical, Physical and Engineering Sciences*, volume 463, pages 1639–1664. The Royal Society, 2007.

[39] Rune Brincker, Lingmi Zhang, and Palle Andersen. Modal identification of output-only systems using frequency domain decomposition. *Smart materials*

*and structures*, 10(3):441, 2001.

[40] Pizhong Qiao, Kan Lu, Wahyu Lestari, and Jialai Wang. Curvature mode shape-based damage detection in composite laminated plates. *Composite Structures*, 80(3):409–428, 2007.

[41] A Tomaszewska. Influence of statistical errors on damage detection based on structural flexibility and mode shape curvature. *Computers & structures*, 88 (3-4):154–164, 2010.

[42] Wang-Ji Yan, Wei-Xin Ren, and Tian-Li Huang. Statistic structural damage detection based on the closed-form of element modal strain energy sensitivity. *Mechanical Systems and Signal Processing*, 28:183–194, 2012.

[43] E Peter Carden and James MW Brownjohn. Arma modelled time-series classification for structural health monitoring of civil infrastructure. *Mechanical systems and signal processing*, 22(2):295–314, 2008.

[44] Haitao Zheng and Akira Mita. Damage indicator defined as the distance between arma models for structural health monitoring. *Structural Control and Health Monitoring*, 15(7):992–1005, 2008.

[45] Mustafa Gul and F Necati Catbas. Statistical pattern recognition for structural health monitoring using time series modeling: Theory and experimental verifications. *Mechanical Systems and Signal Processing*, 23(7):2192–2204, 2009.

[46] YQ Ni, XT Zhou, JM Ko, and BS Wang. Vibration-based damage localization in ting kau bridge using probabilistic neural network. *Advances in structural dynamics*, 2:1069–1076, 2000.

[47] Hoon Sohn, Keith Worden, and Charles R Farrar. Statistical damage classification under changing environmental and operational conditions. *Journal of intelligent material systems and structures*, 13(9):561–574, 2002.

[48] Keith Worden, Wieslaw J Staszewski, and James J Hensman. Natural computing for mechanical systems research: A tutorial overview. *Mechanical Systems and Signal Processing*, 25(1):4–111, 2011.

[49] Chang Kook Oh and Hoon Sohn. Damage diagnosis under environmental and operational variations using unsupervised support vector machine. *Journal of*

*sound and vibration*, 325(1-2):224–239, 2009.

[50] Sheng-Fa Yuan and Fu-Lei Chu. Support vector machines-based fault diagnosis for turbo-pump rotor. *Mechanical Systems and Signal Processing*, 20(4): 939–952, 2006.

[51] Qifeng Zhou, Hao Zhou, Qingqing Zhou, Fan Yang, and Linkai Luo. Structure damage detection based on random forest recursive feature elimination. *Mechanical Systems and Signal Processing*, 46(1):82–90, 2014.

[52] W Zhou, D Chakraborty, N Kovvali, A Papandreou-Suppappola, D Cochran, and A Chattopadhyay. Damage classification for structural health monitoring using time-frequency feature extraction and continuous hidden markov models. In *Signals, Systems and Computers, 2007. ACSSC 2007. Conference Record of the Forty-First Asilomar Conference on*, pages 848–852. IEEE, 2007.

[53] Edward Glaessgen and David Stargel. The digital twin paradigm for future nasa and us air force vehicles. In *53rd AIAA/ASME/ASCE/AHS/ASC Structures, Structural Dynamics and Materials Conference 20th AIAA/ASME/AHS Adaptive Structures Conference 14th AIAA*, page 1818, 2012.

[54] Gyuhae Park, Amanda C Rutherford, Hoon Sohn, and Charles R Farrar. An outlier analysis framework for impedance-based structural health monitoring. *Journal of Sound and Vibration*, 286(1-2):229–250, 2005.

[55] Keith Worden. Structural fault detection using a novelty measure. *Journal of Sound and vibration*, 201(1):85–101, 1997.

[56] Hoon Sohn, Jerry A Czarnecki, and Charles R Farrar. Structural health monitoring using statistical process control. *Journal of structural engineering*, 126 (11):1356–1363, 2000.

[57] K Worden, EJ Cross, I Antoniadou, and A Kyprianou. A multiresolution approach to cointegration for enhanced SHM of structures under varying conditions–an exploratory study. *Mechanical Systems and Signal Processing*, 47(1):243–262, 2014.

[58] Jyrki Kullaa. Damage detection of the z24 bridge using control charts. *Mechanical Systems and Signal Processing*, 17(1):163–170, 2003.

[59] Hoon Sohn. Effects of environmental and operational variability on structural

health monitoring. *Philosophical Transactions of the Royal Society of London A: Mathematical, Physical and Engineering Sciences*, 365(1851):539–560, 2007.

[60] P Cornwell, Charles R Farrar, Scott W Doebling, and Hoon Sohn. Environmental variability of modal properties. *Experimental techniques*, 23(6):45–48, 1999.

[61] YL Xu, B Chen, CL Ng, KY Wong, and WY Chan. Monitoring temperature effect on a long suspension bridge. *Structural Control and Health Monitoring*, 17(6):632–653, 2010.

[62] Peter Moser and Babak Moaveni. Environmental effects on the identified natural frequencies of the dowling hall footbridge. *Mechanical Systems and Signal Processing*, 25(7):2336–2357, 2011.

[63] Yinghong Cao, Jinsuk Yim, Yang Zhao, and Ming L Wang. Temperature effects on cable stayed bridge using health monitoring system: a case study. *Structural Health Monitoring*, 10(5):523–537, 2011.

[64] Nicholas de Battista, James MW Brownjohn, Hwee Pink Tan, and Ki-Young Koo. Measuring and modelling the thermal performance of the tamar suspension bridge using a wireless sensor network. *Structure and Infrastructure Engineering*, 11(2):176–193, 2015.

[65] Dennis Keith Watson and RKND Rajapakse. Seasonal variation in material properties of a flexible pavement. *Canadian Journal of Civil Engineering*, 27 (1):44–54, 2000.

[66] Bart Peeters and Guido De Roeck. One-year monitoring of the Z24-Bridge: environmental effects versus damage events. *Earthquake Engineering & Structural Dynamics*, 30(2):149–171, 2001.

[67] Georgios Konstantinidis, Paul D Wilcox, and Bruce W Drinkwater. An investigation into the temperature stability of a guided wave structural health monitoring system using permanently attached sensors. *IEEE Sensors Journal*, 7(5):905–912, 2007.

[68] Gyuhae Park, Kazuhisa Kabeya, Harley H Cudney, and Daniel J Inman. Impedance-based structural health monitoring for temperature varying appli-

cations. *JSME International Journal Series A Solid Mechanics and Material Engineering*, 42(2):249–258, 1999.

[69] Mousumi Majumder, Tarun Kumar Gangopadhyay, Ashim Kumar Chakraborty, Kamal Dasgupta, and Dipak Kumar Bhattacharya. Fibre bragg gratings in structural health monitoringpresent status and applications. *Sensors and Actuators A: Physical*, 147(1):150–164, 2008.

[70] Yong Xia, Hong Hao, Giovanna Zanardo, and Andrew Deeks. Long term vibration monitoring of an rc slab: temperature and humidity effect. *Engineering Structures*, 28(3):441–452, 2006.

[71] K Mathioudakis and A Tsalavoutas. Uncertainty reduction in gas turbine performance diagnostics by accounting for humidity effects. In *ASME Turbo Expo 2001: Power for Land, Sea, and Air*, pages V004T04A003–V004T04A003. American Society of Mechanical Engineers, 2001.

[72] QS Li, JQ Fang, AP Jeary, CK Wong, and DK Liu. Evaluation of wind effects on a supertall building based on full-scale measurements. *Earthquake engineering & structural dynamics*, 29(12):1845–1862, 2000.

[73] HF Zhou, YQ Ni, JM Ko, and KY Wong. Modeling of wind and temperature effects on modal frequencies and analysis of relative strength of effect. *Wind and Structures*, 11(1):35–50, 2008.

[74] Metwally Mahmoud, Masato Abe, and Yozo Fujino. Analysis of suspension bridge by ambient vibration measurement using time domain method and its application to health monitoring. In *Proceedings of the International Modal Analysis Conference-IMAC*, volume 1, pages 504–510. Society for Experimental Mechanics, 2001.

[75] EJ Cross, KY Koo, JMW Brownjohn, and K Worden. Long-term monitoring and data analysis of the Tamar Bridge. *Mechanical Systems and Signal Processing*, 35(1):16–34, 2013.

[76] Ser-Tong Quek, Quan Wang, Liang Zhang, and Kian-Keong Ang. Sensitivity analysis of crack detection in beams by wavelet technique. *International journal of mechanical sciences*, 43(12):2899–2910, 2001.

[77] Gyuhae Park and Daniel J Inman. Impedance-based structural health moni-

toring. *Damage prognosis for aerospace, civil and mechanical systems*, pages 275–292, 2005.

[78] Lei Gong. *Dynamic analysis of long-span bridge subjected to traffic loading.* PhD thesis, University of Ottawa (Canada), 2008.

[79] Robert Westgate, Ki-Young Koo, and James Brownjohn. Effect of vehicular loading on suspension bridge dynamic properties. *Structure and Infrastructure Engineering*, 11(2):129–144, 2015.

[80] T Ramesh Babu, S Srikanth, and AS Sekhar. Hilbert–huang transform for detection and monitoring of crack in a transient rotor. *Mechanical Systems and Signal Processing*, 22(4):905–914, 2008.

[81] E Cabal-Yepez, RJ Romero-Troncoso, A Garcia-Perez, and RA Osornio-Rios. Single-parameter fault identification through information entropy analysis at the startup-transient current in induction motors. *Electric Power Systems Research*, 89:64–69, 2012.

[82] Zhipeng Feng, Ming Liang, and Fulei Chu. Recent advances in time–frequency analysis methods for machinery fault diagnosis: A review with application examples. *Mechanical Systems and Signal Processing*, 38(1):165–205, 2013.

[83] YQ Ni, HF Zhou, and JM Ko. Generalization capability of neural network models for temperature-frequency correlation using monitoring data. *Journal of structural engineering*, 135(10):1290–1300, 2009.

[84] N Dervilis, M Choi, SG Taylor, RJ Barthorpe, G Park, CR Farrar, and K Worden. On damage diagnosis for a wind turbine blade using pattern recognition. *Journal of sound and vibration*, 333(6):1833–1850, 2014.

[85] Romualdo Ruotolo and Cecilia Surace. Using svd to detect damage in structures with different operational conditions. *Journal of Sound and Vibration*, 226(3):425–439, 1999.

[86] Steve Vanlanduit, Eli Parloo, Bart Cauberghe, Patrick Guillaume, and Peter Verboven. A robust singular value decomposition for damage detection under changing operating conditions and structural uncertainties. *Journal of Sound and Vibration*, 284(3-5):1033–1050, 2005.

[87] Gianluca Ruocci, Gwendal Cumunel, T Le, Pierre Argoul, Nelly Point, and

Lamine Dieng. Damage assessment of pre-stressed structures: A svd-based approach to deal with time-varying loading. *Mechanical Systems and Signal Processing*, 47(1-2):50–65, 2014.

[88] C Zang and M Imregun. Structural damage detection using artificial neural networks and measured frf data reduced via principal component projection. *Journal of sound and vibration*, 242(5):813–827, 2001.

[89] EJ Cross, Graham Manson, Keith Worden, and SG Pierce. Features for damage detection with insensitivity to environmental and operational variations. In *Proc. R. Soc. A*, page rspa20120031. The Royal Society, 2012.

[90] Elizabeth J Cross. *On structural health monitoring in changing environmental and operational conditions*. PhD thesis, University of Sheffield, 2012.

[91] Robert B Gramacy and Herbert K H Lee. Bayesian treed gaussian process models with an application to computer modeling. *Journal of the American Statistical Association*, 103(483):1119–1130, 2008.

[92] K Worden and EJ Cross. On switching response surface models, with applications to the structural health monitoring of bridges. *Mechanical Systems and Signal Processing*, 98:139–156, 2018.

[93] N Dervilis, H Shi, K Worden, and EJ Cross. Exploring environmental and operational variations in shm data using heteroscedastic gaussian processes. In *Dynamics of Civil Structures, Volume 2*, pages 145–153. Springer, 2016.

[94] Keith Worden and AJ Lane. Damage identification using support vector machines. *Smart Materials and Structures*, 10(3):540, 2001.

[95] Luke Bornn, Charles R Farrar, Gyuhae Park, and Kevin Farinholt. Structural health monitoring with autoregressive support vector machines. *Journal of Vibration and Acoustics*, 131(2):021004, 2009.

[96] Adam Santos, Eloi Figueiredo, MFM Silva, CS Sales, and JCWA Costa. Machine learning algorithms for damage detection: Kernel-based approaches. *Journal of Sound and Vibration*, 363:584–599, 2016.

[97] Peter J Brockwell and Richard A Davis. *Introduction to Time Series and Forecasting*. springer, 2016.

[98] Liu-jie Chen and Ling Yu. Structural nonlinear damage identification algorithm based on time series arma/garch model. *Advances in Structural Engineering*, 16(9):1597–1609, 2013.

[99] Tim Bollerslev. Generalized autoregressive conditional heteroskedasticity. *Journal of econometrics*, 31(3):307–327, 1986.

[100] Hoon Sohn and Charles R Farrar. Damage diagnosis using time series analysis of vibration signals. *Smart materials and structures*, 10(3):446, 2001.

[101] J-B Bodeux and J-C Golinval. Modal identification and damage detection using the data-driven stochastic subspace and armav methods. *Mechanical Systems and Signal Processing*, 17(1):83–89, 2003.

[102] Amir A Mosavi, D Dickey, R Seracino, and S Rizkalla. Identifying damage locations under ambient vibrations utilizing vector autoregressive models and mahalanobis distances. *Mechanical Systems and Signal Processing*, 26:254–267, 2012.

[103] Anastasios M Lekkas, John D Hios, and Spilios D Fassois. Output–only damage detection in a composite beam under varying temperatures via vector stochastic models. In *Proceedings of the 5th European Workshop on Structural Health Monitoring–EWSHM*, 2010.

[104] Anthony Liu, Lazhi Wang, Luke Bornn, and Charles Farrar. Robust structural health monitoring under environmental and operational uncertainty with switching state-space autoregressive models. *Structural Health Monitoring*, page 1475921718757721, 2018.

[105] Zoubin Ghahramani and Geoffrey E Hinton. Parameter estimation for linear dynamical systems. Technical report, Technical Report CRG-TR-96-2, University of Totronto, Dept. of Computer Science, 1996.

[106] David Barber. *Bayesian reasoning and machine learning*. Cambridge University Press, 2012.

[107] Tom Minka. From hidden markov models to linear dynamical systems. Technical report, Technical report, MIT, 1999.

[108] Hasan Ocak and Kenneth A Loparo. A new bearing fault detection and diagnosis scheme based on hidden markov modeling of vibration signals. In *Acoustics,*

*Speech, and Signal Processing, 2001. Proceedings.(ICASSP'01). 2001 IEEE International Conference on*, volume 5, pages 3141–3144. IEEE, 2001.

[109] Qiang Miao and Viliam Makis. Condition monitoring and classification of rotating machinery using wavelets and hidden markov models. *Mechanical systems and signal processing*, 21(2):840–855, 2007.

[110] Chen Lin and Viliam Makis. Optimal bayesian maintenance policy and early fault detection for a gearbox operating under varying load. *Journal of Vibration and Control*, 22(15):3312–3325, 2016.

[111] Jann N Yang, Silian Lin, Hongwei Huang, and Li Zhou. An adaptive extended kalman filter for structural damage identification. *Structural Control and Health Monitoring*, 13(4):849–867, 2006.

[112] Chenhao Jin, Shinae Jang, Xiaorong Sun, Jingcheng Li, and Richard Christenson. Damage detection of a highway bridge under severe temperature changes using extended kalman filter trained neural network. *Journal of Civil Structural Health Monitoring*, 6(3):545–560, 2016.

[113] Arnaud Doucet, Nando De Freitas, and Neil Gordon. An introduction to sequential monte carlo methods. In *Sequential Monte Carlo methods in practice*, pages 3–14. Springer, 2001.

[114] Eleni N Chatzi and Andrew W Smyth. Particle filter scheme with mutation for the estimation of time-invariant parameters in structural health monitoring applications. *Structural Control and Health Monitoring*, 20(7):1081–1095, 2013.

[115] Jian Chen, Shenfang Yuan, Lei Qiu, Jian Cai, and Weibo Yang. Research on a lamb wave and particle filter-based on-line crack propagation prognosis method. *Sensors*, 16(3):320, 2016.

[116] Sourav Banerjee, Xinlin P Qing, Shawn Beard, and Fu-Kuo Chang. Prediction of progressive damage state at the hot spots using statistical estimation. *Journal of Intelligent Material Systems and Structures*, 21(6):595–605, 2010.

[117] Lei Qiu, Shenfang Yuan, Fu-Kuo Chang, Qiao Bao, and Hanfei Mei. On-line updating gaussian mixture model for aircraft wing spar damage evaluation under time-varying boundary condition. *Smart Materials and Structures*, 23

(12):125001, 2014.

[118] Lei Qiu, Fang Fang, Shenfang Yuan, Christian Boller, and Yuanqiang Ren. An enhanced dynamic gaussian mixture model–based damage monitoring method of aircraft structures under environmental and operational conditions. *Structural Health Monitoring*, page 1475921718759344, 2018.

[119] Johan Maeck and Guido De Roeck. Description of z24 benchmark. *Mechanical Systems and Signal Processing*, 17(1):127–131, 2003.

[120] Anne Teughels and Guido De Roeck. Structural damage identification of the highway bridge z24 by fe model updating. *Journal of Sound and Vibration*, 278(3):589–610, 2004.

[121] Tara Baldacchino, Elizabeth J Cross, Keith Worden, and Jennifer Rowson. Variational bayesian mixture of experts models and sensitivity analysis for nonlinear dynamical systems. *Mechanical Systems and Signal Processing*, 66: 178–200, 2016.

[122] Minas D Spiridonakos, Eleni N Chatzi, and Bruno Sudret. Polynomial chaos expansion models for the monitoring of structures under operational variability. *ASCE-ASME Journal of Risk and Uncertainty in Engineering Systems, Part A: Civil Engineering*, 2(3):B4016003, 2016.

[123] N Dervilis, K Worden, and EJ Cross. On robust regression analysis as a means of exploring environmental and operational conditions for shm data. *Journal of Sound and Vibration*, 347:279–296, 2015.

[124] Elizabeth J Cross, Keith Worden, and Qian Chen. Cointegration: a novel approach for the removal of environmental trends in structural health monitoring data. In *Proceedings of the Royal Society of London A: Mathematical, Physical and Engineering Sciences*, volume 467, pages 2712–2732. The Royal Society, 2011.

[125] Elizabeth J Cross and Keith Worden. Cointegration and why it works for SHM. In *Journal of Physics: Conference Series*, volume 382, page 012046. IOP Publishing, 2012.

[126] James Douglas Hamilton. *Time Series Analysis*, volume 2. Princeton University Press, 1994.

[127] Walter Enders. *Applied Econometric Time Series*. John Wiley & Sons, 2008.

[128] Roger Perman. Cointegration: an introduction to the literature. *Journal of Economic Studies*, 18(3), 1991.

[129] David A Dickey and Wayne A Fuller. Distribution of the estimators for autoregressive time series with a unit root. *Journal of the American Statistical Association*, 74(366a):427–431, 1979.

[130] Robert F. Engle and C. W. J. Granger. Co-integration and error correction: Representation, estimation, and testing. *Econometrica*, 55(2):251–276, 1987. ISSN 00129682, 14680262. URL `http://www.jstor.org/stable/1913236`.

[131] Chris Bracegirdle and David Barber. Bayesian conditional cointegration. *arXiv preprint arXiv:1206.6459*, 2012.

[132] Søren Johansen. *Likelihood-Based Inference in Cointegrated Vector Autoregressive Models*. Oxford University Press, 1995.

[133] H Shi, K Worden, and E J Cross. A nonlinear cointegration approach with applications to structural health monitoring. In *Journal of Physics: Conference Series*, volume 744, page 012025. IOP Publishing, 2016.

[134] Haichen Shi, Keith Worden, and Elizabeth J Cross. An exploratory study on removing environmental and operational effects using a regime-switching cointegration method. In *Dynamics of Civil Structures, Volume 2*, pages 329–337. Springer, 2017.

[135] HAICHEN SHI, KEITH WORDEN, and ELIZABETH J CROSS. A time series decomposition method for heteroskedastic data in structural health monitoring. *Structural Health Monitoring 2017*, 2017.

[136] Haichen Shi, Keith Worden, and Elizabeth J Cross. A regime-switching cointegration approach for removing environmental and operational variations in structural health monitoring. *Mechanical Systems and Signal Processing*, 103: 381–397, 2018.

[137] Phong B Dao and Wieslaw J Staszewski. Lamb wave based structural damage detection using cointegration and fractal signal processing. *Mechanical Systems and Signal Processing*, 49(1):285–301, 2014.

[138] Ifigeneia Antoniadou, Elizabeth J Cross, and Keith Worden. Cointegration and the empirical mode decomposition for the analysis of diagnostic data. In *Key engineering materials*, volume 569, pages 884–891. Trans Tech Publ, 2013.

[139] EJ Cross and K Worden. Approaches to nonlinear cointegration with a view towards applications in SHM. In *Journal of Physics: Conference Series*, volume 305, page 012069. IOP Publishing, 2011.

[140] Konrad Zolna, Phong B Dao, Wieslaw J Staszewski, and Tomasz Barszcz. Towards homoscedastic nonlinear cointegration for structural health monitoring. *Mechanical Systems and Signal Processing*, 75:94–108, 2016.

[141] Phong B Dao, Wieslaw J Staszewski, and Andrzej Klepka. Stationarity-based approach for the selection of lag length in cointegration analysis used for structural damage detection. *Computer-Aided Civil and Infrastructure Engineering*, 32(2):138–153, 2017.

[142] Gang Liu, Jianxin Zhang, Xuan Yao, and Ping Qin. Damage detection from continuous long-term static response using cointegration and mewma control chart. In *Sustainable Development of Critical Infrastructure*, pages 421–429. 2014.

[143] Anna Michalak, Jacek Wodecki, Agnieszka Wyłomańska, and Radoslaw Zimroz. Application of cointegration to vibration signal for local damage detection in gearboxes. *Applied Acoustics*, 2017.

[144] Svend Hylleberg, Robert F Engle, Clive WJ Granger, and Byung Sam Yoo. Seasonal integration and cointegration. *Journal of econometrics*, 44(1):215–238, 1990.

[145] Phong B Dao, Wieslaw J Staszewski, Tomasz Barszcz, and Tadeusz Uhl. Condition monitoring and fault detection in wind turbines based on cointegration analysis of scada data. *Renewable Energy*, 116:107–122, 2018.

[146] Matteo CORBETTA, Claudio SBARUFATTI, J Elizabeth, and Marco GIGLIO. Removal of temperature-induced strain variations for fatigue crack growth detection in a real aeronautical structure.

[147] R Fuentes, EJ Cross, N Ray, N Dervilis, T Guo, and K Worden. In-process monitoring of automated carbon fibre tape layup using ultrasonic guided

waves. In *Special Topics in Structural Dynamics, Volume 6*, pages 179–188. Springer, 2017.

[148] Gabriele Comanducci, Filipe Magalhães, Filippo Ubertini, and Álvaro Cunha. On vibration-based damage detection by multivariate statistical techniques: Application to a long-span arch bridge. *Structural Health Monitoring*, 15(5): 505–524, 2016.

[149] Keith Worden, Tara Baldacchino, Jennifer Rowson, and Elizabeth J Cross. Some recent developments in SHM based on nonstationary time series analysis. *Proceedings of the IEEE*, 104(8):1589–1603, 2016.

[150] Gilles Dufrénot and Valérie Mignon. *Recent Developments in Nonlinear Cointegration with Applications to Macroeconomics and Finance*. Springer Science & Business Media, 2012.

[151] J Lin and C Granger. Testing nonlinear cointegration. *Jaromir Antoch COMPSTAT 2004 Proceedings in Computational Statistics*, pages 1413–1419, 2004.

[152] Clive WJ Granger and Jeff Hallman. Nonlinear transformations of integrated time series. *Journal of Time Series Analysis*, 12(3):207–224, 1991.

[153] Ingolf Dittmann and Clive WJ Granger. Properties of nonlinear transformations of fractionally integrated processes. *Journal of Econometrics*, 110(2): 113–133, 2002.

[154] Joon Y Park and Peter CB Phillips. Nonlinear regressions with integrated time series. *Econometrica*, 69(1):117–161, 2001.

[155] Yoosoon Chang, Joon Y Park, and Peter CB Phillips. Nonlinear econometric models with cointegrated and deterministically trending regressors. *The Econometrics Journal*, 4(1):1–36, 2001.

[156] Hans Arnfinn Karlsen, Terje Myklebust, Dag Tjøstheim, et al. Nonparametric estimation in a nonlinear cointegration type model. *The Annals of Statistics*, 35(1):252–299, 2007.

[157] Qiying Wang and Peter CB Phillips. Structural nonparametric cointegrating regression. *Econometrica*, 77(6):1901–1948, 2009.

[158] Jörg Breitung. Rank tests for nonlinear cointegration. *Journal of Business &*

*Economic Statistics*, 19(3):331–340, 2001.

[159] In Choi and Pentti Saikkonen. Tests for nonlinear cointegration. *Econometric Theory*, 26(3):682–709, 2010.

[160] Tony Van Gestel, Marcelo Espinoza, Bart Baesens, Johan AK Suykens, Carine Brasseur, and Bart De Moor. A bayesian nonlinear support vector machine error correction model. *Journal of forecasting*, 25(2):77–100, 2006.

[161] Carl Edward Rasmussen and Christopher KI Williams. *Gaussian processes for machine learning*, volume 1. MIT press Cambridge, 2006.

[162] Stephen Roberts, Michael Osborne, Mark Ebden, Steven Reece, Neale Gibson, and Suzanne Aigrain. Gaussian processes for time-series modelling. *Phil. Trans. R. Soc. A*, 371(1984):20110550, 2013.

[163] Joaquin Quiñonero-Candela and Carl Edward Rasmussen. A unifying view of sparse approximate gaussian process regression. *Journal of Machine Learning Research*, 6(Dec):1939–1959, 2005.

[164] Andrew Wilson and Ryan Adams. Gaussian process kernels for pattern discovery and extrapolation. In *Proceedings of the 30th International Conference on Machine Learning (ICML-13)*, pages 1067–1075, 2013.

[165] Johan Maeck, Bart Peeters, and Guido De Roeck. Damage identification on the z24 bridge using vibration monitoring. *Smart materials and structures*, 10 (3):512, 2001.

[166] Miguel Lázaro-Gredilla and Michalis Titsias. Variational heteroscedastic gaussian process regression. 2011.

[167] Kristian Kersting, Christian Plagemann, Patrick Pfaff, and Wolfram Burgard. Most likely heteroscedastic gaussian process regression. In *Proceedings of the 24th international conference on Machine learning*, pages 393–400. ACM, 2007.

[168] Nathan S Balke and Thomas B Fomby. Threshold cointegration. *International Economic Review*, pages 627–645, 1997.

[169] Bruce E Hansen and Byeongseon Seo. Testing for two-regime threshold cointegration in vector error-correction models. *Journal of Econometrics*, 110(2):

293–318, 2002.

[170] Ming Chien Lo and Eric Zivot. Threshold cointegration and nonlinear adjustment to the law of one price. *Macroeconomic Dynamics*, 5(04):533–576, 2001.

[171] Allan W Gregory and Bruce E Hansen. Residual-based tests for cointegration in models with regime shifts. *Journal of Econometrics*, 70(1):99–126, 1996.

[172] Ryan Prescott Adams and David JC MacKay. Bayesian online changepoint detection. *arXiv preprint arXiv:0710.3742*, 2007.

[173] K Worden. Inferential parameterisation using principal curves. In *3rd International Conference on Identification in Engineering Systems, University of Wales Swansea, UK*, 2002.

[174] WeiYin Loh. Classification and regression trees. *Wiley Interdisciplinary Reviews: Data Mining and Knowledge Discovery*, 1(1):14–23, 2011.

[175] K Worden, E Cross, and E Barton. Damage detection on the npl footbridge under changing environmental conditions. In *6th European Workshop on Structural Health Monitoring*, pages 1–8, 2012.

[176] Douglas C Montgomery. *Introduction to statistical quality control*. John Wiley & Sons (New York), 2009.

[177] Robert B Cleveland, William S Cleveland, and Irma Terpenning. Stl: A seasonal-trend decomposition procedure based on loess. *Journal of Official Statistics*, 6(1):3, 1990.

[178] Charles C Holt. Forecasting seasonals and trends by exponentially weighted moving averages. *International Journal of Forecasting*, 20(1):5–10, 2004.

[179] Rob Hyndman, Anne B Koehler, J Keith Ord, and Ralph D Snyder. *Forecasting with Exponential Smoothing: The State Space Approach*. Springer Science & Business Media, 2008.

[180] Alysha M De Livera, Rob J Hyndman, and Ralph D Snyder. Forecasting time series with complex seasonal patterns using exponential smoothing. *Journal of the American Statistical Association*, 106(496):1513–1527, 2011.

[181] Piotr Omenzetter and James Mark William Brownjohn. Application of time

series analysis for bridge monitoring. *Smart Materials and Structures*, 15(1): 129, 2006.

[182] Valerie Livina, Elena Barton, and Alistair Forbes. Tipping point analysis of the npl footbridge. *Journal of Civil Structural Health Monitoring*, 4(2):91–98, 2014.

[183] E Barton and T Esward. The origins of measurement uncertainty in SHM-NPL footbridge case study. In *6th European Workshop on Structural Health Monitoring*, 2012.

[184] Michalis Titsias. Variational learning of inducing variables in sparse gaussian processes. In *Artificial Intelligence and Statistics*, pages 567–574, 2009.